

University of Naples Federico II

Department of Biology



Doctorate School in Biology

XXIX cycle

Coordinator: Prof. Salvatore Cozzolino

**“Local control of TH action in cancer
growth and stemness”**

Daniela Di Girolamo

Supervisor: Prof. Domenico Salvatore

“Era tale l'entusiasmo generato in me dalla scoperta che ogni mio pensiero, di giorno e di notte, era fisso su questo fenomeno.”

Elogio dell'imperfezione – Rita Levi Montalcini

“Such was the excitation generated in me by the discovery that every thought, by day and by night, was steadily fixed on this phenomena.”

Elogio dell'imperfezione – Rita Levi Montalcini

List of publications

1. **Di Girolamo D**, Ambrosio R, De Stefano MA, Mancino G, Porcelli T, Luongo C, Di Cicco E, Scalia G, Vecchio LD, Colao A, Dlugosz AA, Missero C, Salvatore D, Dentice M. “*Reciprocal interplay between thyroid hormone and microRNA-21 regulates hedgehog pathway-driven skin tumorigenesis.*” J Clin Invest. 2016 Jun
2. Miro C, Ambrosio R, De Stefano MA, **Di Girolamo D**, Di Cicco E, Cicatiello AG, Mancino G, Porcelli T, Raia M, Del Vecchio L, Salvatore D, Dentice M.” *The concerted action of type 2 and type 3 deiodinases regulates the cell cycle and survival of basal cell carcinoma cells.*” Thyroid. 2017 Jan 15.

Index

1 Summary	1
1.1 Local control of TH action in cancer growth and stemness	1
1.1 Il controllo locale dell'azione dell'OT nella crescita tumorale e nella staminalità	2
2 Introduction	4
2.1 Basal cell carcinoma and Shh signaling	4
2.2 Mechanism of thyroid hormone action and deiodinase	7
2.3 Type 3 deiodinase and cancer.....	11
2.4 MicroRNA and cancer : focus on miR-21	13
2.5 Stem cells in skin cancer.....	17
3 Aim of the project	22
4 Results	23
4.1 TH and microRNA: down-regulation of miR21 TH-dependent in BCC	23
4.2 miR21 is overexpressed in mouse BCC cells and tumors	25
4.3 TH regulates miR21 through it's binding a specific gene region	26
4.4 miR21 positively regulates D3 expression	28
4.5 GRHL3, a described miR21 target, suppresses D3 expression	29
4.6 GRHL3 directly inhibits D3 expression	32
4.7 The miR21-GRHL3-D3 axis	33
4.8 GRHL3 is positively regulated by TH.....	34
4.9 Generation of D3KO cells using CRISPR/Cas9 technology and production of miR21 overexpressing cells.....	35
4.10 BCC tumorigenesis required an intact miR21-GRHL3-D3 axis	37
4.11 Genetic D3 depletion reduces BCC-like tumor growth <i>in vivo</i>	39
4.12 The miR21-GRHL3-D3 axis is recapitulated in human BCC	42
4.13 TH and cancer stem cells: generation of conditional D3KO mice	44
4.14 D3 is overexpressed in Smo- and Ptch1- dependent BCC	46
4.15 TH metabolism affect skin cancer stem cells population	48
4.16 Sox 9 is negatively regulated by TH	50
4.17 TH regulates SOX9 through it's binding a specific gene region	51
5 Discussion	52

6 Materials and Methods	59
6.1 Cell cultures and transfections	59
6.2 Plasmid and reagents	59
6.3 Genome-editing of the <i>dio3</i> locus using the CRISPR/Cas9 technology	60
6.4 Luciferase assay	60
6.5 Western blot analysis	61
6.6 miRNA Northern blot	61
6.7 Animals, histology and immunostaining	62
6.8 Real time PCR	62
6.9 TaqMan miRNA assay	63
6.10 Tumor xenografts	63
6.11 Human samples	64
6.12 ChIP assay	64
6.13 Isolation of epithelial CSCs	64
6.14 Statistical analysis	65
6.15 Sequences of primers	66
7 References	68

1 Summary

1.1 Local control of TH action in cancer growth and stemness

Non-melanoma skin cancers, including basal cell carcinoma (BCC), are keratinocyte-derived tumors, which represent the most frequent cancers worldwide. BCCs can cause significant tissue destruction by local invasion, which is particularly devastating since they usually develop in regions closed to the eyes, nose and ears. The aberrant Hedgehog (Hh) pathway is a pivotal defect implicated in BCC formation. Several studies have demonstrated functional cross-talk between thyroid hormone (TH) and Hh signaling. TH controls a number of cellular processes including cell proliferation, differentiation and survival/apoptosis. Intracellular TH concentration is not simply the mirror of circulating TH levels, but is determined by a balance between the activating and inactivating deiodinases enzymes, D2 and D3. In functional combinations, these regulatory molecules provide the ability to fine-tune TH action at cell level. TH deregulation is frequent in human tumors, in particular type 3 iodothyronine deiodinase (D3), the thyroid hormone (TH)-inactivating enzyme, is an oncofetal protein rarely expressed in adult life, but re-activated in proliferating and neoplastic contexts. By terminating TH action within the tumor microenvironment, D3 enhances cancer cell proliferation. We aimed to understand how the TH action regulates multiple aspects of tumorigenesis, ranging from cancer formation to progression.

Here we describe reciprocal regulation between TH action and the cancer-associated microRNA-21 (miR21) in BCC skin tumors. We found that, besides being negatively regulated by TH at transcriptional level, miR21 attenuates the TH signal by increasing D3 levels. The ability of miR21 to positively regulate D3 was mediated by *GRHL3*, a tumor suppressor gene and a hitherto unrecognized D3 transcriptional inhibitor. Moreover, we found that keratinocyte-specific D3-depletion significantly reduced tumor growth in a BCC mouse model, which establishes the functional relevance of this network in vivo. A second aim of this study was to underscore the role of TH and deiodinase D3 in the control of skin CSCs behavior. In vivo and in vitro evidences demonstrate that TH represses the transcription of the stemness gene Sox9. Furthermore, D3-depletion causes a variation of number of CD34⁺ cells demonstrating

that TH metabolism is important not only for the control of tumor growth and maintenance, but also for the behavior of CSCs.

Elucidating the functional role of TH in the landscape of tumorigenesis is crucial for the use of hormonal regulation as a new tool in a therapeutic context.

1.2 Il controllo locale dell'azione dell'OT nella crescita tumorale e nella staminalità

I tumori cutanei non melanomatosi, tra cui i carcinomi basocellulari (o basaliomi), sono tumori di derivazione cheratinica, che rappresentano uno dei tipi di cancro più diffusi al mondo. Il basalioma è un tumore ad invasione locale ma può essere deturpante in quanto insorge generalmente in prossimità di occhi, naso ed orecchie. La principale causa del basalioma è un'aberrante espressione del pathway di Hedgehog (Hh). Diversi studi hanno dimostrato l'esistenza di un cross-talk tra l'ormone tiroideo (OT) e il pathway di Hedgehog. L'OT controlla una serie di processi cellulari tra cui la proliferazione, il differenziamento ed i meccanismi di sopravvivenza/apoptosi. La concentrazione intracellulare dell'OT non rispecchia semplicemente i livelli circolanti di OT, ma è determinata da un equilibrio tra l'attivazione e inattivazione dell'ormone stesso mediata da due enzimi, D2 e D3. Il complesso sistema delle desiodasi svolge, quindi, un ruolo fondamentale nel regolare la quantità di ormone tiroideo a livello cellulare. Molti tumori sono influenzati dal signaling dell'ormone tiroideo, in particolare, la desiodasi di tipo 3, ovvero l'inattivatore dell'OT, è una proteina oncofetale raramente espressa nell'adulto, ma che viene riattivata in contesti di iperproliferazione e trasformazione neoplastica. Terminando l'azione dell'OT all'interno del microambiente tumorale, D3 aumenta la proliferazione delle cellule cancerose. Lo scopo principale del presente lavoro è stato quello di comprendere come l'azione dell'OT potesse regolare i molteplici aspetti della tumorigenesi, che vanno dalla formazione del cancro alla sua progressione.

Abbiamo dimostrato l'esistenza di una reciproca interazione tra l'azione dell'OT e il microRNA-21 (miR21) nel basalioma. Abbiamo, infatti, scoperto che, oltre ad essere regolato negativamente dall'OT a livello trascrizionale, il miR21 attenua il segnale dell'OT aumentando i livelli di D3. La capacità di miR21 di regolare positivamente D3 è mediata da GRHL3, un gene soppressore del tumore nonché un inibitore trascrizionale

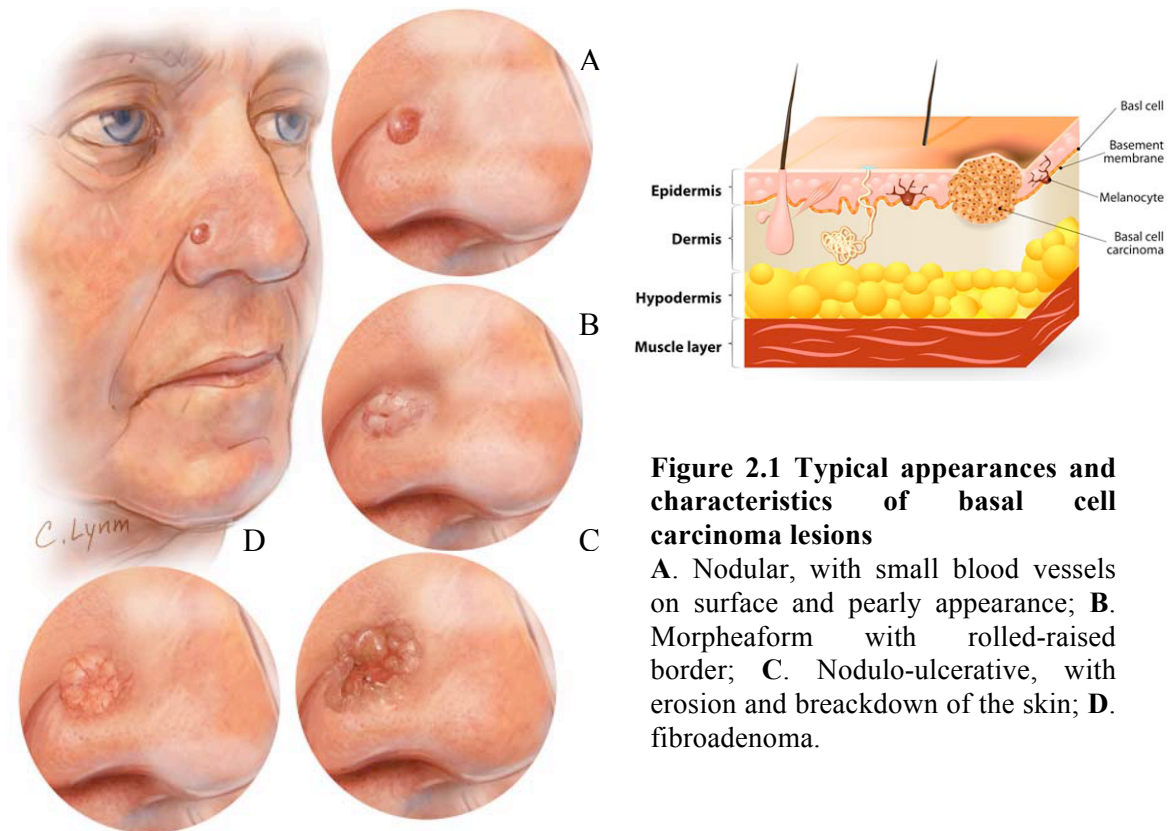
di D3, fino a ad oggi sconosciuto. Inoltre, abbiamo dimostrato che, la deplezione di D3 specificatamente in cheratinociti, riduce significativamente la crescita tumorale in un modello murino di basalioma, sottolineando l'importanza funzionale di questa rete in vivo. Un secondo scopo di questo lavoro è stato indagare gli effetti dell'OT e della D3 nella regolazione delle CSCs della pelle. I nostri dati hanno dimostrato che l'OT reprime la trascrizione del gene Sox9 coinvolto nella staminalità delle cellule epiteliali. Inoltre, la deplezione di D3 provoca una variazione del numero di cellule CD34⁺ dimostrando che il metabolismo dell'OT è importante per il controllo della crescita tumorale e il mantenimento delle cellule staminali cancerose. Chiarire il ruolo funzionale dell'OT durante la tumorigenesi è di cruciale importanza per l'uso della regolazione ormonale come un nuovo strumento in contesti terapeutici.

2 Introduction

2.1 Basal cell carcinoma and Shh signaling

Basal cell carcinoma (BCC) is the most common cutaneous cancer of epithelial origin and account for approximately 80% of all non-melanoma skin cancer. One of principal etiological factors in the development of BCC is the exposure to the ultraviolet (UV) fraction of sun light (1). Areas of body that are exposed to sun are more prone to develop BCC; in fact about 90% are located in the head and neck region, with a particular predilection for the upper central part of the face. However, there are additional etiological factors, which play a role in the development of BCC as injury to the skin by X-ray, chronic inflammation, congenital malformations and genetic alterations such as point mutations in the Ras-oncogene (2). BCC is most common in Causasian population and rarely affects black- and other dark skinned population. The clinical forms of BCC are extremely variable: nodulo-ulcerative, superficial, morpheaform, pigmented, fibroadenoma. (3). The nodulo-ulcerative lesions are the most common type, accounting for 75% of cases of BCC. The typical clinical appearance is a well-circumscribed nodule or plaque with pearly border and overlying telangiectasia and may be combined with rodent ulcer. Superficial BCC represents about 10% of BCC. The clinical presentation is discrete erythematous macules or plaques with scaly change and a thin rolled border (3). BCC tends to share the common histopathologic features of a predominant basal cell type, peripheral palisading of lesional cell nuclei, and a mucinous stroma with artificial cleft between the epithelial island and the stroma. In addition, there are variable degrees of cytologic atypia and mitotic activity.

The incidence of BCC is 30% higher in man than in women and the age is further most important factor influencing incidence. Person aged higher then 55 years have a 100-fold hiegher incidence of BCC than persons of age below 20 years. BCC usually does not metastasize. In fact, rate of metastasis in BCC have been estimated as 0,1%, (4) however this malignancy can be very aggressive due to a highly infiltrate and invasive growth pattern by direct extension into adjacent tissue, leading to a severe destruction of affected skin. Especially in the case of facial BCC, the growth characteristic can be highly disfiguring and is therefore associated with severe morbidity (Fig. 2.1).



The origin of the cells which forms BCC is not yet entirely defined but the aberrant Hedgehog (Hh) pathway is a pivotal defect implicated in BCC formation. (5-7). In a silent Hedgehog pathway, where the Hh peptide is absent, the transmembrane receptor Patched-1 (Ptch1) is exerting an inhibitory action on another transmembrane protein Smoothed (Smo) that is a key activator of the Gli pathway. In this situation, the Gli proteins are retained to the cytoplasm. In the opposite situation, when the Hh signal peptide is present and binds to and inactivates Ptch1 (or when Ptch1 inactivation is due to a loss of function mutation), Smo is no longer controlled by Ptch1 thereby activating Gli factors that translocate to the nucleus and induce transcription of Hh target genes (Fig. 2.2) (8). Uncontrolled activation of this pathway results in such cancers, as brain, muscle, skin and gastro-intestinal tract cancers. In particular, aberrant Hh pathway signaling has been detected in patients with nevoid BCC syndrome as well as in over 95% of patients with sporadic BCCs. The Hh signaling has been shown to play a critical role not only in embryonic development, but also in other normal processes, such as

regulation of stem cells and maintenance of tissue homeostasis (9). The initial association between the Hh pathway and human cancers was made as a result of the discovery that loss-of-function mutations in human *Ptch1* are associated with Gorlin syndrome, a rare and hereditary disorder. Patients with Gorlin syndrome show a broad spectrum of developmental defects and have a predisposition to develop basal cell carcinoma (BCC) and medulloblastoma (10). It was found that sporadic BCCs also have a high frequency of loss-of-function mutations in *Ptch1* and, to a lesser extent, activating mutations in *SMO*. Notably, the downstream effectors of the Hh pathway (Gli1/2/3) are rarely found to be mutated in sporadic BCCs. Inactivating mutations in *Ptch1* occur in about 70%–80% of BCCs, and they mostly produce a truncated protein or are frameshift or missense mutations (11, 12). In another fraction of BCCs, activation of Hh signaling results from gain-of-function mutations in *SMO* (about 6%–21%). Based on these informations, in the last few years, several mouse models using tissue-specific activation of the Hh pathway have provided a powerful tool to investigate the mechanisms of Hh-mediated development of BCC and to identify the BCC cell of origin. All current BCC mouse models target different components of Hh signaling, from the Shh ligand, to the transmembrane proteins Ptch1 and Smo, and the Gli transcription factors. Because homozygous *Ptch1* knockdown leads to embryonic lethality due to heart and neural tube closure defects, skin-specific knockout of *Ptch1* has been generated, under the promoter of keratin 14 (K14CRE), keratin 5 (K5CRE), or keratin 6a (K6aCRE). In addition to Ptch1 inactivation, skin-specific knockin SmoM2 mice (K14CRE-ER/Rosa26-SmoM2) develop multiple BCCs (13, 14). Furthermore, overexpression of *Gli2* in mouse skin leads to development of BCC (15). In this context it is important to note that tumors developing in the mouse may not always fully mimic human BCCs but represent various stages in a spectrum of benign to malignant Hh pathway– induced BCC-like tumors, likely reflecting a similar variation in humans, where benign hamartomas and BCCs appear to be driven by different levels of Hh pathway activation (16).

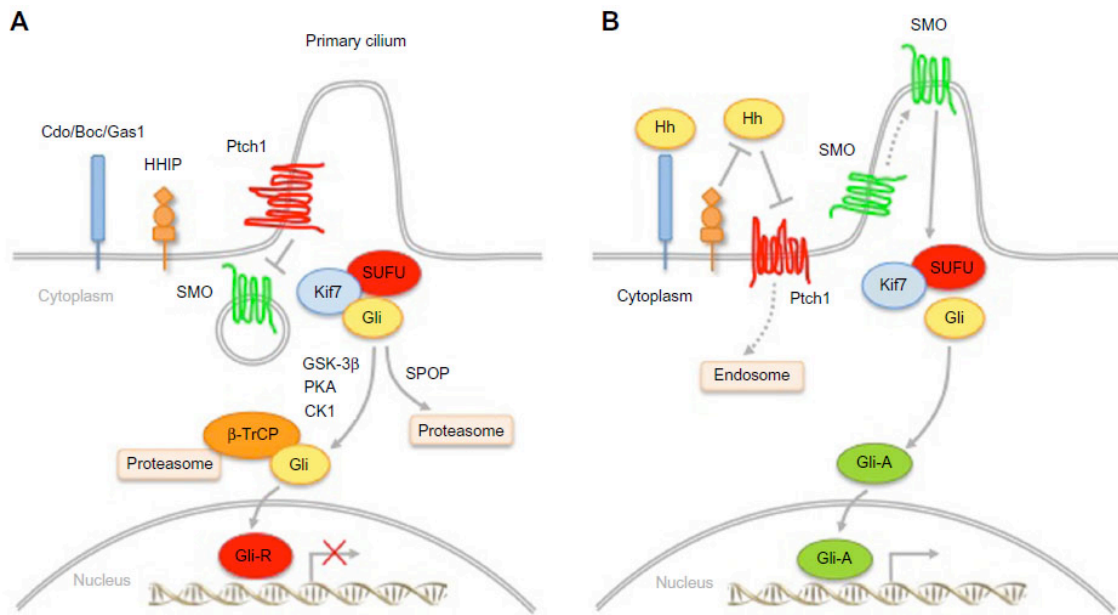


Figure 2.2 Schematic representation of Hedgehog signaling pathway

A. In the absence of Hh ligand, the Gli transcription factors are bound to a multiprotein complex with the negative regulator Sufu. Phosphorylation of Gli by PKA, GSK3 β and CK1 targets Gli proteins to proteasome; **B.** Upon binding of Hh ligand to its receptor Ptch, Ptch loses its ability to inhibit Smo, which moves into the cytoplasm, thus stimulating the pathway and preventing Gli cleavage. The activated forms of Gli bind to Gli-promoters in the nucleus and stimulate transcription of target genes (Silvia Pandolfi and Barbara Stecca 2015).

2.2 Mechanism of thyroid hormone action and deiodinases

Thyroid hormone (TH) is a pleiotropic agent that controls the development and homeostasis of several organs in vertebrates. It is produced for ~ 90% by the thyroid gland in the form of the biologically inactive precursor thyroxine (T₄) and its action is initiated by the activation of T₄ into T₃, catalyzed by two seleno-proteins, the type 1 or type 2 iodothyronine deiodinase (D1 or D2). Both, T₄ and T₃ undergo inner ring deiodination, catalyzed by another seleno-protein, type 3 deiodinase (D3), generating inactive metabolites that do not interact with T₃ receptors, reverse triiodothyronine (rT₃) and 3,3'-diiodothyronine (T₂), respectively (17). Therefore, depending on whether the deiodination occurs on the inner (IDR) or outer ring (ODR) of the iodothyronine substrate, the deiodination results in activating pathway or inactivating pathway. In fact, while ~ 20% of T₃ is secreted by the thyroid, most of T₃ is derived

from outer ring deiodination of T4 in peripheral tissue where the actions of these three deiodinases, together with the uptake of T3 and T4 into the cell by several specific transporters (organic anion transporter 2 and 3, Oatp2 and Oatp3, and monocarboxylate transporter 8 and 10, MCT8 and MCT10) (18), determine the levels of T3 availability and constitute a potent mechanism of pre-receptor control of TH action at cellular level, regardless of the constant plasma T3 levels (Fig. 2.3). Therefore, access to the intracellular compartment is mediated by four different families of transport proteins that have been shown to be involved in the traffic of iodothyronines across the plasma membrane, with different patterns of tissue expression (19). The monocarboxylate 8 (MCT8) is probably the most relevant transporter as mutations in the MCT8 protein have been associated with variable levels of mental retardation in humans combined with lack of speech development, muscle hypotonia and endocrine dysfunctions (19, 20). Once the active hormone T3 is present inside the cells, it can enter the nucleus and reach the TRs, a family of ligand-dependent transcription factors that enhance or inhibit the expression of target genes by binding to specific DNA sequences, known as TH response elements (TREs). Thyroid hormone receptors exist in two isoforms, TR α and TR β , which are encoded by the THRA and THRB genes, respectively (21). As already mentioned, the modern paradigm of thyroid hormone action recognizes that D2 and D3 play antagonistic roles in a number of settings, with D2 increasing thyroid hormone signaling and D3, silencing it, independently of plasma T4 or T3. Thus, at any given moment, thyroid hormone signaling in different tissues and cells can be amplified or dampened, according to the local expression of deiodinases (17). The cloning of all three deiodinases identified the presence of the rare amino acid selenocysteine (Sec) located in the catalytic site (22). Like with the other selenoproteins, deiodinases undergo a unique synthetic mechanism that involves reprogramming of the stop codon, UGA, to a Sec amino acid (23). This takes place with a coordinated effort between the ribosomal machinery and an evolutionary conserved stem loop-shaped RNA element that is found at the 3'UTR of all mammalian selenocysteine proteins (23). This element is called the selenocysteine insertion sequence (SECIS) and functions as a binding site of several accessory proteins that recruit a Sec-charged tRNA and mediates the anti-termination at the UGA codon. This allows the incorporation of a Sec molecule into the selenoprotein growing polypeptide chain. All three deiodinases are integral membrane

proteins of 29-33kDa that share an overall 50 % sequence similarity (24) and are homodimers whose dimerization is required for full catalytic activity (25, 26). The subcellular localization varies among the three enzymes, and this affects their systemic versus cellular contributions to TH homeostasis (27). D1 is the only selenodeiodinase that can function as either an outer- (5') or an inner (5)-ring iodothyronine deiodinase mainly in the liver, kidney and thyroid and was the first to be cloned (23, 28). For its tissue-specific expression, D1 contributes to the regulation of systemic T3 levels, by providing a significant portion of the circulating plasma T3 in euthyroid vertebrates. D1 is an enzyme with a low kinetic efficiency, but its ability to dehalogenate iodine metabolites suggests that could also act as a scavenger enzyme that recycle iodine to replenish the thyroid's iodine reservoir (29).

D2 is considered the main T4-activating enzyme, given its high substrate affinity. D2 is a classical type-1 membrane protein, approximately of 31kDa, residing on the endoplasmic reticulum (ER) membrane, with a half-life of ~ 45 minutes (24). Its relatively short half-life is due to ubiquitination and proteasome uptake, a feature that is accelerated by D2 interaction with its natural substrate, T4 (30). D2 is expressed in many brain areas and is considered to play a major role in local T3 production in the brain. D2 is also expressed in pituitary, brown adipose tissue, placenta and in skeletal muscle (17). In contrast to D1, D2 is involved in outer-ring deiodination exclusively. The preferred substrate for D2 is T4 and, although to a lesser extent, rT3. D2 is regulated by thyroid hormones both pre- and post-transcriptionally as T3 downregulates D2 mRNA expression (31), while T4 as well as rT3 (the substrates of D2) increase D2 ubiquitination and subsequently proteasomal degradation, resulting in decreased D2 activity. D2 is required for normal mouse skeletal muscle differentiation of muscle stem cells (satellite cells) and regeneration (32).

Deiodinase type 3 (D3) is viewed as the thyroid hormone inactivating enzyme, as it can only catalyze the inner-ring deiodination of T4 and T3. Like D1, D3 is present in the plasma membrane. The *Dio3* gene is localized in the imprinted *Dlk-Dio3* region of human chromosome 14 and mouse chromosome 12, and is expressed predominantly by the paternal allele. It comprises a single exon, coding for a protein of 278 residues, with a molecular mass of about 32 kDa, including a selenocysteine-encoding TGA in the catalytic pocket and an SECIS element in the 3'UTR (33).

D3 is highly expressed in placenta and plays an important role during embryonic development protecting protect the fetus from excessive exposure to active thyroid hormone. D3 is also expressed in the brain and skin but in adult, healthy tissues expression levels are very low (17). Several studies have shown that D3 is expressed in activated leukocytes during bacterial and chemical inflammation (34) and that lacking D3 impairs bacterial clearance capacity during infection (35). D3 induction has also been shown during hypoxia in post-mortem liver biopsies of critically ill patients (36) and during myocardial infarction (37). Recent studies have revealed reactivation of D3 expression in specific pathophysiological contexts correlated with hyperproliferation conditions as cancer.

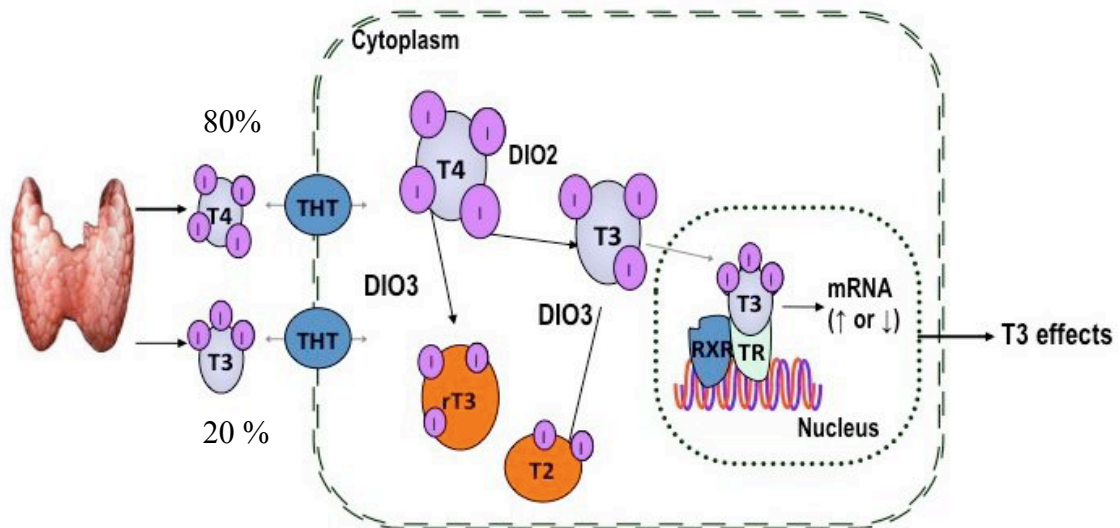


Figure 2.3 Schematic of deiodinase-mediated thyroid hormone metabolism

The thyroid gland produces principally (~ 80%) the biologically inactive precursor of TH, the thyroxine (T4). The TH action is initiated by the activation of T4 into T3, catalyzed by the type 2 iodothyronine deiodinase (D2). Both, T4 and T3 undergo inner ring deiodination, catalyzed by type 3 deiodinase (D3), generating inactive metabolites that do not interact with T3 receptors, reverse triiodothyronine (rT3) and 3,3'-diiodothyronine (T2), respectively.

2.3 Type 3 deiodinase and cancer

Type 3 deiodinase, the main physiologic inactivator of TH, controls TH homeostasis by protecting tissues from an excess of TH. D3 is abundantly present in fetal tissues and in the human placenta, where it blocks the excessive maternal-to-fetal transfer to T4 (38). In contrast, during late neonatal and adult life, D3 expression is more limited and identified in only few postnatal tissues i.e. brain, skin and placenta (39). However, several studies have revealed the re-expression of D3 in different pathophysiological conditions, among which cardiac hypertrophy, chronic inflammation and ischemia (17) (37). Moreover, this oncofetal protein results reactivated in the adult in highly-proliferating and neoplastic cells. This finding suggests a link between deiodinase-mediated TH metabolism and carcinogenesis. Indeed, D3-mediated local hypothyroidism promotes cellular proliferation by regulating the nuclear T3 availability. It has been reported that immortalized cell lines derived from different tumors such as basal-cell carcinoma (BCC), hemangiomas, hepatocarcinomas, breast cancer (MCF-7 cells), colon adenocarcinoma (Caco2, SW280, and HCT116 cells), thyroid cancer, endometrium cancer (ECC-1 cells), and neuroblastoma (SH-SY5Y cells) express elevated D3 levels (40-42). D3 overexpression has been further verified in many human cancer tissues. Vascular tumors (hepatic hemangiomas) show high D3 activity resulting in an accelerated rate of THs degradation leading to a clinically relevant hypothyroidism named “consumptive hypothyroidism” (43, 44). In benign adenomas and in colon carcinomas, D3 expression is significantly higher than in normal tissues but negatively correlated with the histologic grade of the lesions suggesting that D3 could be a marker of the early stages of tumorigenesis. As already mentioned, an abnormal activation of Hedgehog pathway is implicated in the development of different types of cancer. There are several evidences that D3 is under the control of the Shh–Gli pathway. The activation of this pathway results in D3 overexpression in mouse and human BCC (45). By directly inducing D3 in keratinocytes, through Gli2, Shh causes a hypothyroid state at intracellular level resulting in increased cyclin D1 and higher proliferative rate. Shh-induced thyroid hormone degradation via D3 synergizes with the Shh-mediated reduction of the type 2 deiodinase, the thyroxine activating enzyme, and both effects are reversed by cAMP (45). Therefore, it has been shown that D3 expression in BCC cells determines a proliferative advantage for the tumor and that,

conversely, D3 depletion interferes with tumorigenesis, enhancing the apoptotic process. By promoting Gli degradation, through protein kinase A induction, which in turn destabilizes Gli2 protein via its C-terminal degron, T3 blocks its transcriptional activity. Moreover, T3 treatment or D3 depletion reduce tumor growth in a genetically modified mouse model of skin tumorigenesis. By this mechanism, Shh induces TH signaling attenuation contributing to epidermal tumorigenesis *in vivo* by favoring cell proliferation and bypassing T3-induced growth arrest and cell differentiation. Also aberrant activation of the Wnt/ β -catenin signaling pathway causes developmental defects and tumorigenesis. In particular, in colorectal cancers canonical Wnt signaling is aberrantly activated by mutations affecting either APC tumor suppressor gene (85%) or β -catenin-encoding *CTNNb1* oncogene (10%). It has been recently shown that Wnt/ β -catenin pathway directly affects TH signaling by a dual convergent mechanism, which modulates the activity of the deiodinase enzymes in colon cancer cells (42). Specifically, the TH activating D2 enzyme is down regulated by β -catenin while D3 is over-expressed by β -catenin/TCF complex. When D3 is absent, excess of T3 attenuates cell proliferation and promoted differentiation in both cultured cells and in xenograft mouse models. This is due to induction of E-cadherin, which sequestered β -catenin at the plasma membrane and promoted cell differentiation (42). Similarly to colon cancer, it should be postulated that deregulated Wnt pathway could induce D3 expression in other tumors.

2.4 MicroRNA and cancer : focus on miR-21

MicroRNAs are an abundant subclass of non-coding RNAs of 18-25 nucleotides which act as endogenous regulators silencing gene expression through a process of post-transcriptional modification. They exhibit varied and widespread functions during normal development and tissue homeostasis (46). MicroRNAs can be located in either introns and exons and are found in both coding and non-coding transcriptional units (47). Wherever their origin, they are transcribed by RNA polymerase II in the nucleus, generating “pri-miRNA,” a partially self-complementary oligonucleotide strand comprised of a core dsRNA stem-loop region flanked by two single-stranded tails. This precursor is subsequently cleaved by the RNase III enzyme (also called Drosha) into “pre-miRNAs,” a shorter (~70 nucleotides in length) hairpin-shaped dsRNA. This transient precursor exits the nucleus after interacting with Exportin-5, which facilitates its transport into the cytosol. Here, it is further processed by Dicer, an endoribonuclease which severs the loop from the stem, forming a mature (but still double stranded) miRNA duplex. To exert its effect, a mature miRNA depends on the assembly of ribonucleoprotein complexes, referred to as the RNA-Induced Silencing Complexes (RISCs). The RISC facilitates the dissociation of passenger and guide (targeting) strands, allowing the guide strand to inhibit translation by hybridizing to a target mRNA 3'-UTR via partially complementary base pairing. The degree of complementarity appears to be an important predictor of the resulting fate of the mRNA target, as the RISC may instigate either degradation of the mRNA target (if match is highly complementary) or merely blockade translation (if the match is less highly complementary) (46).

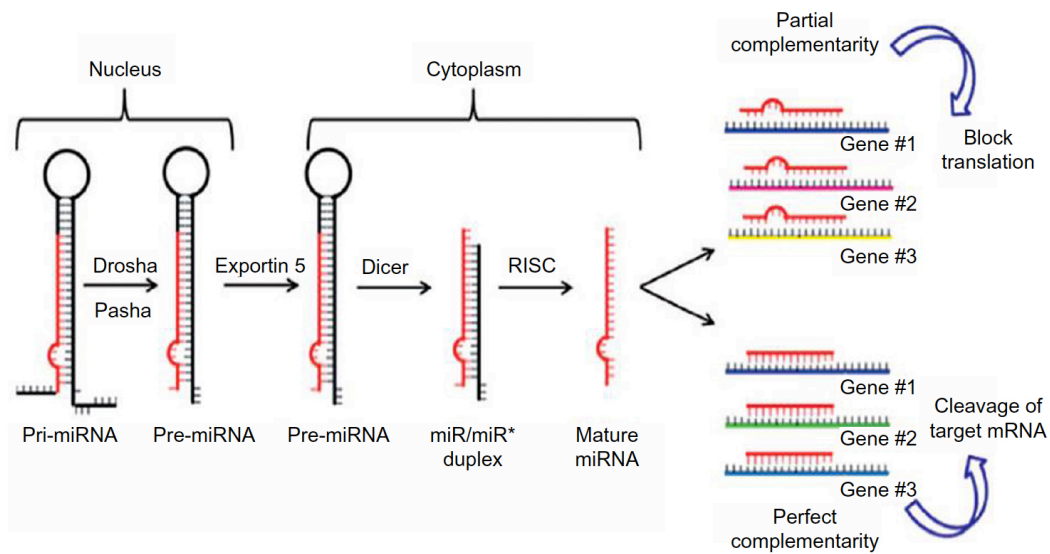


Figure 2.4 Biogenesis and action of miRNAs

miRNAs are transcribed in the nucleus by RNA polymerase II generating a primary miRNA (pri-miRNA) molecule, which is processed into a precursor miRNA (pre-miRNA) by the microprocessor complex comprised of Pasha and Drosha. Pre-miRNAs are exported to the cytoplasm by Exportin 5 where are cleaved to create a microRNA duplex by Dicer enzyme. The duplex unwinds and the mature miRNA assembles into RISC. The miRNA base-pairs with target mRNA to direct gene silencing *via* mRNA cleavage or translation repression based on the level of complementarity between the miRNA and the mRNA target (Athina Markou 2016).

Inspiringly, a recent study showed that a single miRNA may repress more than 100 mRNAs on average and over 60% of human protein-coding genes are conserved targets of miRNAs (48). Given this vast majority of mRNA targets regulated by miRNAs, aberrant miRNA expression profoundly influences a wide variety of cell regulation pathways. Accordingly, miRNAs influence numerous cancer-relevant processes such as proliferation, cell cycle control, apoptosis, differentiation, migration and metabolism (49). In particular, during the past several years it has become clear that alterations in the expression of microRNA genes contribute to the pathogenesis of most, perhaps all, human malignancies. These alterations can be caused by a variety of mechanisms, including deletions, amplifications or mutations involving microRNA loci, by epigenetic silencing or by deregulations of transcription factors targeting specific microRNAs. In the context of cancer biology, miRNAs are often placed within a simple classification scheme as either an oncogenic miRNA (frequently abbreviated as

“oncomir”) or as a tumor suppressor miRNA. Deregulation of miRNAs can result in either increased or decreased expression depending on the scenario. In this way, both reduced and enhanced miRNA expression can promote tumorigenesis if the miRNAs subject to such events are tumor suppressors and oncomirs respectively. Among all cancer-related miRNAs, miR21 has been related to the pathogenesis of various malignant tumors, including glioblastoma, prostate, gastric, colon, breast and lung cancer (50-53). Its up-regulation has been shown to be self-sufficient in promoting proliferation and can evade apoptosis by targeting several tumor suppressors like PTEN and PDCD4 (54, 55). Furthermore, transgenic overexpression of miR21 results in B cell lymphoma demonstrating that miR21 is an “oncomiR”. In fact, when miR21 was inactivated, the tumors regressed completely in a few days. It has been shown that miR-21 is transcriptionally activated by Stat3 (signal transducer and activator of transcription 3) in the IL-6 signaling pathway (56). miR-21 exerts an anti-apoptotic function in k-Ras-dependent lung tumors by inhibiting expression of Apaf-1, an important component of the intrinsic mitochondrial apoptotic pathway, and decreases protein levels of Fas ligand, a key initiator of the extrinsic apoptotic pathway. The function of miR-21 was further confirmed by the observation that ectopic expression of miR-21 protected cancer cells from gemcitabine-induced apoptosis. miR-21’s role is well characterized in invasion and metastasis. In fact, miR-21 promotes cell motility and invasion by directly targeting PTEN, a tumor suppressor known to inhibit cell invasion by blocking the expression of several MMPs (matrix metalloprotease) (57) (Fig. 2.5).

Apart from being involved in cancerogenesis, miR21 plays a crucial role in a plethora of biological functions and diseases, namely development, cardiovascular diseases and inflammation (58) miR21 is also expressed in skin, and its potential role as a regulator of skin homeostasis is demonstrated by its up-regulation in such diseases as psoriasis, atopic dermatitis, melanoma and squamous cell carcinoma (SCC) (59-61). However, nothing is known about miR21 expression in BCC.

Among the few known targets of miR21 is grainyhead-like3 (GRHL3), a transcription factor expressed in the skin in the differentiated suprabasal layers and essential for epidermal differentiation and barrier formation at the end of mouse embryogenesis by regulating multiple genes important for executing the differentiation program in skin (62, 64). These genes encode for structural proteins, lipid metabolizing enzymes and

cell-cell adhesion molecules. GRHL3 knock-out mice exhibit impaired epidermal differentiation and decreased expression of several genes involved in barrier formation (64). Furthermore, it was shown that epidermal-specific GRHL3 knockout mice exhibit thickened, hyperproliferative epidermis, as well as accelerated tumor formation and increased tumor and carcinoma numbers than the wild-type controls. These mice show also increased Akt activation and reduced PTEN levels. Accordingly, in humans, dominant-negative GRHL3 mutations are associated with defective periderm development in Van der Woude syndrome (65). Moreover, GRHL3 was found to be a potent tumor suppressor in mouse and human SCC, and an upstream regulator of PTEN (62). In particular, it was identified a miR-21 proto-oncogenic network that simultaneously targets GRHL3 and PTEN leading to amplification of PI3K/AKT/mTOR signaling, cell hyperproliferation and induction of SCC (62).

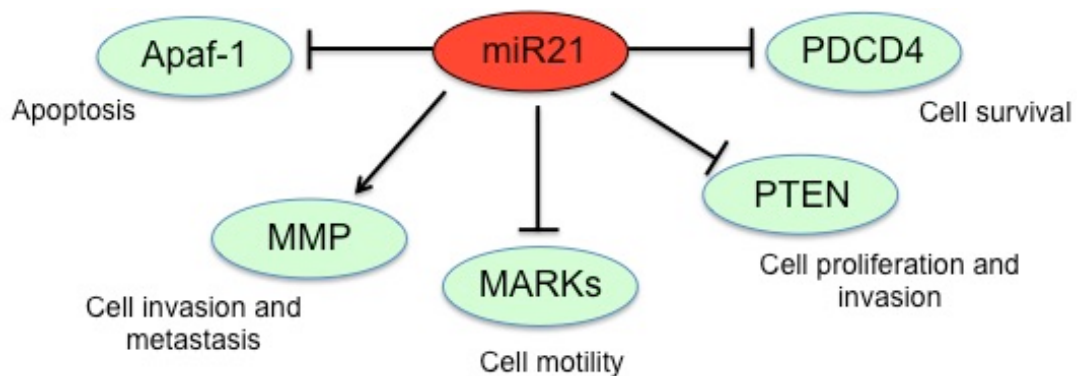


Figure 2.5 miR21 targets

miR21 can influence positively and negatively several biological processes, from block of apoptosis to promotion of cell proliferation, mobility and invasion through its effect on a number of targets (PDCD4, programmed cell death protein 4; PTEN, phosphatase and tensin homolog; MARKs, microtubule-affinity-regulating kinases; MMP, matrix metalloproteinase; Apaf-1, apoptotic protease activating factor-1)

2.5 Stem cells in skin cancer

Skin is a complex tissue made of a structured combination of cell types. It has a remarkable regenerative capacity and contains several different kinds of stem cells (SCs). As in many adult tissues, also in the skin, stem cells (SCs) are responsible for tissue homeostasis and regeneration. Upon division, SCs can give rise to transit-amplifying (TA) cell populations which, after several rounds of divisions, will terminally differentiate and eventually be lost from the tissue. In addition, adult SCs are activated following injuries, rapidly expand, and contribute actively to tissue repair (66). There is no unique marker of tissue-specific SCs, and SCs are usually defined by their functional properties, namely by their capacity for long-term self-renewal and their capacity to differentiate into one or multiple cell lineages (67). Epithelial skin stem cells (ESSCs) are thought to reside in a specialized area of the hair follicle called “the bulge”. Cells in this compartment possess the ability to differentiate, at least under stress conditions, into different cell lineages to regenerate not only the hair follicle but also the sebaceous gland (SG) and the epidermis. However, more recent studies presented compelling evidence for the existence of independent IFE (interfollicular epidermis) stem cells, as well as for isthmus stem cells, sebaceous gland (SG) stem cells and other epidermal progenitors (68, 69). Lineage-tracing experiments reveal that during homeostasis, the different compartments of the epidermis are self-sustained by their own resident stem cells. Hair follicle bulge stem cells expressing the typical markers keratin 15 (K15), CD34 and Lgr5 (leucine-rich repeat-containing G-protein-coupled receptor 5) mediate hair follicle regeneration; Lgr6⁺ isthmus stem cells mediate turnover of the sebaceous gland cells and possibly of other epidermal lineages; and IFE stem and progenitor cells expressing keratin 14 (K14) sustain IFE homeostasis and maintenance of the skin barrier. Although under physiological conditions bulge stem cells do not contribute to the maintenance of the IFE, almost all stem cell populations of the epidermis, including the hair follicle bulge, Lgr6⁺ isthmus and IFE stem cells, can contribute to healing of the IFE after wounding (70- 73) (Fig. 2.6).

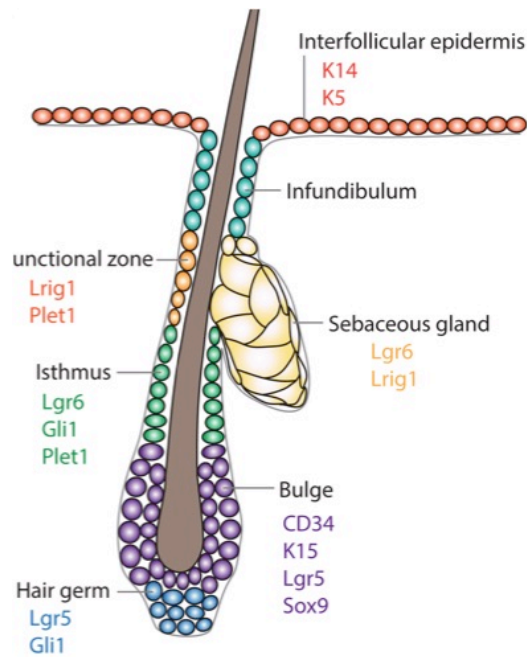


Figure 2.6 Skin stem cells localization and markers

The hair follicle structure is subdivided into distinct compartments. In each compartment exist basal cell populations that possess stem cell properties and are defined by distinct molecular markers.

Unlike epidermal keratinocytes, which are committed to undergo terminal differentiation, skin stem cells have a long life span and this result in an ability to accumulate multiple genetic mutations that are necessary to induce cancer formation (74). When stem cells possess the ability to originate tumors they are called cancer stem cells (CSCs) (75). These tumor-initiating cells (TICs), are defined as a subpopulation of cancer cells with self-renewing capacity that possess high tumorigenic potential and can undergo multilineage differentiation to give rise to all types of cells present within the malignancies (76). In particular, different models have been proposed to explain tumor growth and heterogeneity. In the stochastic model of tumor growth, all cancer cells have the same intrinsic properties to contribute to tumors growth and choose between self-renewal and differentiation in a stochastic manner (77, 78). In contrast, in the cancer stem cell (CSC) model, tumors are hierarchally organized, with only some tumor cells, called CSCs, presenting greater renewing potential that sustain long-term tumor growth

(77, 78). Many recent studies using prospective isolation of a fraction of tumor cells followed by their transplantation into immunodeficient mice have demonstrated that certain populations of tumor cells contain cells with higher probability to reform secondary tumor upon transplantation, supporting the existence of CSC (77, 79). According to the CSC model, CSCs drive tumor growth and these cells are considered to be a cause of tumor relapse and disease progression, perhaps through their resistance to therapy and metastatic potential. Therefore, CSCs are currently extensively studied in various cancers.

The field of CSC research truly started about 20 years ago when Dick and colleagues (80) published their pioneer studies demonstrating that only minor subpopulation of acute myeloid leukemia cells with CD34⁺/CD38⁻ phenotype presents the potential to initiate leukemia in the immunodeficient mice (80). Since then, large body of evidence has been published that supports the essential role of CSCs in initiation and progression of several hematological malignancies and of a wide range of solid tumors (81). In fact, many other groups have now demonstrated that in solid tumors only a fraction of cancer cells present the capacity to reform secondary tumors following their transplantation into immunodeficient mice (82). In particular, different solid tumors, including pancreatic cancer (83), squamous cell carcinomas (SCCs) (84), colon cancer (85), and melanoma (86), have been shown to contain subpopulations of tumor cells with greater ability to propagate the tumors in xenotransplantation assays.

Recently, it was demonstrated that CD34-expressing tumor propagating cells (TPCs) with increased clonogenic potential and the ability to form secondary tumors upon transplantation into immune deficient mice have been isolated from DMBA/TPA-induced skin SCC (87). However, it was later shown that both CD34^{HI} and CD34^{LO} tumor epithelial cell (TECs) populations from DMBA/TPA-induced skin SCC cultured in vitro 4 days before their transplantation present similar ability to reform secondary tumor upon transplantation into immune deficient mice (88). These two conflicting studies raise questions to whether CD34 expression can be used as marker to enrich for TPCs in skin SCCs. This matter was clarified using transplantation of limiting dilution of different populations of FACS-isolated tumour cells from four distinct mouse models of squamous skin tumours in order to investigate the frequency of tumour propagating cells (TPCs) at different stages of tumour progression. It was found that benign

papillomas, despite growing rapidly in vivo and being clonogenic in vitro, reformed secondary tumours upon transplantation at very low frequency and only when tumour cells were co-transplanted together with tumour-associated fibroblasts or endothelial cells. In two models of skin squamous cell carcinoma (SCC), TPCs increased with tumour invasiveness. Interestingly, the frequency of TPCs increased in CD34HI but not in CD34LO SCC cells with serial transplantations, while the two populations initially gave rise to secondary tumors with the same frequency (89).

In this contest, several studies are coming out in order to establish the cells of origin from BCC and the possibility to use CD34 not only to isolate TPCs from SCC but also from BCC. However, in this regard no information are available yet, but the cellular origin of BCC has been debated for a long time. BCC was originally thought to derive from hair follicle stem cells due to its histological and biochemical similarities to hair follicles (90). However, recently studies demonstrated that BCCs can arise from the bulge, sebaceous glands, and IFE after Gli2 induction, and interestingly, different subtypes of BCCs (superficial versus nodular) developed depending on which compartments were being targeted for induction (91). Prior to this observation, recent studies using Cre-mediated cell-specific targeting both by lineage tracing and specific activation of Hh signaling in distinct skin cell populations gave unexpected results. Using clonal analysis of oncogene-targeted cells, Youssef and colleagues showed that more than 90% of SmoM2-induced BCCs arise from long-lived progenitors residing in the IFE, the rest arising from the upper infundibulum (92). Bulge SCs generate hyperplastic or dysplastic lesions upon SmoM2 expression, which do not progress into invasive cancer (92). Soon afterwards, Wang et al. presented conflicting data using lineage tracing (K15CrePR transgenic mice) in adult *Ptch1*^{+/-} mice to demonstrate that X-ray induced BCC arise exclusively from the follicular bulge, and that deletion of p53 enhanced BCCs development from both the bulge and IFE in *Ptch1*^{+/-} mice (93). Taken together, these studies suggest that BCC primarily originate from hair follicle bulge stem cells but may be derived from other epidermal compartments under certain conditions (94).

In a new study, using a genetic mouse model of BCC, some researchers report that Sox9, directly controls skin cancer formation by regulating the expansion of tumor initiating cells and the invasive properties of cancer cells. In fact, while Sox9 is not

expressed in the normal skin cells, Sox9 begins to be expressed in pre-cancerous lesions and is maintained in invasive tumors. Deletion of Sox9 prevents skin cancer formation demonstrating the essential role of Sox9 during tumorigenesis and leads to the progressive disappearance of the oncogene expressing cells. Moreover, Sox9 controls the long term maintenance and expansion of oncogene expressing cells by promoting self-renewing division and inhibiting differentiation. The authors uncover the cellular and molecular mechanisms, as well as the gene network regulated by Sox9 during the early steps of skin tumor initiation and demonstrate that Sox9 controls the long term maintenance and expansion of oncogene expressing cells by promoting self-renewing division and inhibiting differentiation. In addition, Sox9 acts also as key orchestrator of the extracellular matrix remodeling, cell adhesion and cytoskeleton dynamics required for tumor invasion. These results have important implications for the development of novel strategies to block tumor formation and invasion in the most frequent cancer in humans (95). Although considered as a stem cell marker, no studies so far have directly investigated its regulation by TH.

It was recently introduced the concept that TH might modulate the behavior of CSCs. In particular, in the colon cancer stem cells TH influences stemness through its action on Wnt and BMP pathways. In fact, D2 and D3 are differentially expressed in different subpopulations of colon cancer stem cells according to their stem-like versus differentiated shape. Moreover, TH induces the differentiation of colon cancer stem cells and attenuates symmetric cancer cell division. In particular, D3 depletion increases the intracellular availability of TH that induced cell differentiation and sharply mitigated tumor formation. Furthermore, BMP4 is a direct thyroid hormone target and is involved in a positive feedback loop that modulates thyroid hormone signaling (115). However, few are the information about the influence of TH on skin cancer stem cells.

3 Aim of the project

Thyroid Hormone (TH) is a pleotropic agent that has widespread biological functions such as control of cellular growth, development, tissue homeostasis and neoplastic transformation. At tissue level, TH action is regulated by the expression and activity of three selenodeiodinases, which catalyze TH activation (D1 and D2) and catabolism deiodinases (D3). The deiodinase system is often altered in such pathological conditions as cancer. In fact, the type III deiodinase, that normally is absent in adult tissues, results re-activated in various types of human cancers where plays a critical role in the regulation of cell proliferation. Several studies have been demonstrated that D3 is overexpressed also in Basal Cell Carcinoma (BCC), the most frequent skin cancer (45). However, the precise role of TH in the BCC formation and maintenance is still unknown. Because SCs exist and proliferate for extended periods in adult tissue, they present, in theory, a higher chance of accumulating the necessary mutations to induce cancer formation (83). Based on above considerations, **my PhD project aimed to understand how the local control of TH action can affect tumor growth in mouse models of BCC, which molecular mechanisms are involved in this regulation and how the intracellular concentration of TH can influence skin cancer stem cells maintenance.** The functional interplay between TH and oncogenic pathways is likely to have broad implications, not only for the role of TH action in skin, but also for the identification of novel potential therapeutic strategies aimed at interfering with these signalings in other pathological contexts.

4 Results

4.1 TH and microRNA: down-regulation of miR21 TH-dependent in BCC

It was previously showed that TH regulates the proliferative potential of BCC cells in vitro and in vivo. In particular, It was demonstrate the existence of a cross talk between TH and Shh/Gli2, where Shh, through Gli2, directly induces D3 in mouse and human BCCs and, on the contrary, TH mediates Gli2 inactivation (45, 106). There were several reports indicating the involvement of miRNAs in many type of cancer. However, the regulation of these miRNAs has been poorly investigated and still remain largely unknown. TH is a pleotropic agent that has widespread biological functions nevertheless, no studies so far have directly investigated its functional role in regulation of microRNA. To explore whether TH action in BCC involves the regulation of miRNAs, we analyzed the differential expression of mature miRNAs (miChip) in D3-silenced mouse BCC cells. We used a microarray platform of miRNA, the Exiqon platform, to compare the expression of miRNAs in BCC cells transfected with a control scrambled shRNA oligo versus the D3-targeting shRNA oligo. As showed by *vulcano plot* we found 46 miRNAs differentially expressed where the miR21 was the most sensitive target upon D3 depletion (Fig. 4.1 A). We validated miR21 as a negative TH target gene by measuring the mature miR21 transcript by TaqMan reverse transcriptase-PCR (Fig. 4.1 B) and Northern blotting (Fig. 4.1 C and D) of BCC cells treated with 30 nM T3 and in BCC cells transfected with D3-targeting shRNA, in which the TH signal was amplified (45). Moreover, the same analisis was conduced in BCC cells transfected with empty vector (CTR) or D3-overexpressing plasmid and in BCC cells grown in normal serum or in charcoal stripped serum for 48h (Fig. 4.1 E and F). Accordingly, while repressed by TH treatment and D3-depletion, miR21 was up-regulated by D3 overexpression and by TH deprivation in serum.

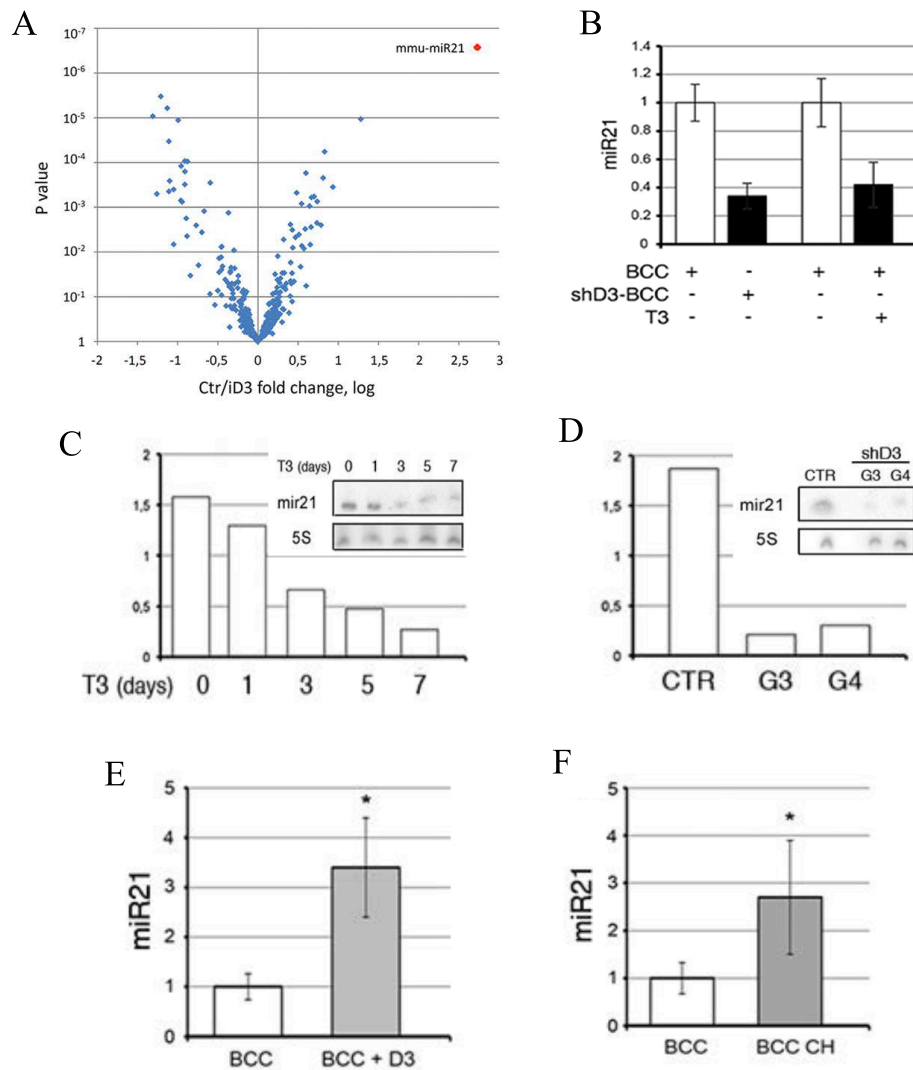


Figure 4.1 Thyroid hormone reduce miR21 expression

A. Genome-wide miRNA expression analysis in D3-depleted and control BCC cells. Selected deregulated miRNAs in shD3 relative to control cells are plotted against the p value; **B.** miR21 expression was measured by Taqman real time PCR in cDNAs from control BCC, shD3 and BCC cellstreated with 30 nM T3 for 48hours; **C-D.** Northern blot of pre-miR21 expression in BCC cells treated with 30nM T3 for the indicated days and in control BCC cells versus D3-depleted clones; quantification of miR21/5S ratio; **E-F.** miR21 expression in BCC cells grown in normal serum or in charcoal stripped serum-containing medium for 48h.

4.2 miR21 is overexpressed in mouse BCC cells and tumors

miR21 overexpression is an hallmark of tumorigenesis and mi21 has been found to be overactive in many tumors. In the skin, miR21 has been demonstrated to have oncogenic potential in squamous cell carcinomas (SCCs) and melanomas (61) but its relevance and expression in BCC has not been explored. Our studies indicate that TH influences miR21 expression in BCC cells. In order to explore the role of miR21 in BCC, we first validate the expression of miR21 in BCCs. Therefore, we analyzed miR21 expression by Taqman real time PCR in mouse BCC cells and tumors, from ear and tail regions, compared with normal skin and keratinocytes, respectively. We observed a robust over-expression of miR21 in both mouse BCC cells and tumors versus the normal counterparts (Fig. 4.2 A and B).

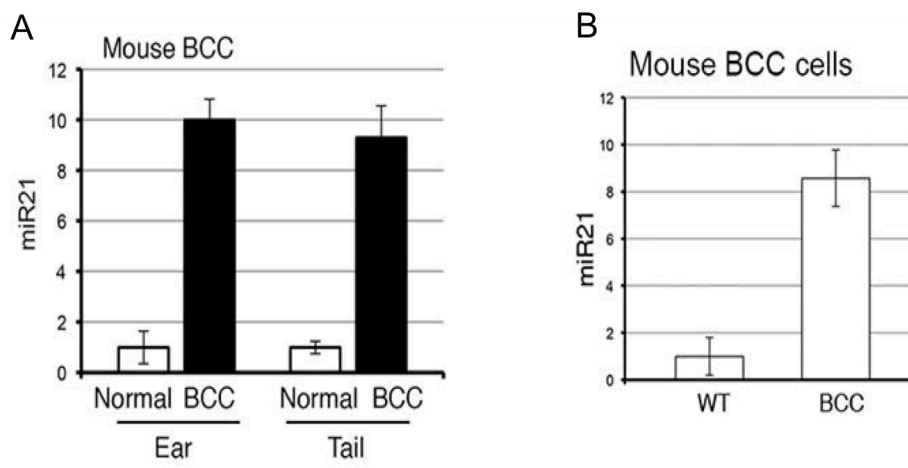


Figure 4.2 miR21 is highly expressed in mouse BCC

A. miR21 was measured by Taqman real time PCR in mouse BCC tumors from ears and tails and the normal skin counterparts; **B.** miR21 was measured by Taqman real time PCR in BCC cells compared to keratinocytes.

4.3 TH regulates miR21 through it's binding a specific gene region

Given that TH down-regulates the miR21 expression we explore the possibility that TH directly inhibits miR21 transcription. To this aim, we analyzed the sequence of the miR21 enhancer region. In silico analysis revealed a conserved thyroid hormone responsive element-binding site (TRE) within the miR21 enhancer region (Fig. 4.3 A). We cloned 389 bp of the enhancer within the pGL3-basic vector to perform functional studies in the human embryonic kidney (HEK) 293 cell line and in mouse BCC cells. As shown in Figures 4.3 B and C, the miR21 enhancer was efficiently down-regulated by TH and by double TR-transfection-TH treatment in both cell lines, thus demonstrating that TH represses the transcription of the pre-miR21. To further demonstrate the interaction between the TH-TR and the TRE present into miR21 enhancer regions, we performed a chromatin immunoprecipitation assay in BCC cells. As expected, chromatin immunoprecipitation analysis revealed that the thyroid receptor (TR) physically binds to the newly identified TRE (Fig. 4.3 D). Together, these results point to a negative regulation of T3 on the miR21 transcription via a direct T3-TR binding to the miR21 enhancer.

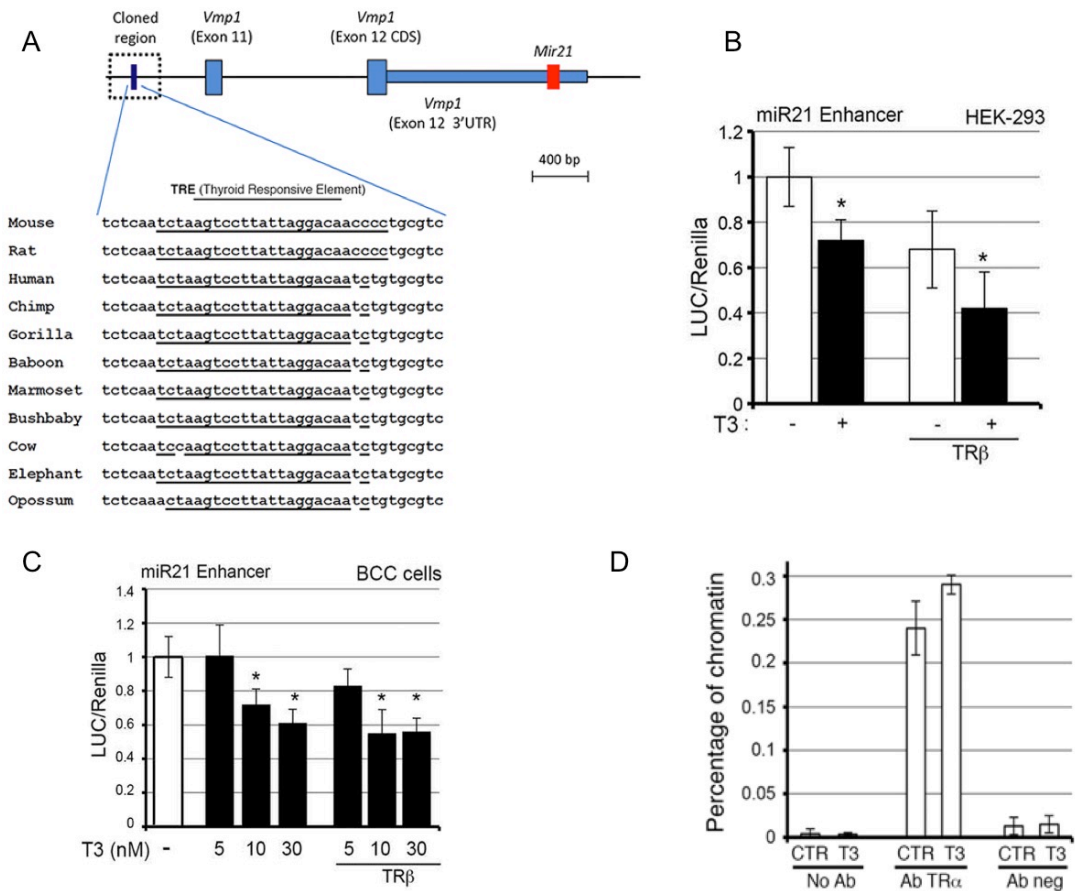


Figure 4.3 TH reduces miR21 by regulating miR21 enhancer region

A. Organization of miR21 gene; **B.** HEK293 cells were transfected with miR21-Enhancer-Luc plasmid +/- TRβ and treated with T3; **C.** BCC cells were transfected with miR21-Enhancer-Luc plasmid +/- TRβ and treated with T3; **D.** ChIP analysis of the interaction between TRα and miR21 enhancer region.

4.4 miR21 positively regulates D3 expression

Next, we asked whether miR21 is able to modulate TH signal in BCC cells. To this aim, we measured the expression of deiodinases D2 and D3 and other TH signaling modulators (TR α and TR β , MCT8 and MCT10) in BCC cells transiently transfected with miR21. While mRNA of D2, thyroid hormone receptors and transporters were not modified by miR21 expression (Fig. 4.4 A), overexpression of miR21 strongly induced D3 levels in a time-dependent manner (Fig 4.4 A and B). In order to further investigate these findings, we inhibited miR21 in BCC cells by transfecting the LNA oligonucleotide complementary to miR-21 (LNA-antimiR-21) or with a control LNA oligonucleotide (LNA-scrambled, CTR). In accordance with its role as an inducer of D3 expression, miR21 inhibition reduced D3 expression levels at mRNA and protein levels (Fig. 4.4 C). Importantly, the overexpression of miR21 also attenuated TH signal as demonstrated by the co-transfection of increasing amounts of miR21 along with an artificial T3-responsive promoter in BCC cells (Fig. 4.4 D).

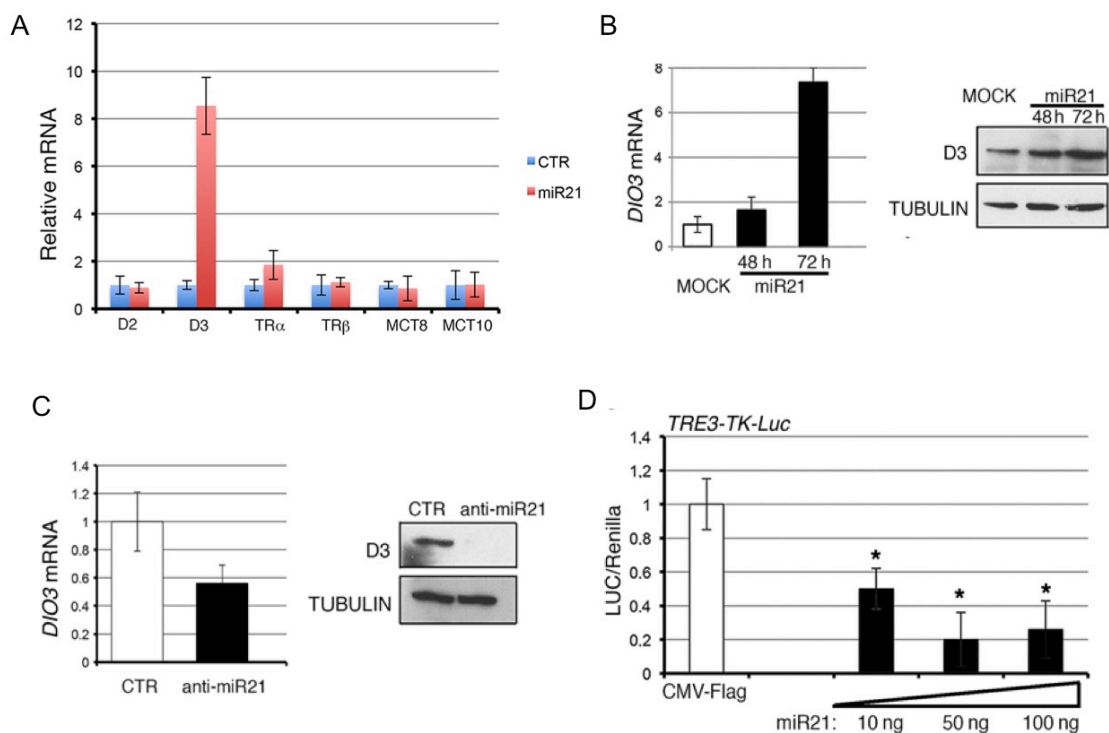


Figure 4.4 miR21 up-regulates D3

A. BCC cell were transfected with miR21 and TH modulators were analyzed by real time PCR; **B.** real time PCR and western blot for D3 in BCC cells transfected with miR21; **C.** real time PCR and western blot for D3 in BCC cells transfected with anti-miR21; **D.** BCC cells were transfected with artificial T3-responsive promoter TRE3-TK and CMV-renilla as control.

4.5 GRHL3, a described miR21 target, suppresses D3 expression

miRNAs are well known to act inhibiting messenger RNA expression at post-transcriptional level. Since D3 is induced by miR21, we tested the hypothesis that a direct miR21-target, and putative suppressor of D3, might mediate this effect. To this aim, we searched for miR21 downstream targets that could potentially inhibit D3 expression. By using the computational algorithm Target Scan together with published and/or validated miR21 target genes, we obtained a list of genes potentially controlled by miR21. This list was further analyzed with the DAVID program for functional classification (96). By selecting the categories of “Regulation of transcription”, “Epidermal development” and “Tumor suppressor”, we found only a few genes that were present in all these three categories (Fig. 4.5 A). We tested the ability of three different genes belonging to these categories (TP63, KLF5 and GRHL3) to affect D3 expression. We thus transfected $\Delta Np63\alpha$, KLF5 and GRHL3 in BCC cells and we analyzed D3 expression by western blot and real time PCR (Fig. 4.5 B and C). Among these, only one gene repressed D3 expression, namely GRHL3. In fact, GRHL3 overexpression causes a D3 reduction in a time-dependent manner (Fig. 4.5 D).

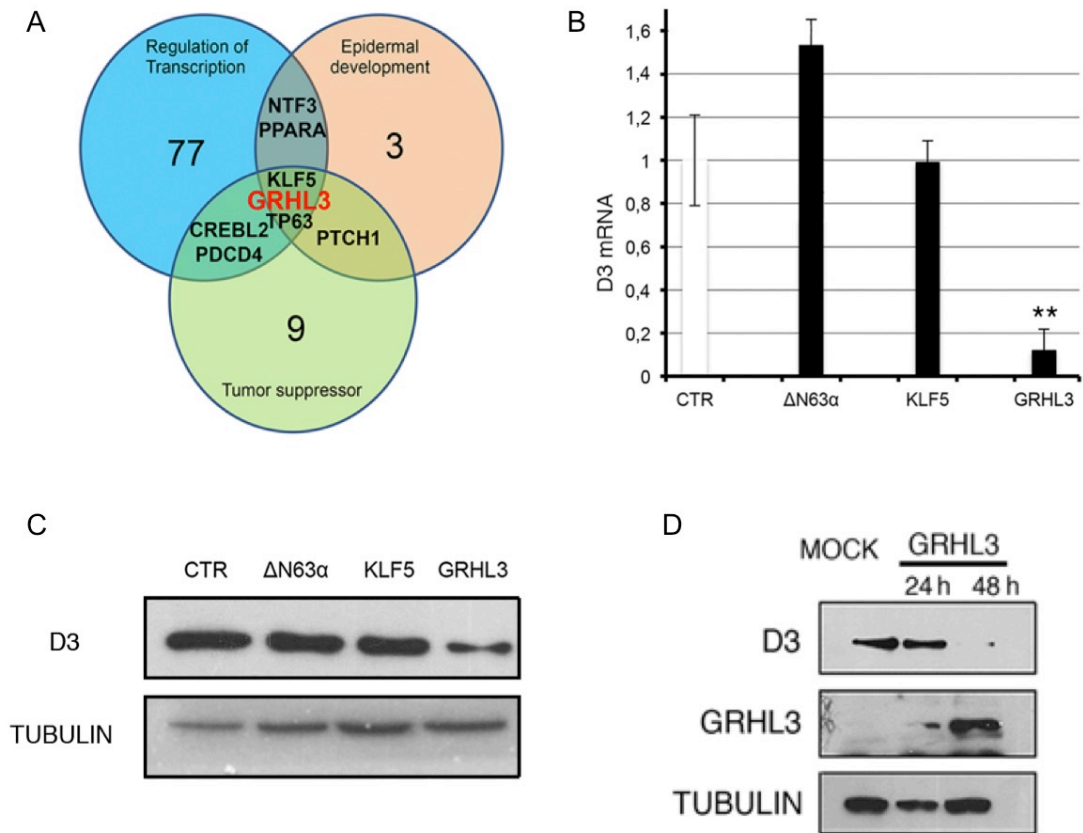


Figure 4.5 miR21 up-regulates D3 by targeting GRHL3

A. miR21 target genes were classified using DAVID program; **B.** real time PCR for D3 in BCC cells transfected with indicated plasmid; **C.** western blot for D3 in BCC cells transfected with indicated plasmid; **D.** BCC cells were transfected with Flag-GRHL3 plasmid and D3 expression was measured by western blot.

GRHL3 is a transcription factor expressed in the skin in the differentiated suprabasal layers and essential for epidermal differentiation and barrier formation. Recently, it was demonstrated to work also as a tumor suppressor in mouse and human SCC (62, 64). We tested whether GRHL3 is a miR21 downstream target in the BCC cells, as already demonstrated in other cell contexts (62). To address this point, BCC cells transfected with miR21 or with anti-miR21 LNA were analyzed for GRHL3 mRNA and protein expression. We found that miR21 overexpression reduced GRHL3, while miR21 silencing increased GRHL3 levels, thus validating GRHL3 as a miR21 target in the BCC cell context (Fig. 4.6 A and B). Importantly, the same effects were observed in primary cultures of keratinocytes in which, thanks to the very low level of endogenous miR21, overexpression of miR21 changed D3 and GRHL3 to a much greater extent than it did in BCC cells (Fig. 4.6 C). To determine whether GRHL3 negatively regulates D3 we knocked-down the endogenous protein using two different siRNA oligos (siGRHL3-1 and siGRHL3-2). As expected, D3 levels were significantly higher in BCC cells transfected with one or more siGRHL3 oligos, than in BCC cells transfected with scrambled oligos (siCTR). This result confirms that GRHL3 is a novel repressor of D3 expression (Fig. 4.6 D).

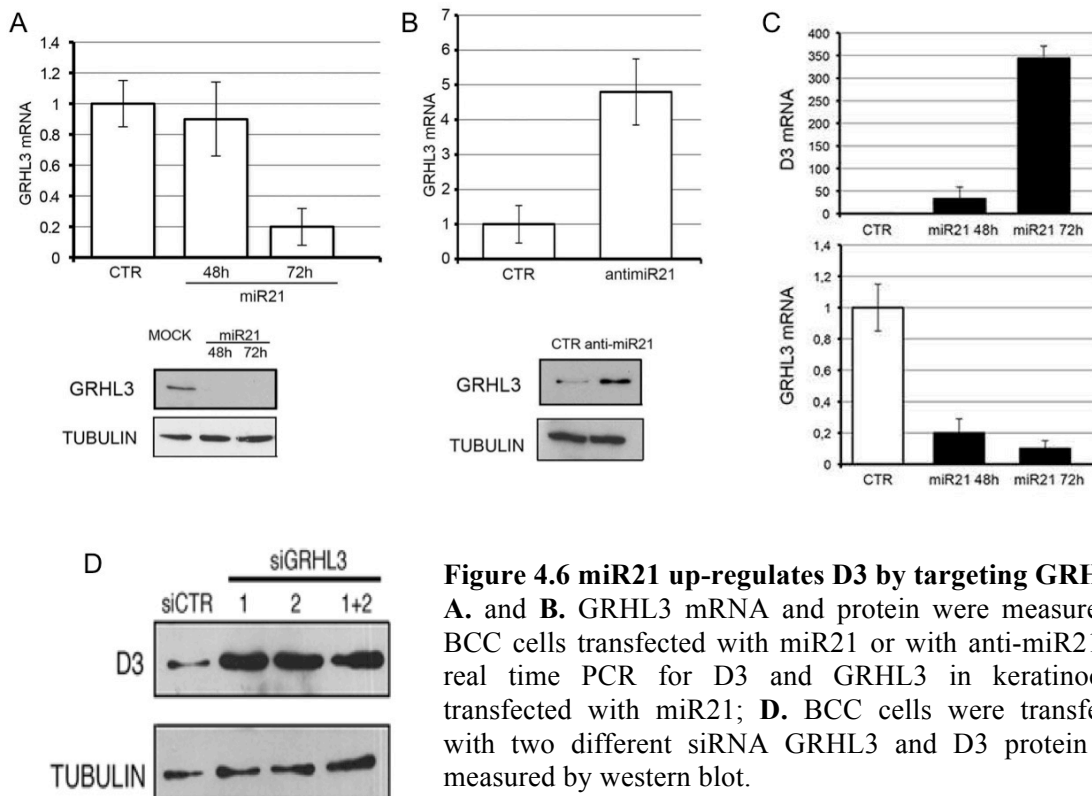


Figure 4.6 miR21 up-regulates D3 by targeting GRHL3
A. and **B.** GRHL3 mRNA and protein were measured in BCC cells transfected with miR21 or with anti-miR21; **C.** real time PCR for D3 and GRHL3 in keratinocytes transfected with miR21; **D.** BCC cells were transfected with two different siRNA GRHL3 and D3 protein was measured by western blot.

4.6 GRHL3 directly inhibits D3 expression

All together our findings lead us to think that GRHL3 effectively is a D3 inhibitor. To this end, we tested whether GRHL3 directly binds to the *Dio3* promoter. In silico analysis revealed a putative GRHL3 binding site within the promoter region of the *Dio3* gene (G1: GCGAACCGGAGCT), which is highly conserved, and located 436-bp from the ATG codon (Fig. 4.7 A). Functional studies demonstrated that GRHL3 binds to the G1 site and represses the activity of the *Dio3* promoter. Indeed, co-transfection of the mouse *Dio3* promoter (pmD3- Luc) with increasing amounts of GRHL3 showed that the *Dio3* promoter is potently inhibited by GRHL3 (Fig. 4.7 C). To further demonstrate this regulation we mutagenize the G1 site within the *Dio3* Promoter. As expected, mutation of the G1 site revealed that, while the basal activity of the mutated promoter was increased, the GRHL3-induced repression was abolished (Fig. 4.7 C and B). These data indicate that the tumor suppressor GRHL3 is a direct repressor of D3.

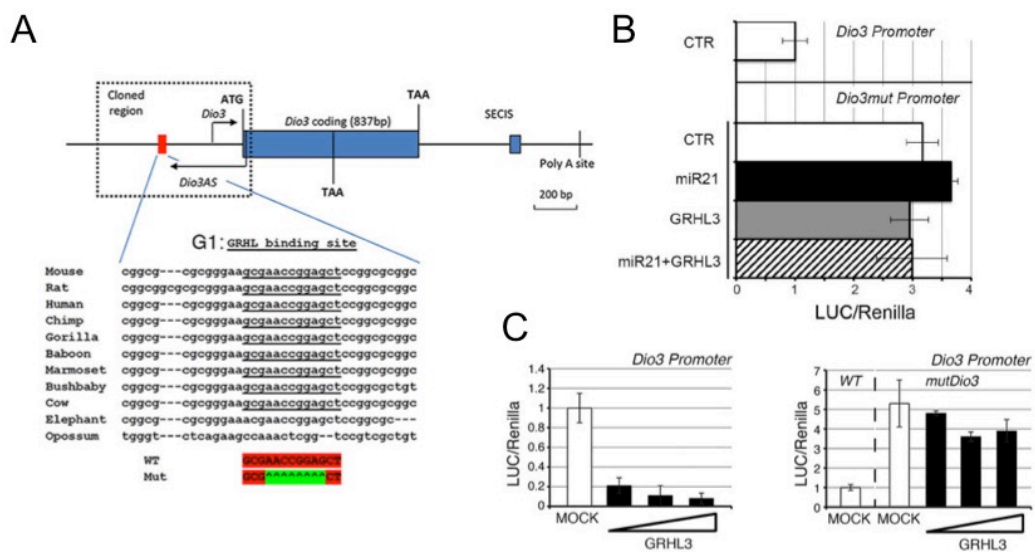


Figure 4.7 GRHL3 is a direct D3 inhibitor

A. Representation of G1 site responsive to GRHL3 within *Dio3* locus; **B.** BCC cells were co-transfected with the wild type or mutant in the G1 site *Dio3* promoter and were analyzed for luciferase activity; **C.** BCC cells were transfected with *Dio3*-Luc promoter or mut-*Dio3*-Luc promoter and with increasing amounts of GRHL3 plasmid to analyzed the relative luciferase activity.

4.7 The miR21-GRHL3-D3 axis

To assess the contribution of GRHL3 to the miR21-dependent D3 up-regulation, we transfected miR21 or GRHL3 or both in BCC cells. The forced expression of GRHL3 down-regulated D3 expression and, most importantly, abolished the miR21-mediated induction of D3 (Fig. 4.8 A). This observation was confirmed by co-transfection of the *Dio3* promoter with miR21 alone and with miR21 plus GRHL3. Also in this context, GRHL3 antagonized the effects induced by miR21 on D3 (Fig. 4.8 B). Interestingly, concomitant miR21 overexpression and GRHL3 down-regulation by siRNA did not result in synergistic D3 up-regulation, which reinforces the concept that suppression of GRHL3 is the mechanism by which miR21 enhances D3 (Fig. 4.8 C and D). Notably, miR21 and GRHL3 expression ultimately decreased and increased, respectively, the effect of TH in the nucleus (Fig. 4.8 E). The idea that emerges from these results is that miR21 up-regulates D3 expression by inhibiting the D3-repressor GRHL3.

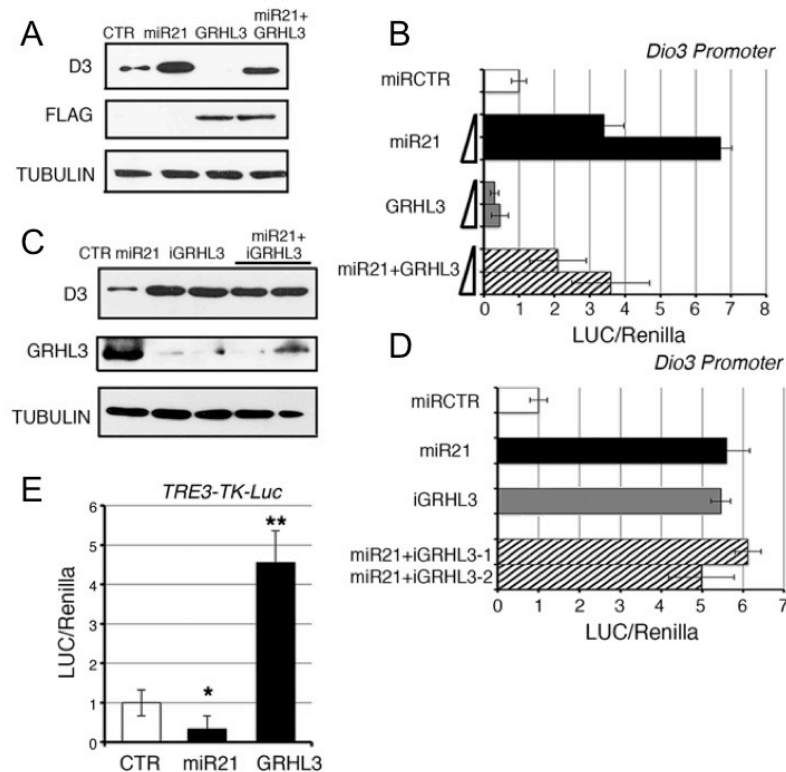


Figure 4.8 The miR21/GRHL3 axis regulates D3 expression

A. D3 protein levels were measured by western blot from BCC cells transfected with miR21 and GRHL3 or both plasmids; **B.** BCC cells were co-transfected with the *Dio3*-Luc promoter and miR21, GRHL3 or both the extracts were analyzed for luciferase activity; **C.** BCC cells were transfected with miR21 and siRNA targeting GRHL3 and D3 expression was analyzed by western blot; **D.** BCC cells were co-transfected with *Dio3*-Luc promoter and miR21, siGRHL3 or both and the luciferase activity was measured; **E.** the T3-responsive promoter TRE3-TK-Luc was co-transfected with miR21 or GRHL3 and luciferase activity was measured.

4.8 GRHL3 is positively regulated by TH

Since TH negatively regulates miR21, we tested the possibility that TH treatment could in turn increase GRHL3 expression. BCC cells were treated with 30nM T3 for 1, 2, 3, 5 days and GRHL3 expression was analyzed by western blot. We observed that T3 treatment positively regulates GRHL3 in a time-dependent manner (Fig. 4.9 A). Moreover, to verify if this effect is mediated by miR21 we treated BCC cells with or without T3 and transfected with anti-miR21 or with LNA-control. The western blot analysis showed that treatment with T3 reduces the GRHL3 overexpression mediated by miR21 silencing (Fig. 4.9 B). Moreover, the immunofluorescence analysis of BCC cells treated with T3, and transfected or not with miR21, revealed that the increase of GRHL3 TH-dependent is mediated by miR21 (Fig. 4.9 C).

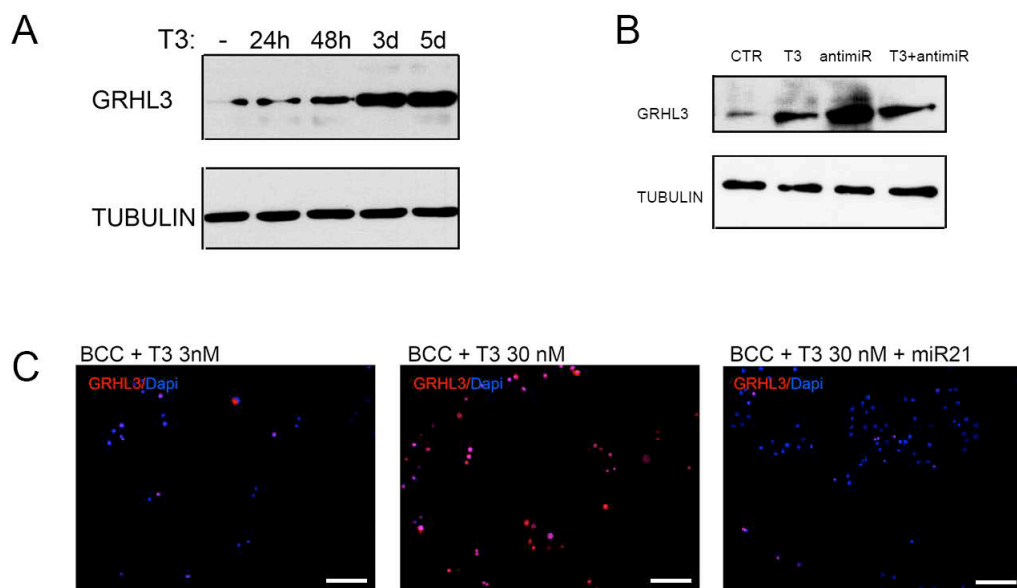


Figure 4.9 GRHL3 is positively regulated by TH

A. BCC cells were treated with 30nM T3 for the indicated times and protein were analyzed by western blot for GRHL3 expression; **B.** BCC cells were transfected with anti-miR21 and treated with or without T3 and protein were analyzed for GRHL3 expression; **C.** BCC cells were treated with 30nM T3 and transfected with miR21. The GRHL3 expression was analyzed by immunofluorescence.

4.9 Generation of D3KO cells using CRISPR/Cas9 technology and production of miR21 overexpressing cells

To get insights into the mechanism by which miR21-D3 work we decided to use CRISPR/Cas9 technology to genetically deplete D3 in BCC cells (D3KO clones). We also stably overexpressed miR21 in BCC cells (miR cells). One representative D3KO clone was subsequently stably transfected with the miR21 plasmid, and, double D3KO-miR21 overexpressing cells were selected (D3KO-miR cells). In this regards, we first confirmed D3 depletion in D3KO clones analyzing the generated clones by PRC, using the oligos shown in Fig. 4.10 A, and by western blot analysis for D3 (Fig. 4.10 B and C). In the same way, we analyzed the miR21 overexpressing clones by Taqman real time PCR for miR21 (Fig. 4.10 D). The D3 overexpression was verified in these clones by western blot analysis (Fig. 4.10 E). Finally, the double D3KO-miR21 overexpressing cells were analyzed by Taqman real time PCR and western blot analysis (Fig. 4.10 F and G).

Because the level of miR21 was higher in BCC tissue than in normal skin, we tested whether the increase of miR21 exceeded its basal levels of transcription. Indeed, we observed that miR21 is 10-fold overexpressed in miR clones versus control BCC cells (Fig. 4.10 D). As shown, GRHL3 expression was very low in all generated cells, and was further suppressed by miR21 overexpression (Fig. 4.10 H and I).

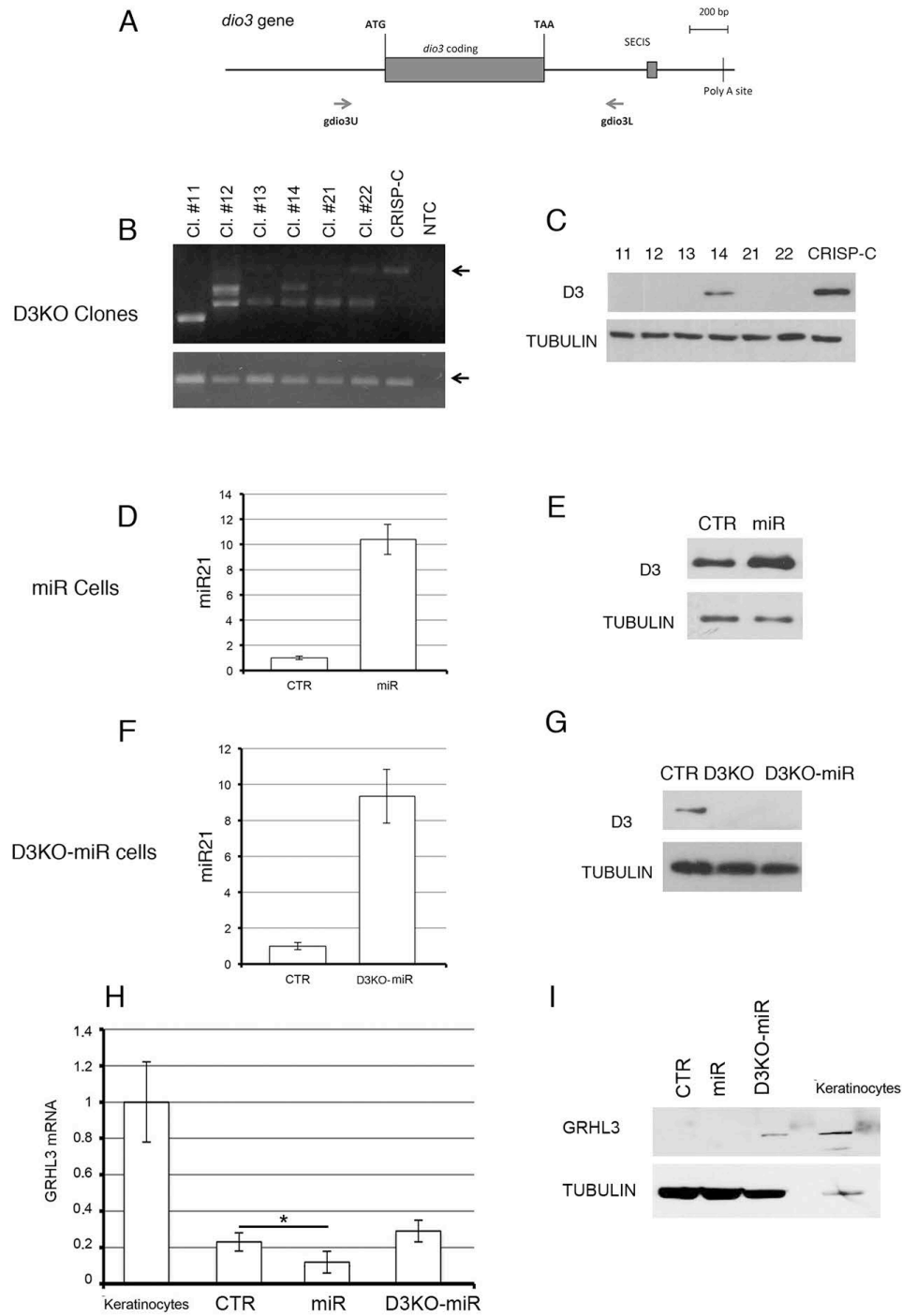


Figure 4.10 Characterization of D3KO cells

A. Representation of *Dio3* locus and oligos used for PCR analysis; **B.** PCR analysis in clones generated using CRISPR/Cas9 technology; **C.** Western blot for D3 in clones generated using CRISPR/Cas9 technology; **D.** Taqman PCR analysis in miR21 overexpressing clones; **E.** western blot for D3 in clones in miR21 overexpressing clones; **F.** Taqman PCR analysis in D3KO-miR21 overexpressing clones; **G.** western blot for D3 in clones in D3KO-miR21 overexpressing clones; **H.** and **I.** GRHL3 mRNA and protein in generated cells was measured by real time PCR and western blot.

4.10 BCC tumorigenesis required an intact miR21-GRHL3-D3 axis

To assess the functional role of the newly identified network, we next subcutaneously injected the cells generated above into athymic (nude) mice and examined the weight and morphology of the resulting subcutaneous xenograft tumors. Tumors originating from miR cells grew rapidly, and were palpable 2 weeks after injection (Fig. 4.11 A and B). D3KO-miR cells generated much smaller tumors, which become palpable 3 weeks after injection, while D3KO cells did not generate tumors (Fig. 4.11 A-C). Importantly, miR21 overexpression exacerbated tumorigenesis versus control BCC cells (Fig. 4.11 A-C). On the contrary, D3 ablation almost completely abolished the tumorigenic advantage acquired upon miR21 overexpression, consequently, D3 depletion results in a potent anti-tumoral effect even in the presence of an excess of mir21. Analyzing the formed xenograft we found a 3.54-fold reduction in tumor weight derived from D3KO-miR cells and a 2.04 increase in tumor weight derived from miR21 cells, and a 4.2-fold reduction and a 2.2 increase in tumor volume derived from D3KO-miR and miR21 cells respectively, compared to control cell-generated tumors (Fig. 4.11 D and E). Accordingly, H&E staining, Ki-67 and TUNEL staining showed that control and miR-derived tumors have a high mitotic grade, while D3KO-miR-derived tumors showed multiple areas of cell death (Fig. 4.11 F and G).

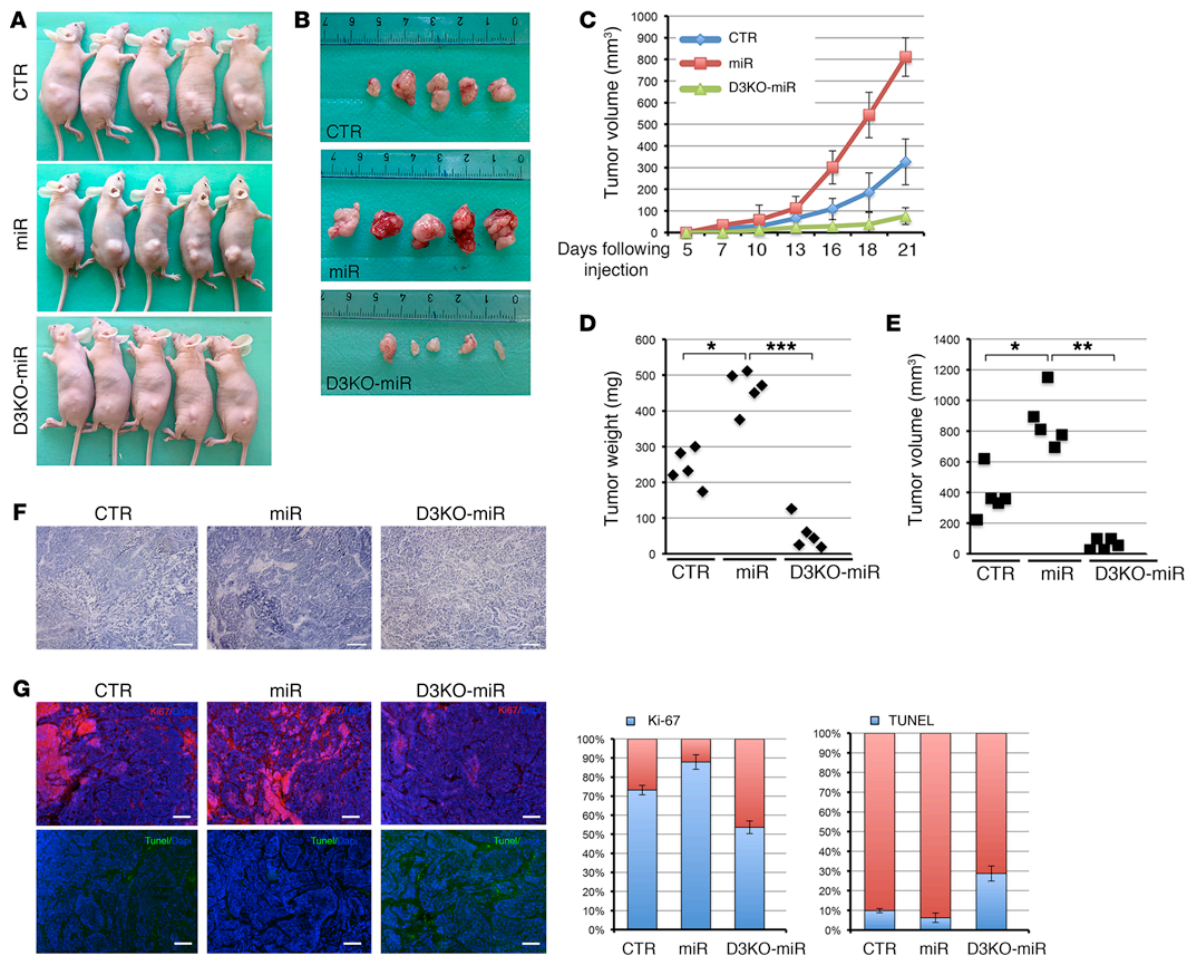


Figure 4.11 D3 depletion reduces tumorigenic capacity of BCC *in vivo*

A. $1 \times 10^6/100 \mu\text{l}$ of control CRISPR-CTR cells (CTR), stable miR21 overexpressing (miR) BCC cells, CRISPR/Cas9-D3KO cells (D3KO) and double D3KO-miR cells were injected subcutaneously into the flanks of nude mice; **B.** Tumors were collected three weeks after injection; **C.** Tumor volume was measured with a caliper for three weeks in CTR, miR and D3KO-miR cells deriving tumors; **D.** and **E.** Tumor weight and volume measured three weeks after cell injection; **F.** and **G.** Tumor sections were analyzed by H&E staining and by immunofluorescence for Ki67 and TUNEL expression in the indicated tumors.

4.11 Genetic D3 depletion reduces BCC-like tumor growth *in vivo*

Having shown that D3 depletion drastically attenuates BCC tumorigenesis and miR21 oncogenic potential in xenografts, we evaluated the role of D3 depletion in genetically-induced BCC tumors *in vivo*. To this aim, we generated a keratinocyte-specific conditional D3 null mouse (K14Cre^{+/-}/D3^{fl/fl}) in a mouse model developing BCCs-like tumors (K5-Gli2) (15), thereby generating a spontaneously forming mouse BCC-like model in an epidermal-specific D3 null background, namely, K5Gli2/K14Cre^{+/-};D3^{fl/fl}, henceforth referred to as “Gli2;D3KO”, while K5Gli2/K14Cre^{-/-}/D3^{fl/fl} mice (referred to as “Gli2”) served as controls (Fig. 4.12 A). Constitutive activation of Gli2 in keratinocytes of Gli2 mice resulted in epidermal hyperplasia, BCC and basaloid follicular hemartoma with conspicuous down-growth, arising mostly on the ears of mice at six months of age. Strikingly, D3 deletion in Gli2;D3KO mice reduced the number and size of tumors (Fig. 4.12 B). The few lesions that developed on the ears of Gli2;D3KO mice were much smaller than those found in Gli2 mice as shown by hematoxylin and eosin staining (Fig. 4.12 C).

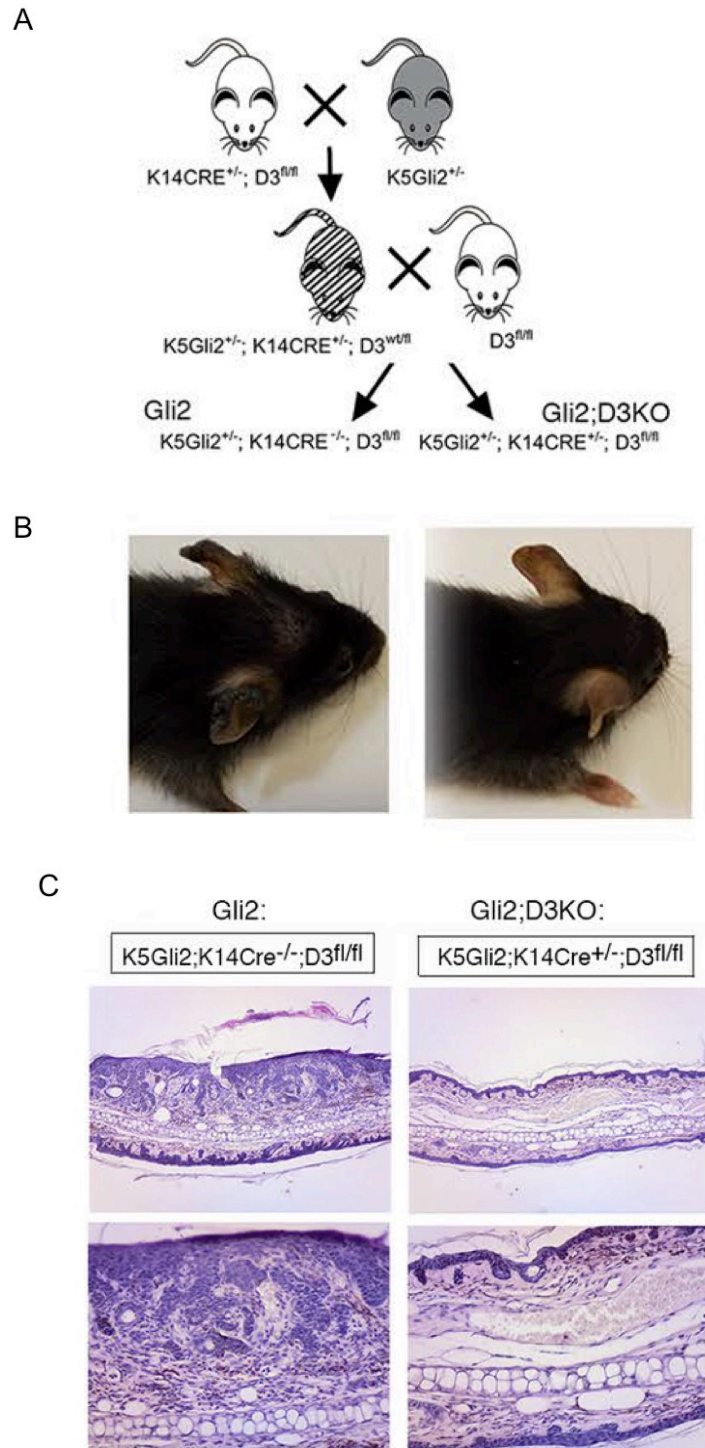


Figure 4.12 D3 depletion reduces Gli2-briven BCC-like *in vivo*

A. Genetic D3-depletion was specifically induced in keratinocytes by crossing K5Gli2;K14Cre^{-/+} with D3fl/fl mice; **B.** Mice were analyzed at 6 months of age when BCC-like formations were abundant and readily visible on the ears of control (Gli2) mice (n= 11); **C.** Histological analysis for hematoxylin and eosin stainings were performed on sections of ears from Gli2 and Gli2;D3KO mice.

To confirm that the BCC tumorigenesis was reduced in Gli2;D3KO mice compared to Gli2 mice we have analyzed by real time PCR and immunofluorescence the expression of classic markers of BCC. Accordingly, the expression of K17, cyclinD1, Ptch1 and Sox9 was drastically reduced in D3-depleted mice (Fig. 4.13 A and B). Additionally, K10, a marker of the differentiating layers of the epidermis, was significantly down-regulated in Gli2 mice, while it was well preserved in Gli2;D3KO mice (Fig. 4.13 B).

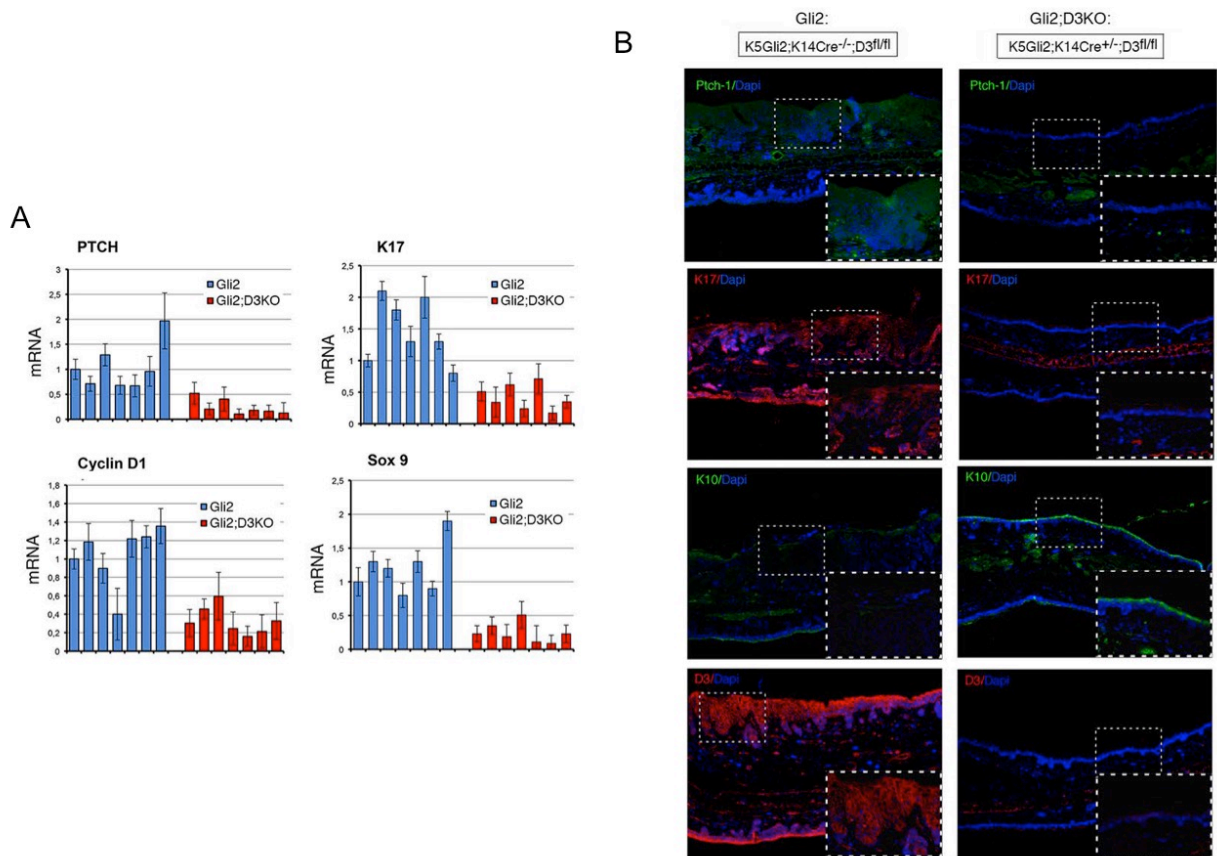


Figure 4.13 *in vivo* D3 depletion reduces BCC markers

A. Real time PCR for PTCH1, K17, Cyclin D1 and Sox9 in Gli2 vs Gli2;D3KO mice;
B. Immunofluorescence staining for PTCH1, K17, K10 and D3 in Gli2 vs Gli2;D3KO mice.

4.12 The miR21-GRHL3-D3 axis is recapitulated in human BCC

Lastly, we sought to address whether the regulation of T3 on miR21 and GRHL3 is recapitulated also in human BCC. To this aim, we evaluated miR21 levels in 16 human BCC tissues versus samples of healthy skin from the same patients by TaqMan real-time RT-PCR. According to the concept that miR21 is a marker of tumorigenesis, miR21 was expressed at significantly higher levels in BCC tissue than in the healthy skin samples (Fig. 4.14 A). We also measured GRHL3 and D3 expression in the human samples by real time PCR. As expected, GRHL3 was highly expressed in normal skin and drastically repressed in most of the BCC samples (Fig. 4.14 B). On the contrary, D3 expression correlated with miR21 expression being higher in BCC tumors compared to normal skin (Fig. 4.14 C). Taken together, these results confirm the model established in our study and suggest that targeting D3 and increasing the TH signal might represent a therapeutic approach to BCC.

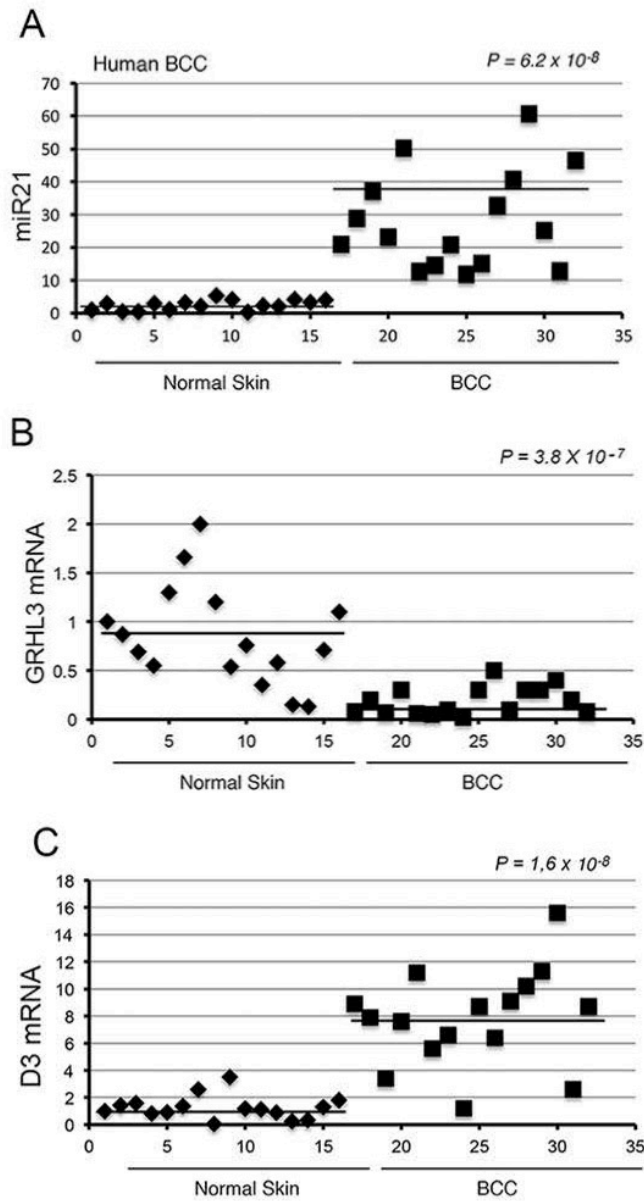


Figure 4.14 miR21, GRHL3 and D3 correlation in human BCCs

A. The expression of miR21 in 16 human BCC tumors compared with normal skin; **B.** The expression of GRHL3 was measured in 16 human BCC tumors compared with normal skin; **C.** The expression of D3 was measured in 16 human BCC tumors compared with normal skin

4.13 TH and cancer stem cells: generation of conditional D3KO mice

Hedgehog pathways deregulation leads to development of basal cell carcinoma, however the cell of origin for BCC is unclear. Several studies demonstrated that even in solid tumors only a fraction of cancer cells present the capacity to reform secondary tumors following their transplantation into immunodeficient mice. These cells, with increased renewal capacity and ability to recapitulate the heterogeneity founded in primary tumors, were referred to as cancer stem cells (CSCs) (78). Two critical properties contribute to the functional role of CSCs in the establishment and recurrence of cancerous tumors: their self-renewal capacity and their potential to differentiate into unlimited heterogeneous populations of cancer cells. These findings suggest that regulation of CSCs may represent an important mechanism to control the tumor progression. In this regard, we tested the possibility that TH metabolism affect the CSCs behavior. We thus generated two mouse model K14CRE-ER/Rosa-SmoM2-YFP/D3^{fl/fl} and K14CRE-ER/Ptch1^{fl/fl}/D3^{fl/fl} crossing K14CRE-ER/Rosa-SmoM2-YFP mice, that present a constitutive active SMO, and K14CRE-ER/Ptch1^{fl/fl}, that have a conditional depletion of Ptch1, with D3^{fl/fl} mice. In both mouse models D3 is specifically depleted in epidermis (Fig. 4.15 A and B). Furthermore, these models offer the possibility to have in the same cells the expression of SmoM2 or Ptch1 depletion and depletion of D3 contemporarily. Moreover, given that up to 70% of people with sporadic BCC have PTCH1 gene mutations and other 10-20% of patients presents mutations in the SMO these new mouse models better recapitulate the mutations in Hh pathway humans.

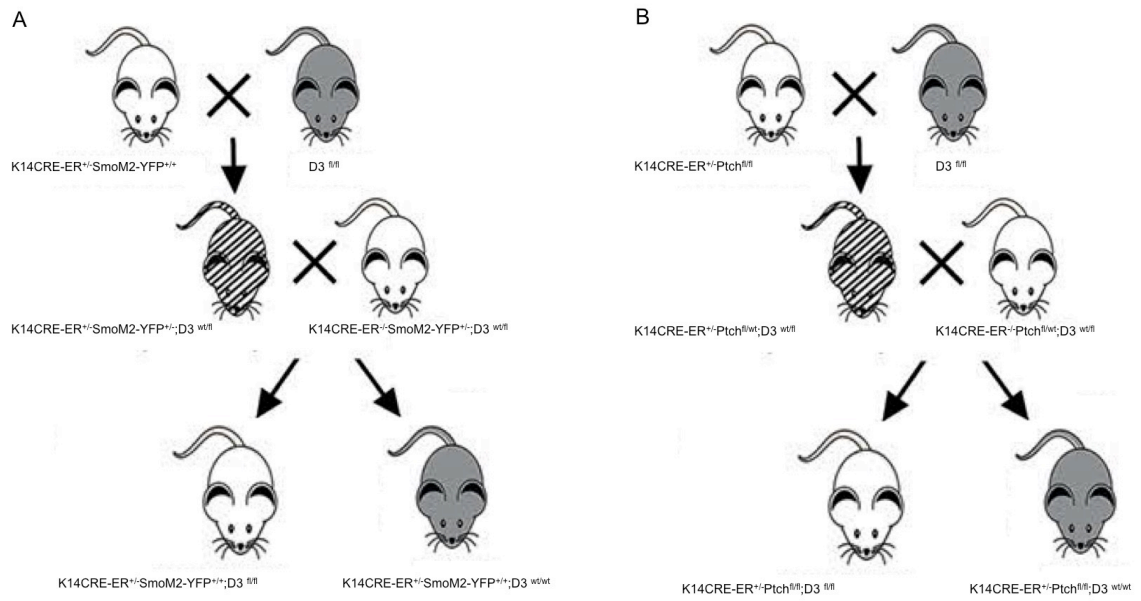


Figure 4.15 generation of D3KO conditional mice

A. Genetic D3-depletion was specifically induced in keratinocytes by crossing K14CRE-ER/Rosa-SmoM2-YFP with D3^{fl/fl} mice; **B.** Genetic D3-depletion was specifically induced in keratinocytes by crossing K14CRE-ER/Ptch1^{fl/fl} with D3^{fl/fl} mice;

4.14 D3 is overexpressed in Smo- and Ptch1- dependent BCC

To assess the biological relevance of TH on CSCs, we first confirmed D3 overexpression in Smo- and Ptch1- dependent BCC tumors. In this regard, we analyzed the D3 expression in Smo- and Ptch1- dependent BCC tumors by western blot and real time PCR. As expected, D3 is overexpressed in both Smo- and Ptch1- dependent BCC tumors (Fig. 4.16 A and B). In particular, D3 is rapidly activated since 4 weeks of induction in K14CRE-ER/Rosa-SmoM2 mice and continued to be highly expressed at 8 weeks, when BCC-like tumors were apparent, as shown by real time PCR and western blot analysis for D3 (Fig. 4.16 C). Interestingly, D3 co-localizes perfectly with Smo as shown by IF analysis (Fig. 4.16 D). Accordingly, together with an increase of D3 at mRNA level these mice present an overexpression of BCC markers such as K17 and Sox9 (Fig. 4.16 E). The same results were obtained using K14CRE-ER/Ptch1^{fl/fl} mice. All together these data confirmed that D3 is overexpressed in Smo- and Ptch1- dependent BCC and highlight D3 as a potential target for affecting BCC formation.

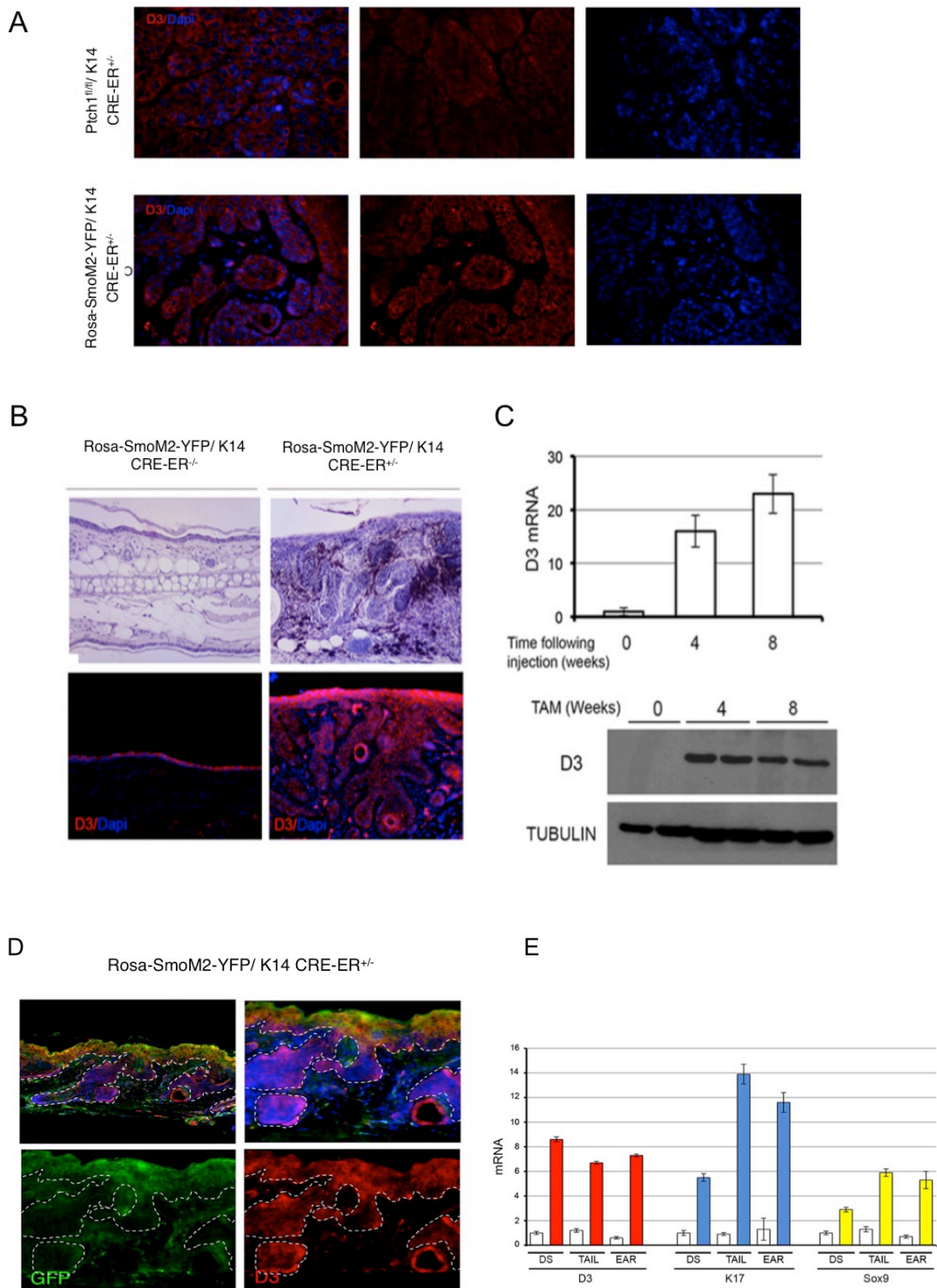


Figure 4.16 D3 expression in Smo- Ptch1- dependent BCC tumors:

A. Immunofluorescence for D3 in K14CRE-ER/Rosa-SmoM2-YFP and K14CRE-ER/Ptch1^{fl/fl} mice; **B.** Hematoxylin and eosin and Immunofluorescence staining in K14CRE-ER/Rosa-SmoM2-YFP; **C.** Real time PCR and western blot analysis for D3 in K14CRE-ER/Rosa-SmoM2-YFP 4 and 8 weeks after TAM administration; **D.** Co-staining for D3 and GFP in K14CRE-ER/Rosa-SmoM2-YFP; **E.** real time PCR for BCC markers.

4.15 TH metabolism affect skin cancer stem cells population

Skin CSCs are a heterogeneous population of stem cells marked by a differential profile of high (Hi) versus low (Lo) CD34 expression, closely linked to the tumorigenic potential and capacity to reform the tumor in transplantation studies (89, 97). To define the impact of TH metabolism on CSC physiology we analyzed the percentage of CSCs in K14CRE-ER^{+/-}/Rosa-SmoM2-YFP/D3^{fl/fl} versus K14CRE-ER^{-/-}/Rosa-SmoM2-YFP/D3^{fl/fl} mice by FACS analysis through co-expression of SmoM2 with YFP (yellow fluorescent protein) and analysis of CD34⁺ population cells. In this regard, 5 weeks old mice, K14CRE-ER^{+/-}/Rosa-SmoM2-YFP/D3^{fl/fl} versus K14CRE-ER^{-/-}/Rosa-SmoM2-YFP/D3^{fl/fl}, were treated with tamoxifen to generate the concomitant D3 depletion and SmoM2-YFP overexpression. The mice were sacrificed 3 and 6 weeks after tamoxifen administration and CSCs were isolated from the tumor bulk using CD34 as marker of bulge CSCs. Interestingly, our data demonstrated that the number of CD34⁺ cells is reduced in D3-depleted epidermis as a result of the increased TH concentration and attenuated proliferative potential.

Furthermore, in order to investigate the relevance of TH metabolism on CSCs, K14CRE-ER^{+/-}/Rosa-SmoM2-YFP/D3^{fl/fl} mice were made systemically hypothyroid by treatment with methimazole for 6 weeks and the CD34⁺ cells were analyzed by FACS analysis. Surprisingly, the treatment with methimazole prevents the reduction of CD34⁺ cells in K14CRE-ER^{+/-}/Rosa-SmoM2-YFP/D3^{fl/fl} mice (Fig.4.17).

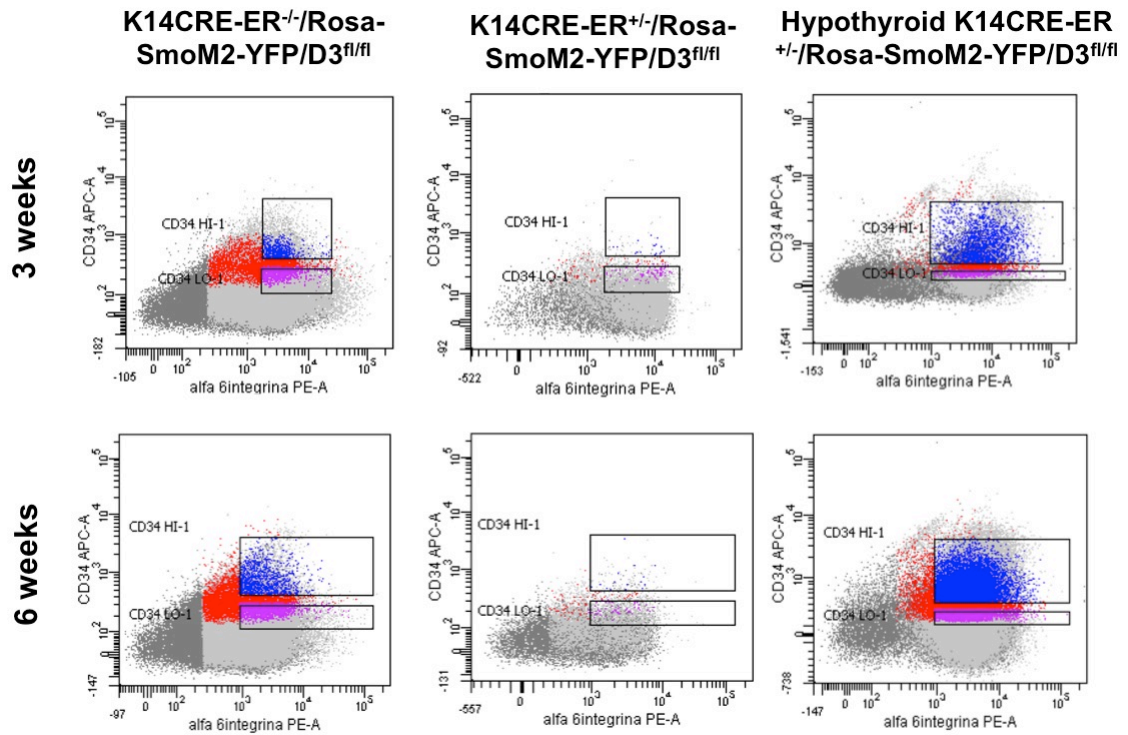


Figure 4.17 D3 depletion reduces a population of CD34⁺ cells

FACS strategy used to isolate YFP⁺/α6-integrin⁺/CD34⁺ (Hi and Lo) cells from K14CRE-ER^{+/-}/Rosa-SmoM2-YFP/D3^{fl/fl} versus K14CRE-ER^{-/-}/Rosa-SmoM2-YFP/D3^{fl/fl} mice.

4.16 Sox 9 is negatively regulated by TH

In the last few years several studies have been demonstrated that Sox9, a bulge stem cells marker, normally involved in the control of cell fate decision during development and homeostasis of a broad range of tissues, is expressed in a wide range of cancers, including BCC. In particular, Sox9 is required for self-renewal of CSC in BCC tumor (95). However, Sox9 regulation is yet unclear. To get insights into the mechanism by which TH could influence the population of CSCs we verify if TH signaling could influence Sox9 expression. To this aim, BCC cells were treated with 30nM T3 and were analyzed by western blot and real time PCR. Our data showed that Sox9 is down-regulated by T3 treatments (Fig.4.18 A and B). Furthermore, D3-depletion in BCC cells, using D3-targeting shRNA oligo versus control scrambled shRNA oligo, also causes a reduction of Sox9 mRNA (Fig. 4.18 C).

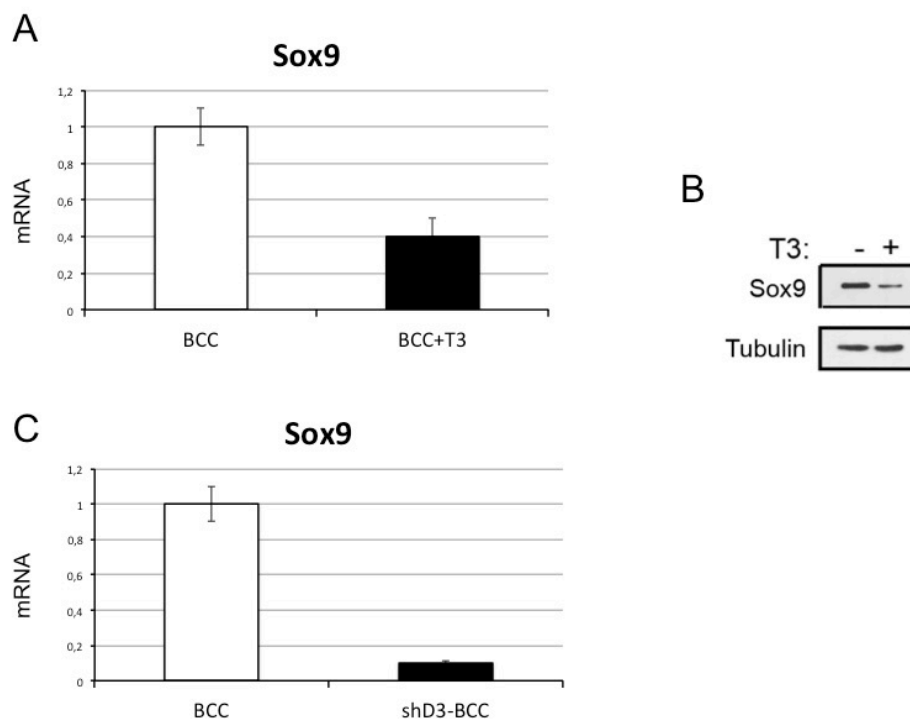


Figure 4.18 Sox9 is downregulated by TH in BCC cells

A. Real time PCR and western blot analysis for Sox9 in BCC cells treated with 30nM T3 for 48h; **B.** western blot analysis for Sox9 in BCC cells treated with 30nM T3 for 48h; **C.** Real time PCR for Sox9 in BCC cells transfected with shD3.

4.17 TH regulates SOX9 through it's binding a specific gene region

To further investigate the mechanism by which TH inhibits Sox9 expression, we analyzed the *Sox9* regulatory region. *In silico* analysis revealed several conserved thyroid hormone responsive element-binding sites (TREs) within the mouse *Sox9* 5'-Flanking regions (Fig. 4.19 A). We cloned 1241 bp of the 5'-Flanking region within the pGL3-basic vector to perform functional studies in mouse BCC cells. As shown in Fig. 4.19 B, the *Sox9* enhancer was efficiently down-regulated by TH and by double TR-transfection-TH treatment in BCC. Finally, to further support these findings, we performed chromatin immunoprecipitation analysis. The results revealed that the thyroid receptor (TR) physically binds to the one of the most conserved TREs (Fig. 4.19 C). Together, these results demonstrate that TH represses the transcription of the stemness gene *Sox9*.

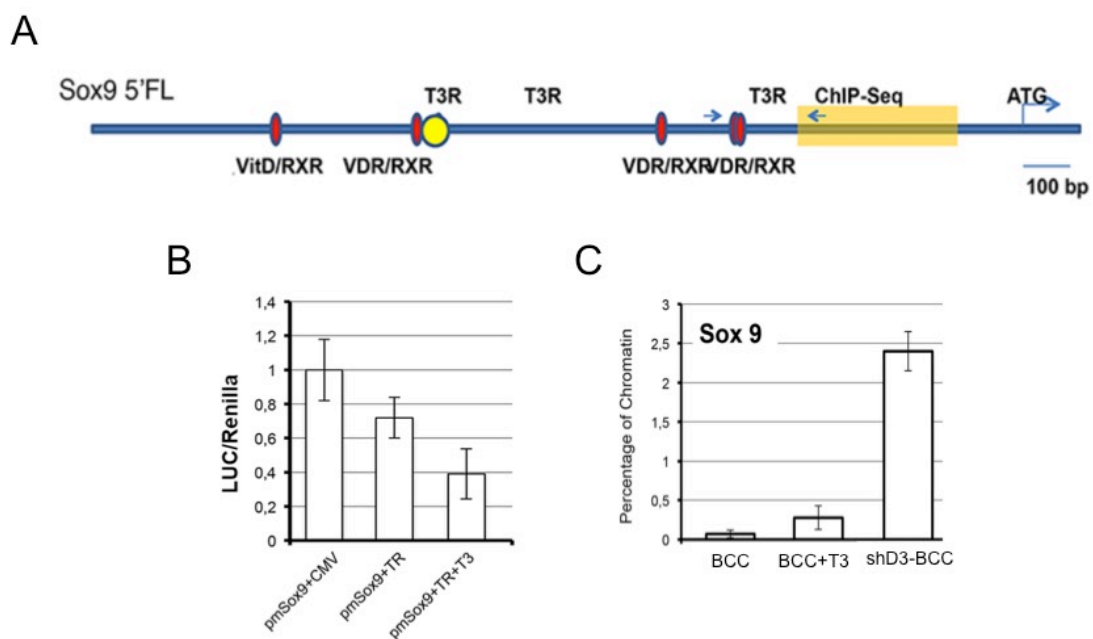


Figure 4.19 TH binds Sox9 5'-Flanking region in BCC cells

A. Representation of *Sox9* 5'-Flanking Regions; **B.** BCC cells transfected with *Sox9*-Luc promoter and luciferase activity was measured; **C.** Chromatin immunoprecipitation analysis revealed that the thyroid receptor (TR) physically binds to the one of the most conserved TREs in *Sox9* 5'-Flanking Regions.

5 Discussion

The thyroid hormone (T3) acts on different signaling pathways to control intrinsic transcription factor networks regulating the balance between proliferation *versus* differentiation in several contexts. Additionally, current literature suggests that TH have an important role in neoplastic transformation. Our studies have identified a novel network through TH signaling, by modulating miRNA expression, interacts with oncogenic pathways to regulate the growth of BCC tumors. Specifically, we provided evidence that T3 suppresses miR21 expression, thus attenuating BCC formation. Moreover, TH action is contextually regulated by miR21 through the control of the TH-inactivating enzyme, D3. Of note, thyroid hormone deregulation is frequent in human tumors, but it is unknown whether it is a bystander event or if it could drive or control *in vivo* cancer growth. Presently, not much evidence exist in literature regarding the cross-talk between TH signaling and microRNA in cancer. Notably, several evidences have indicated that the TH-inactivating enzyme D3 is up-regulated in many human tumors and cancer cell lines (38) where, blocking TH action, enhances the proliferation of malignant cells (45). Here we described a TH functional role in the control of miR21-dependent oncogenic action. Importantly, using a unique skin-specific D3-KO mouse model, we provided the first *in vivo* genetic evidence that D3 depletion, which is equivalent to TH treatment, drastically reduces BCC formation. In particular, the primary TH mode action is its binding to TH receptors in the nucleus, which are able to binding to TH response elements (TREs) and impose a gene expression signature that activates or inhibits target genes transcription. However, a direct TR-TRE mechanism may not explain all TH actions. Therefore, miRNAs represent an additional mechanism by which TH could regulate target genes. miRNAs are involved in many biological processes and functions, which control protein expression principally through mRNA degradation (47). Moreover, studies in the past 10 years have evidenced that alteration in microRNA expression and regulation contributes to the pathogenesis of most malignancies (51-55). Similarly, TH signaling is often compromised in carcinogenesis as demonstrated by the reduced expression or deletion of the TR genes in human cancers, suggesting that TRs could function as tumor suppressors. The inverse association between TH and cancer was confirmed by the demonstration that the *v-erb-a*

oncogene, which is the avian erythroblastosis gene, is a mutated form of the *Thra* gene (coding for the TRa protein) (98). It antagonizes T3 function AEV-transformed erythroleukemic in cells thus blocking T3-dependent cell differentiation. Therefore, both T3/thyroid hormone receptor signaling and miRNAs affect tumor cell progression. As such, in the current work we explored the miRNAs' role in governing TH action in BCC context. In this light, it is of critical relevance the novel finding of a negative control exerted by T3 on miR21 expression. Established as "onco-miR" miR21 was demonstrated acts in a plethora of cancer (57, 99, 100). In skin, miR21 has been implicated in tumorigenesis of SCC and melanomas (62, 101), but also in psoriasis (102) and wound healing (103). Here, we provide the first evidence that miR21 is overexpressed in human and mouse BCC, while it is barely detectable in normal skin. Our data demonstrate that miR21 is suppressed by TH at transcriptional level by directly binding to a TRE located within the miR21 enhancer region. Indeed, decreased expression of D3 or TH treatment of BCC cells contributes to miR21 down-regulation levels. Furthermore, we described the existence of a loop between T3 and miR21 due to the fact that miR21 is also an upstream regulator of D3, the T3-inactivating enzyme. It is been known that miRNAs reduce gene expression by targeting the 3-UTR regions of downstream mRNAs and blocking their translation. The positive correlation between miR21 and D3 suggests the existence of an intermediate factor that mediates such regulation. To accomplish this, we have screened a downstream target of miR21, transcription factors express in the epithelium, as a putative suppressor of D3 expression. Consequently, we discovered a novel D3 repressor, grainyhead-like 3 (GRHL3). Our data demonstrate that the developmental factor and tumor suppressor GRHL3 represses D3 transcription and mediates the positive regulation of D3 expression by miR21. Consistent with the computational analysis, some studies have demonstrated that GRHL3 is down-regulated by miR21 in SCCs (62, (64). Accordingly, here we demonstrated that GRHL3 is down-regulated by miR21 in BCC and this inhibition increases the D3 expression. This is consistent with the poor D3 expression in adult tissues and its reactivation in many tumor contexts (38). Remarkably, forced GRHL3 expression prevents miR21-dependent D3 transcription, thus providing a genetic proof for a miR21-GRHL3-D3 network (Fig. 5.1).

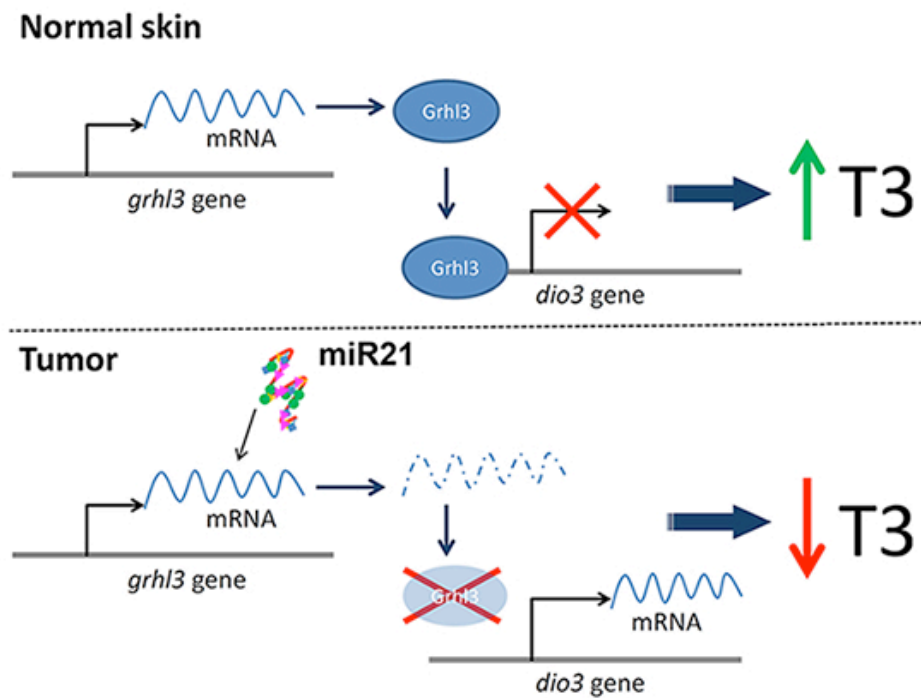


Figure 5.1 miR21-GRHL3-D3 axis

Schematic representation of miR21-GRHL3-D3 axis through BCC cells regulates intracellular T3 availability

Our findings suggest that TH metabolism has a critical role in the skin. Consistent with these results, both miR21 and GRHL3 play crucial roles in skin cancer formation (64). Particularly, keratinocytes derived from $GRHL3^{-/-}$ mice displayed increased tumorigenesis when injected in nude mice, demonstrating a tumor suppressor role in skin cancer. Accordingly, previous reports have shown the oncogenic activity of miR-21 including high proliferation, low apoptosis, and high invasion and metastasis potential. Moreover, Hatley et al. (2010) revealed, for the first time, a miR-21 oncogenic potential *in vivo* by using gain-of-function transgenic mice and loss-of-function knockout mice of miR-21 allele in combination with the $K\text{-ras}^{LA2}$ mouse model of NSCLC ($CAG\text{-miR-21}$; $K\text{-ras}^{LA2}$ and the $miR\text{-21}^{-/-}$; $K\text{-ras}^{LA2}$, respectively). Indeed, miR21 inhibition in $miR\text{-21}^{-/-}$; $K\text{-ras}^{LA2}$ mice drastically attenuates tumor growth. These observations reinforce the idea that D3 expression, and in general TH metabolism, play a critical role in skin cancer. Furthermore, it was previously demonstrated that D3 overexpression enhances keratinocyte proliferation (45), and that

D3 is normally absent in adult tissues while is re-activated in many hyper-proliferative conditions (38). The inverse correlation between miR21 and GRHL3, and consequently of D3 and GRHL3, shown by our studies, underline the opposite roles played by the two genes in BCC tumorigenesis. In addition, miR21 and GRHL3 are also related to others pathologies of skin in which the proliferation control is enhanced, such as psoriasis and wound healing (104) thus suggesting that D3-mediated control of T3 signaling might also be active in these conditions. Finally, given that GRHL3 is a critical factor for keratinocyte differentiation and skin barrier formation and that *Grhl3*^{-/-} mice exhibit impaired epidermal differentiation and decreased expression of multiple differentiation genes (105), we can suppose that D3 suppression and TH regulation could influence the differentiation program of keratinocytes. Such a speculation might have important clinical relevance, since alterations of thyroid hormone levels in patients are associated with cutaneous manifestations and generalized myxedema (increased glycosaminoglycan deposition in skin, which appears cold, dry and pale, with abundant hair loss) is the classical clinical sign of hypothyroid patients (106). Although thyroid dysfunctions affect the skin phenotype and many people with hypothyroidism and hyperthyroidism have skin-related conditions (106), there is no evidence of an association between thyroid dysfunctions and BCC formation. This apparent lack of an association may be explained in one of two ways. Firstly, BCCs grow very slowly while alterations of thyroid hormone circulation at plasma levels are acute conditions that generally do not become chronic. Secondly, the deiodinase family represents a potent homeostatic mechanism when thyroid dysfunction induces a minimal variation of TH, and is thus able to preserve intracellular “normal” T3 concentrations even in the presence of altered thyroid status at plasma level.

Taken note of these considerations, we sought to assess the pathologic role of the newly identified circuit in vivo. For this purpose, we used a CRISPR/Cas9 technology to genetically deplete D3 in BCC cells. Additionally, we create a miR21-overexpressing BCC cells and D3ko- miR21-overexpressing BCC cells. Our results demonstrated that D3 depletion potently attenuates BCC cell proliferation in vivo xenograft. On the contrary, miR21 overexpression enhances the oncogenic potential of BCC cells. Most remarkably, the ability to form tumors of miR21-overexpressing cells was significantly compromised by D3 depletion, which strongly supports the concept that the TH

inactivation pathway plays a pivotal role in tumor growth. Furthermore, the intracellular TH regulation by D3 seems to be critical for tumorigenic potential in an *in vivo* model of BCC-like tumor formation. Indeed, we demonstrate that skin-specific D3 depletion drastically reduces tumor occurrence in mice with spontaneously-forming BCC tumors, and prevents miR21 overexpression in these tumors. Interestingly, our data demonstrate that it is possible attenuates skin cancer formation by blocking the down-regulation of TH signaling. However, even if D3 depletion potentially attenuates BCC growth driven by the Shh-Gli2 pathway and by miR21 overexpression, BCC cells still generate tumors when miR21 is overexpressed and D3 is depleted, thus suggesting that increasing the intracellular thyroid hormone signaling is not sufficient to eradicate BCC tumorigenesis. Collectively, these findings suggest that TH may regulate the cellular levels of miRNA which, in turn, regulate the TH intracellular availability. To our knowledge, this represents the first observation of strong link between miR21 expression and D3 overexpression. Besides in cancer, there are many other contexts in which miR21 functions, D3 expression and TH metabolism are linked. For instance, miR21 is implicated in many types of cardiac stress, including the myocardial remodeling that occur after infarction, in which both D3 and miR21 are induced (107). Moreover, miR21 is induced during immune cell activation (58, 108). The analogy of miR21 with D3 expression in multiple settings suggests that the miR21-D3 axis is a potential therapeutic target. In conclusion, the first part of this work leads us to conclude that exist a common route by which tumor cells attenuate the TH signal in the tumor microenvironment (Fig. 5.2).

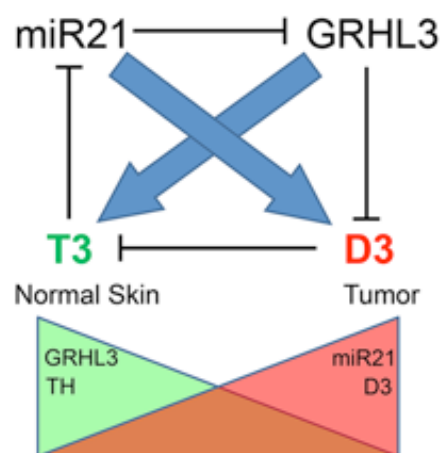


Figure 5.2 TH-miR21 loop

Schematic representation of the mutual, negative-feedback loop by which TH regulates miR21 and miR21 controls intracellular TH through GRHL3.

In the second part of this study, we provide the first evidence that TH controls the skin cancer stem cells maintenance. Here we demonstrated that TH act not only down-regulating and important stemness gene, Sox9, but also reducing the proportion of CD34⁺ in the bulk of tumor. Sox9 exhibits several functions in embryogenesis, sex determination as well as maintenance of stemness properties (109). Apart from their physiological functions, numerous studies have also highlighted the important involvements of Sox9 in tumorigenesis of a number of human malignancies such as colorectal, pancreatic, prostate cancers and skin (110, 111). In the normal skin, Sox9 is expressed in the sebaceous gland and in the bulge (112). In epidermal keratinocytes Sox9 plays an important role in proliferation, differentiation and apoptosis processes (113). Several studies have been demonstrated that Sox9 depletion in early stem cells can block hair follicle morphogenesis and epidermal wound repair (112). In this regard, the role of Sox9 as a cell fate determiner during embryonic development has been well characterized. In particular, Sox9 expression is related to differentiation of cells derived from all three germ layers into a several specialized tissues. However, Sox9 is express not only in pluripotent progenitors but also in adult stem cells, suggesting its role in cell maintenance and specification during adult life. During last few years, several studies have characterized the versatile role of Sox9 as a stem cell regulator. Indeed, recent data have demonstrated that Sox9 controls the long-term maintenance and expansion of oncogene expressing cells by promoting self-renewing division and inhibiting differentiation (114). This versatility of Sox9 may be explained by a combination of pre- and post-transcriptional regulations. Accordingly, it was demonstrated that TH regulates the self-renewal of colon cancer stem cells through the activation of canonical Notch pathway (115). Other studies provide the evidence that TH promotes cell self-renewal and drugs resistance also in HCC cells (116).

Here we described the ability of T3 to regulate Sox9 expression. In particular, our data suggest that Sox9 is down-regulated by T3 treatment and specifically the thyroid receptor physically binds the TRE within Sox9 5'-Flanking Regions. Most remarkably, D3-depletion in BCC cells also causes a reduction of Sox9 levels. These data lead us to hypothesize that TH may have a yet uncharacterized functional role in the regulation of skin stemness genes. In line with this idea, we have analyzed the role of TH on BCC-CSCs. Several studies have demonstrated that BCCs can arise from CSC of bulge,

sebaceous glands, and IFE (91, 92, 94). The cell surface glycoprotein CD34 marks mouse hair follicle bulge cells (117) that are thought to be major target of carcinogens and the cells of origin for skin tumors in mice and humans (118). Because of that, we have generated two mouse model (K14CRE-ER/Rosa-SmoM2-YFP/D3^{fl/fl} and K14CRE-ER/Ptch1^{fl/fl}/D3^{fl/fl}), in which D3 is specifically depleted in epidermis simultaneously with the Smo overexpression or Ptch1 depletion. We demonstrated that skin specific D3-depletion, leading to increased TH action, causes a reduction of CD34⁺ cells in BCC. Most importantly, systemically hypothyroidism of these mice prevents the percentage diminution of CD34⁺ population.

We thus speculate that TH signaling is essential for the maintenance of bulge CSC. Although these findings provide the first evidence that the absence of D3 dramatically impairs CSC population, yet a key question remains open: which is the mechanism through TH signaling can act in modulating cancer stem cells.

In conclusion, our findings identify the TH-inactivating enzyme D3 as a potential target of anti-cancer therapy for human BCC and demonstrate that TH functions as a suppressor of BCC tumors by regulating multiple pathways, including regulation of CSCs.

6 Materials and Methods

6.1 Cell cultures and transfections

BCC cells were cultured under low calcium conditions with 8% Ca²⁺-chelated fetal bovine serum and keratinocyte growth factor (Sigma). HEK-293 cells were cultured in DMEM with 10% fetal bovine serum (FBS), 2 mM L-glutamine, and 10 U/mL penicillin/streptomycin. All transient transfections for BCC cells were performed using Lipofectamine 2000 (Life Technologies, Ltd) according to the manufacturer's instructions. HEK-293 cells were transfected using IBAfect reagent (IBA BioTAGnology). Mouse primary keratinocytes were isolated from C57BL/6 newborn mice and cultured under low calcium conditions (0.05 mM) in the presence of 4% calcium-chelated fetal bovine serum (FBS) (Invitrogen, Carlsbad, CA, USA) and epidermal growth factor (EGF, Invitrogen).

6.2 Plasmid and reagents

For the pmD3Luc (*Dio3* Promoter) a genomic mouse DNA was used as a PCR template; the oligonucleotides pmD3U and pmD3L (see paragraph 6.15) generated a 750-bp fragment containing the mouse *dio3* 5' flanking region. For the miR21-Enhancer-Luc plasmid, we used the oligos mMiR21U and mMiR21L to amplify 389 bp of the miR21 5' flanking region. The amplified regions were cloned into the NheI/BglII (pmD3Luc) or SacI/XhoI (miR21-Enhancer-Luc) sites of a pGL3-basic vector (Promega). The mutated plasmid pmD3Luc-del was obtained from the pmD3Luc by recombinant PCR with two sets of oligonucleotides. Briefly, the two PCR products, pmD3U/pmD3mGRHLL2 and pmD3mGRHLU/pmD3L to obtain pmD3Luc-del were combined by PCR using outside oligonucleotides, and the final PCR products were reinserted into the pGL3-basic vector (Promega). The Flag-GRHL3 plasmid was generated by PCR on mouse normal skin cDNA; the coding sequence of mouse *grhl3* was amplified by PCR with specific oligonucleotides (mGRHL3clonU and mGRHL3clonL); the PCR product was inserted into the HindIII/EcoRI sites of the pFLAG-CMV-2 vector (Sigma). To generate the pmSox9Luc plasmid, we used a genomic mouse DNA as template in a PCR with oligonucleotides: pmSox9U and

pmSox9L2 to isolate 1241 bp from the mouse *Sox9* 5' flanking region. The amplified region were cloned into Xho/HindIII sites of a pGL3-basic vector (Promega).

GRHL3 silencing was performed with siRNA technology: two siRNA targeting GRHL3 were purchased from Life Technology (cod. s106644, s106646). Stealth RNAi negative control duplex (Invitrogen) served as control. The primer sequence is reported at paragraph 6.15. The miR21-overexpressing plasmid was kindly provided by Prof. G. De Vita (University of Naples Federico II, Naples, Italy). Knockdown of miR-21 was performed by transient transfection of anti-miR21 LNA (ID mh10206, Ambion). LNA-scrambled CTR served as control.

6.3 Genome-editing of the *dio3* locus using the CRISPR/Cas9 technology

Targeted depletion of D3 in mouse BCC cells was obtained with CRISPR/Cas9 technology by using the CRISPR/Cas9 system from Santa Cruz Biotechnology (*dio3* CRISPR/Cas9 KO Plasmid, Cod. sc-430733) and control plasmid (Control CRISPR/Cas9 Plasmid, cod. sc-418922). The D3 CRISPR/Cas9 KO plasmid consists of a pool of 3 plasmids, each encoding the Cas9 nuclease and a target-specific 20 nucleotide guide RNA. CRISPR/Cas9-guided mutagenesis in this case resulted in a deletion in the *dio3* coding region. Briefly, BCC cells were transfected with 500 ng of the D3 CRISPR/Cas9 KO plasmid or control plasmid with Lipofectamine 2000 (Life Technology). Three days after transfection, the cells were FACS-sorted for green fluorescent protein expression, and single clones were selected and analyzed by PCR to verify D3 coding sequence integrity using specific oligonucleotides (g_{dio3U}: cgaccaagatttctggggca and g_{dio3L}: agcagagtctcaagttagccagac). Effective D3 depletion was confirmed by western blot analysis.

6.4 Luciferase assay

The Luc plasmids (pmD3Luc, miR21-Enhancer-Luc or T3TRETkLc, pmSox9Luc) and CMV-Renilla reporters were co-transfected into BCC and HEK-293 cells, and treated with 30 nMT3 as indicated. Luciferase activities were measured 48 hours after transfection by using the Dual Luciferase Reporter Assay System (Promega), and differences in transfection efficiency were corrected relative to the level of Renilla

activity. Each construct was studied in triplicate in at least 3 separate transfection experiments.

6.5 Western blot analysis

Total protein extracts from BCC cells were run on a 10% SDS–PAGE gel and transferred on Immobilon-P transfer membrane (Millipore). The membrane was then blocked with 5% non-fat dry milk in phosphate buffered saline (PBS), probed with appropriate antibodies (anti-D3 polyclonal antibodies (1:500); anti-Flag M2-Sigma (1:1000); cyclin D1 (1:1000) Santa Cruz, sc-246) for 2 h, washed and incubated with horseradish peroxidase-conjugated donkey anti-rabbit IgG or anti-mouse secondary antibody (1:3000) and detected by chemiluminescence (Millipore). After extensive washing, the membrane was incubated with anti-Tubulin-specific antibodies (sc -8035, 1:10000; Santa Cruz) as loading control. All Western blots were run in triplicate, and bands were quantitated in one representative gel.

6.6 miRNA Northern blot

Total RNA was isolated from BCC cells treated or not with T3, using Trizol (Invitrogen) and quantitated at 260 nm using a standard spectrometry. 10 μ g of total RNA was resuspended in 2 X tris/borate/EDTA (TBE) urea sample buffer (Invitrogen) to a final volume of 10 μ l. Samples were heated at 70 °C for 5 min and loaded onto a 15% polyacrylamide gel containing TBEurea. Electrophoresis was performed in 1 X TBE running buffer at 120 V with a run time between 60–90 min. After electrophoresis, the gel was rinsed in deionised water, followed by a 5 min wash in 1 X TBE. RNA was transferred onto a Hybond N+ membrane for 30 min at 20 V using a BioRadMiniprotean II apparatus. The nylon membrane was placed in the Stratagene UV Cross linker® and RNA cross-linked at 1200 kJ. As miR21 probe, we designed the oligonucleotide Mir21probe (see paragraph 6.15) containing the mature miRNA sequence. The oligo was hybridized to the OprobAAA: 5' TTTTTTTTTTCTCTGTCC-3' and elongated with klenowexo- and ATPalpha P32 to generate a tail of radioactive adenine. To normalize the RNA, we used the 5s subunit of ribosomal RNA (see Supplemental Table 3), which was also hybridized to the OprobAAA and radiolabeled.

6.7 Animals, histology and immunostaining

.K5Gli2;K14Cre^{+/-}D3^{fl/fl}(Gli2;D3KO) mice were obtained by crossing a keratinocyte-specific conditional D3 null mouse (K14Cre^{+/-}D3^{fl/fl}) with the mouse model K5-Gli2(119). Female 5-week-old BALB/C (nude) mice were purchased from Charles River Laboratories (Milan, Italy). K14CRE-ER/Rosa-SmoM2-YFP/D3^{fl/fl} mice were obtained by crossing K14CRE-ER/Rosa-SmoM2-YFP mice with D3^{fl/fl} mice. K14CRE-ER/Ptch1^{fl/fl}/D3^{fl/fl} were obtained by crossing K14CRE-ER/Ptch1^{fl/fl} with D3^{fl/fl} mice.

For immunofluorescence and histology, ears from Gli2;D3KO and control mice at 6 months of age and xenograft tumors were and embedded in paraffin, cut, into 7 μm sections, and hematoxylin and eosin stained. Slides were baked at 60 °C, deparaffinized by xylenes, dehydrated with ethanol, rehydrated in PBS, and permeabilized by 0.5% Triton X-100 in PBS. Antigen retrieval was performed by incubation in 0.01 M citrate buffer (pH 6.0) or 0.5 M Tris buffer (pH 8.0) at 95 °C for 15 minutes. Sections were blocked in 1% BSA/0.05% Tween/PBS for 30 min at 37 °C. Primary antibody (Anti-K17 (Novocastra, NCL-CK17), K10 (PRB-159P), Sox9 (AbCam, ab26414) and Ptch-1 (Novus Bio 2113) GFP (AbCam, ab13970)) incubation was carried out overnight at 4 °C in blocking buffer followed by washing in 0.2% Tween-PBS. Secondary antibody incubation was carried out at room temperature for 1 hour, followed by washing in 0.2% Tween-PBS. Images were acquired with an IX51 Olympus microscope and the Cell*F software.

6.8 Real time PCR

mRNAs were extracted with TRIzol reagent (Life Technologies Ltd). cDNAs were prepared with SuperScript VILO Master Mix (Life Technologies Ltd) as indicated by the manufacturer. The cDNAs were amplified by PCR in an iQ5 Multicolor Real-Time Detector System (Bio-Rad) with the fluorescent double-stranded DNA-binding dye SYBR Green (Applied Biosystems). Specific primers for each gene were designed to work under the same cycling conditions (95°C for 10 min followed by 40 cycles at 95°C for 15 s and 60°C for 1 min), generating products of comparable sizes (~200 bp for each amplification). Primer combinations were positioned whenever possible to span an exon-exon junction and the RNA digested with deoxyribonuclease to avoid genomic DNA interference. For each reaction, standard curves for reference genes were

constructed based on 6 4-fold serial dilutions of cDNA. All samples were run in triplicate. The template concentration was calculated from the cycle number when the amount of PCR product passed a threshold established in the exponential phase of the PCR. The relative amounts of gene expression were calculated with cyclophilin A expression as an internal standard (calibrator). The results, expressed as n-fold differences in target gene expression, were determined as follows: $n \times \text{target} = 2^{(\Delta C_{t\text{sample}} - \Delta C_{t\text{calibrator}})}$.

6.9 TaqMan miRNA assay

miR-21, RNU6B, and Sno234 were analyzed using two-step real-time PCR protocols with TaqMan MicroRNA Assays: hsa-miR-21 cod 000397; RNU6B cod 001093; snoRNA234 cod 001234 (Applied Biosystems). Reverse transcriptase reactions were performed using the TaqMan MicroRNA Reverse Transcription Kit (Applied Biosystems) in a 15 μL of total volume reaction mix with 7 μL of master mix containing 1x RT buffer, 1.0 mM of total dNTPs, 50 U MultiScribe Reverse Transcriptase Enzyme, and 0.25 U of RNase inhibitor; 3 μL of RT primers (Applied Biosystems); and 5 μL of RNA sample. The amplification conditions were as follows: annealing at 16°C for 30 min, extension at 42°C for 30 min, and RT inactivation at 85°C for 10 min. qPCRs were performed on Applied Biosystems Step One Plus Real-Time PCR System (Applied Biosystems) with a 20 μL final volume mixture containing 1x TaqMan Universal PCR Master Mix (Applied Biosystems), 1x MicroRNA Assay (Applied Biosystems), and 3 μL LcDNA (RT product diluted 1:5). Thermal cycling conditions were 10 min at 95°C followed by 40 cycles of 15 sec at 95°C and 1 min. at 60°C. The endpoint of qPCR data is the threshold cycle (Ct), which represents the fractional cycle number at which the fluorescence reaches the fixed threshold. All qPCR reactions were run in duplicate. The relative quantification of miRNA expression was analyzed using $2^{-\Delta\Delta C_t}$ method.

6.10 Tumor xenografts

To evaluate in vivo tumorigenesis, a BCC xenografting mouse model was established. After resuspension in PBS, 1×10^6 in 100 μL of CRISP-CTR BCC cells (control), one D3KO clone (D3KO n.12, Supplemental Figure 4), miR21 and D3KO-miR21 cells

were injected subcutaneously into the flanks of 5-week-old female BALB/c-nu mice. Mice were examined twice a week, and the tumor was measured with a caliper and then weighed three weeks after injection. All animals were maintained in a sterile environment on a daily 12 h light/12 h dark cycle. Tumor volume was calculated according to the formula, volume (mm^3) = $4/3 \times p \times (\text{length}/2) \times (\text{width}/2) \times (\text{height}/2)$. Tumor xenografts were harvested, weighed, and snap-frozen for immunofluorescence analysis.

6.11 Human samples

Human BCC samples were collected at the Istituto Nazionale Tumori Ospedale Pascale in Naples. This work was approved by the appropriately constituted research ethics committee of the University of Naples Federico II.

6.12 ChIP assay

Approximately 8×10^6 cells were fixed with 1% formaldehyde in growth medium at 37°C for 30 min. Glycine was added to a final concentration of 0.125 M to stop cross-linking. Sonicated, cross-linked chromatin was centrifuged at 12,000 rpm for 30 min to remove insoluble material. The soluble chromatin was diluted 10-fold in dilution buffer and used directly for chromatin immunoprecipitation (ChIP) assays. Five percent of total DNA was used as a positive control for PCR assays (denoted “input DNA”). Six optical density (A_{260}) units of chromatin from BCC cells were mixed with 10 μl (0.3 $\mu\text{g}/\mu\text{l}$) of anti-TR α and incubated at 4°C for 3 h before precipitation with protein A/G Sepharose (Sigma Chemical Co., St. Louis, MO). After five rounds of washing, bound DNA-protein complexes were eluted by incubation with 1% sodium dodecyl sulfate-0.1 M NaHCO₃ elution buffer. Formaldehyde cross-links were reversed by incubation in 200 mM NaCl at 65°C. Samples were extracted twice with phenol-chloroform and precipitated with ethanol. DNA fragments were recovered by centrifugation, resuspended in 50 μl of H₂O, and used for real-time PCRs

6.13 Isolation of epithelial CSCs

Remove the dorsal skin from back of mice, gently scrape away the fat and blood vessels covering the dermis until the dermis is clearly and uniformly exposed. The dorsal skin

were plated on 10 mm dish, dermis side down, and incubated overnight in 0,25% trypsin at 4°C (Gibco). The next day the epidermis was separated from the dermis, chopped and incubated for 10 min in 0.25% trypsin at 37°C. Trypsin was neutralized by adding DMEM containing 10% Chelex serum. The cell suspension was then passed twice through a 70 µM cell strainer (Corning 431751). After isolation of keratinocytes, immunostaining was carried out using conjugated APC-anti-CD34 (clone MEC14.7; Biolegend) and PE-conjugated anti-α6- integrin (BD biosciences 555736).

Living SmoM2-expressing epidermal cells were gated by forward scatter, by side scatter and by expression of SmoM2-YFP. Fluorescence activated, YFP⁺/α6-integrin⁺/CD34⁺ cell-sorting analysis was carried out using FACS Aria and FACS Diva software (BD Biosciences). Similarly, Tail skins were separated from the tail bone and processed as described above.

6.14 Statistical analysis

The results are shown as means ± SD throughout. Differences between samples were assessed by the Student's two-tailed t test for independent samples. In all experiments, differences were considered significant when p was less than 0.05. Asterisks indicate significance at *p < 0.05, **p < 0.01, and ***p < 0.001 throughout. Differences of mRNA levels in human BBC samples versus normal skin samples were analyzed by using a one-way ANOVA, and P 0.05 was considered significant. Relative mRNA levels (in which the control sample was arbitrarily set as 1) are reported as results of real-time PCR, in which expression of cyclophilin A was used as a housekeeping gene. The relationship between the miR21/GRHL3, miR21/D3 and GRHL3/D3 expression was analyzed using Pearson's correlation.

6.15 Sequences of primers

Oligonucleotides used for plasmid generation and mutagenesis		
Name	Sequence (5' → 3')	
mGRHL3clonU	GCCGAAGCTTTTGAATGAACCTGATTTTCAGGTC	
mGRHL3clonL	TAATGAATTCTCATAGCTCCTTCAGGATGATC	
pmD3U	GCCGGCTAGCTGTGAGCGCGCGGGAGGCGG	
pmD3L	GCCGAGATCTGGTGGCCGCGGGCCCCGAAGCC	
mMir21U	ATTAGAGCTCATGTACAGGAGTTTCTGGGCA	
mMir21L	ATTACTCGAGCACACTGCTGTGGCACAAAGA	
pmD3mGRHLU	GCGCGCGGGAAGCGCTCCGGCGCGGCGCT	
pmD3mGRHLL2	CCGCGCCGAGCGCTTCCCGCGCGCCGCCCA	
pGL3biss	ATTACGCCAGCCCAAGCTACC	
pGL3-R	AATTGTTCCAGGAACCAGGGCGTAT	
mHmir21dU	ATTACCCGGGCACTGCCTCACTGTTTGCCATTG	
mHmir21dL	GCCGCTCGAGCAAGCAAGCAGTTGCTTTCC	
mMir21mutU	ACGCAGGGGTTGTTTTTAATAAAAACTTAGATTGAGAA	
mMir21mutL	TTCTCAATCTAAGTTTTTATTAACAACCCCTGCGT	
pmSox9U	ATTACTCGAGCCTAGAGCTTCGCCCTCTTAG	
pmSox9L2	CGCAAGCTTCTCTCTTGCAAAGAAAAGTTC	
Oligonucleotides used for genome analysis of CrispR/CAS clones		
gdio3U	CGACCCAAGATTTCTGGGGCA	
gdio3L	AGCAGAGTCTCAAGTTAGCCAGAC	
mHMIR21mutU	ACGCAGGGGTTGTTTTAATAAAA	
mHMIR21wtU	ACGCAGGGGTTGTCTTAATAAGG	
mHMIR21wtL	CACACTGCTGTGGCACAAAGA	
Oligonucleotides used for Northern Blot		
Mir21probe	TGGCAACAGCAGTCGATGGGCTGTCGGACAGAG	
5Sprobe	TTAGCTTCCGAGATCAGACGAGGACAGAG	
OprobAAA	TTTTTTTTTTCTCTGTCC	
Oligonucleotides used for real-time PCR		
Gene	Forward primer (5' → 3')	Reverse primer (5' → 3')
<i>cyclophilin A</i>	CGCCACTGTCGCTTTTTCG	AACTTTGTCTGCAAACAGCTC
<i>CYCLOPHILIN A</i>	AGTCCATCTATGGGGAGAAATTTG	GCCTCCACAATATTCATGCCTTC
<i>dio2</i>	CTTCCTCCTAGATGCCTACAAAC	GGCATAATTGTTACCTGATTCAGG
<i>dio3</i>	CCGCTCTCTGCTGCTTCAC	CGGATGCACAAGAAATCTAAAAGC
<i>thral</i>	CCTGGATGACACGGAAGTGGCT	GGGCACTCGACTTTCATGTG
<i>thrb1/2</i>	CACAGGGTACCCTATCGCTGC	CAGCACCAGTCTGTTGCCATGC
<i>mct8</i>	TTCGGCTGGATAGTGGTGTGTTGCA	ATCATGCCCATAGCGAGGGCTC
<i>mct10</i>	CCATCGTGAGTGTCTTCACGGACAT	GGAGCAGGATTGTGAAGACGCTGC
<i>grhl3</i>	TCATCGACGTAGCTGACTGT	TTCATCATCGCGCATCTTCC
<i>GRHL3</i>	TCATTGACGTGGCTGACTGC	CTCGTCATCGCGCATCTTCC
<i>ptch1</i>	ATTCCCTAATGGAAGTATTGC	GCTCCTTGACTCAATAGATGA
<i>cyclin D1</i>	GCTCCTGTGCTGCGAAGTGGAA	TCATGGCCAGCGGGAAGACCT

Local control of thyroid hormone action in cancer growth and stemness

<i>sox9</i>	tcagcaagactctgggcaag	actttgccagcttgacgtcg
<i>krt17</i>	CTCCGTACCAAGTTTGAGAC	CGGTTCTTCTCCGCCATCTTC

7 References

1. Krickler A, Armstrong BK, English DR, and Heenan PJ. A dose-response curve for sun exposure and basal cell carcinoma. *International journal of cancer*. 1995;60(4):482-8.
2. Zak-Prelich M, Narbutt J, and Sysa-Jedrzejowska A. Environmental risk factors predisposing to the development of basal cell carcinoma. *Dermatologic surgery : official publication for American Society for Dermatologic Surgery [et al]*. 2004;30(2 Pt 2):248-52.
3. Ouyang YH. Skin cancer of the head and neck. *Seminars in plastic surgery*. 2010;24(2):117-26.
4. Ting PT, Kasper R, and Arlette JP. Metastatic basal cell carcinoma: report of two cases and literature review. *Journal of cutaneous medicine and surgery*. 2005;9(1):10-5.
5. Xie J, Murone M, Luoh SM, Ryan A, Gu Q, Zhang C, Bonifas JM, Lam CW, Hynes M, Goddard A, et al. Activating Smoothed mutations in sporadic basal-cell carcinoma. *Nature*. 1998;391(6662):90-2.
6. Gailani MR, Stahle-Backdahl M, Leffell DJ, Glynn M, Zaphiropoulos PG, Pressman C, Uden AB, Dean M, Brash DE, Bale AE, et al. The role of the human homologue of Drosophila patched in sporadic basal cell carcinomas. *Nature genetics*. 1996;14(1):78-81.
7. Ruiz i Altaba A, Sanchez P, and Dahmane N. Gli and hedgehog in cancer: tumours, embryos and stem cells. *Nature reviews Cancer*. 2002;2(5):361-72.
8. Ingham PW, and McMahon AP. Hedgehog signaling in animal development: paradigms and principles. *Genes & development*. 2001;15(23):3059-87.
9. Petrova R, and Joyner AL. Roles for Hedgehog signaling in adult organ homeostasis and repair. *Development*. 2014;141(18):3445-57.
10. Gorlin RJ. Nevoid basal cell carcinoma syndrome. *Dermatologic clinics*. 1995;13(1):113-25.
11. Uden AB, Holmberg E, Lundh-Rozell B, Stahle-Backdahl M, Zaphiropoulos PG, Toftgard R, and Vorechovsky I. Mutations in the human homologue of Drosophila patched (PTCH) in basal cell carcinomas and the Gorlin syndrome: different in vivo mechanisms of PTCH inactivation. *Cancer research*. 1996;56(20):4562-5.
12. Reifemberger J, Wolter M, Knobbe CB, Kohler B, Schonicke A, Scharwachter C, Kumar K, Blaschke B, Ruzicka T, and Reifemberger G. Somatic mutations in the PTCH, SMOH, SUFUH and TP53 genes in sporadic basal cell carcinomas. *The British journal of dermatology*. 2005;152(1):43-51.
13. Mao J, Ligon KL, Rakhlin EY, Thayer SP, Bronson RT, Rowitch D, and McMahon AP. A novel somatic mouse model to survey tumorigenic potential applied to the Hedgehog pathway. *Cancer research*. 2006;66(20):10171-8.
14. Wong SY, Seol AD, So PL, Ermilov AN, Bichakjian CK, Epstein EH, Jr., Dlugosz AA, and Reiter JF. Primary cilia can both mediate and suppress Hedgehog pathway-dependent tumorigenesis. *Nature medicine*. 2009;15(9):1055-61.

15. Grachtchouk M, Mo R, Yu S, Zhang X, Sasaki H, Hui CC, and Dlugosz AA. Basal cell carcinomas in mice overexpressing Gli2 in skin. *Nature genetics*. 2000;24(3):216-7.
16. Kasper M, Jaks V, Hohl D, and Toftgard R. Basal cell carcinoma - molecular biology and potential new therapies. *The Journal of clinical investigation*. 2012;122(2):455-63.
17. Gereben B, Zavacki AM, Ribich S, Kim BW, Huang SA, Simonides WS, Zeold A, and Bianco AC. Cellular and molecular basis of deiodinase-regulated thyroid hormone signaling. *Endocrine reviews*. 2008;29(7):898-938.
18. Visser WE, Friesema EC, Jansen J, and Visser TJ. Thyroid hormone transport in and out of cells. *Trends in endocrinology and metabolism: TEM*. 2008;19(2):50-6.
19. Visser WE, van Mullem AA, Jansen J, and Visser TJ. The thyroid hormone transporters MCT8 and MCT10 transport the affinity-label N-bromoacetyl-[(125)I]T3 but are not modified by it. *Molecular and cellular endocrinology*. 2011;337(1-2):96-100.
20. Dumitrescu AM, Liao XH, Best TB, Brockmann K, and Refetoff S. A novel syndrome combining thyroid and neurological abnormalities is associated with mutations in a monocarboxylate transporter gene. *American journal of human genetics*. 2004;74(1):168-75.
21. Cheng SY, Leonard JL, and Davis PJ. Molecular aspects of thyroid hormone actions. *Endocrine reviews*. 2010;31(2):139-70.
22. St Germain DL, and Galton VA. The deiodinase family of selenoproteins. *Thyroid : official journal of the American Thyroid Association*. 1997;7(4):655-68.
23. Berry MJ, Banu L, Chen YY, Mandel SJ, Kieffer JD, Harney JW, and Larsen PR. Recognition of UGA as a selenocysteine codon in type I deiodinase requires sequences in the 3' untranslated region. *Nature*. 1991;353(6341):273-6.
24. Arrojo EDR, and Bianco AC. Type 2 deiodinase at the crossroads of thyroid hormone action. *The international journal of biochemistry & cell biology*. 2011;43(10):1432-41.
25. Curcio-Morelli C, Gereben B, Zavacki AM, Kim BW, Huang S, Harney JW, Larsen PR, and Bianco AC. In vivo dimerization of types 1, 2, and 3 iodothyronine selenodeiodinases. *Endocrinology*. 2003;144(3):937-46.
26. Sagar GD, Gereben B, Callebaut I, Mornon JP, Zeold A, Curcio-Morelli C, Harney JW, Luongo C, Mulcahey MA, Larsen PR, et al. The thyroid hormone-inactivating deiodinase functions as a homodimer. *Mol Endocrinol*. 2008;22(6):1382-93.
27. Bianco AC, and Larsen PR. Cellular and structural biology of the deiodinases. *Thyroid : official journal of the American Thyroid Association*. 2005;15(8):777-86.
28. Mandel SJ, Berry MJ, Kieffer JD, Harney JW, Warne RL, and Larsen PR. Cloning and in vitro expression of the human selenoprotein, type I iodothyronine deiodinase. *The Journal of clinical endocrinology and metabolism*. 1992;75(4):1133-9.
29. Schneider MJ, Fiering SN, Thai B, Wu SY, St Germain E, Parlow AF, St Germain DL, and Galton VA. Targeted disruption of the type 1

- selenodeiodinase gene (Dio1) results in marked changes in thyroid hormone economy in mice. *Endocrinology*. 2006;147(1):580-9.
30. Gereben B, Goncalves C, Harney JW, Larsen PR, and Bianco AC. Selective proteolysis of human type 2 deiodinase: a novel ubiquitin-proteasomal mediated mechanism for regulation of hormone activation. *Mol Endocrinol*. 2000;14(11):1697-708.
 31. Burmeister LA, Pachucki J, and St Germain DL. Thyroid hormones inhibit type 2 iodothyronine deiodinase in the rat cerebral cortex by both pre- and posttranslational mechanisms. *Endocrinology*. 1997;138(12):5231-7.
 32. Dentice M, Ambrosio R, Damiano V, Sibilio A, Luongo C, Guardiola O, Yennek S, Zordan P, Minchiotti G, Colao A, et al. Intracellular inactivation of thyroid hormone is a survival mechanism for muscle stem cell proliferation and lineage progression. *Cell metabolism*. 2014;20(6):1038-48.
 33. Salvatore D, Low SC, Berry M, Maia AL, Harney JW, Croteau W, St Germain DL, and Larsen PR. Type 3 iodothyronine deiodinase: cloning, in vitro expression, and functional analysis of the placental selenoenzyme. *The Journal of clinical investigation*. 1995;96(5):2421-30.
 34. Boelen A, Boorsma J, Kwakkel J, Wieland CW, Renckens R, Visser TJ, Fliers E, and Wiersinga WM. Type 3 deiodinase is highly expressed in infiltrating neutrophilic granulocytes in response to acute bacterial infection. *Thyroid : official journal of the American Thyroid Association*. 2008;18(10):1095-103.
 35. Boelen A, Kwakkel J, Wieland CW, St Germain DL, Fliers E, and Hernandez A. Impaired bacterial clearance in type 3 deiodinase-deficient mice infected with *Streptococcus pneumoniae*. *Endocrinology*. 2009;150(4):1984-90.
 36. Peeters RP, Wouters PJ, Kaptein E, van Toor H, Visser TJ, and Van den Berghe G. Reduced activation and increased inactivation of thyroid hormone in tissues of critically ill patients. *The Journal of clinical endocrinology and metabolism*. 2003;88(7):3202-11.
 37. Simonides WS, Mulcahey MA, Redout EM, Muller A, Zuidwijk MJ, Visser TJ, Wassen FW, Crescenzi A, da-Silva WS, Harney J, et al. Hypoxia-inducible factor induces local thyroid hormone inactivation during hypoxic-ischemic disease in rats. *The Journal of clinical investigation*. 2008;118(3):975-83.
 38. Dentice M, Antonini D, and Salvatore D. Type 3 deiodinase and solid tumors: an intriguing pair. *Expert opinion on therapeutic targets*. 2013;17(11):1369-79.
 39. Bates JM, St Germain DL, and Galton VA. Expression profiles of the three iodothyronine deiodinases, D1, D2, and D3, in the developing rat. *Endocrinology*. 1999;140(2):844-51.
 40. Huang SA, Tu HM, Harney JW, Venihaki M, Butte AJ, Kozakewich HP, Fishman SJ, and Larsen PR. Severe hypothyroidism caused by type 3 iodothyronine deiodinase in infantile hemangiomas. *The New England journal of medicine*. 2000;343(3):185-9.
 41. Kester MH, Kuiper GG, Versteeg R, and Visser TJ. Regulation of type III iodothyronine deiodinase expression in human cell lines. *Endocrinology*. 2006;147(12):5845-54.
 42. Dentice M, Luongo C, Ambrosio R, Sibilio A, Casillo A, Iaccarino A, Troncone G, Fenzi G, Larsen PR, and Salvatore D. beta-Catenin regulates deiodinase

- levels and thyroid hormone signaling in colon cancer cells. *Gastroenterology*. 2012;143(4):1037-47.
43. Howard D, La Rosa FG, Huang S, Salvatore D, Mulcahey M, Sang-Lee J, Wachs M, and Klopper JP. Consumptive hypothyroidism resulting from hepatic vascular tumors in an athyreotic adult. *The Journal of clinical endocrinology and metabolism*. 2011;96(7):1966-70.
 44. Ruppe MD, Huang SA, and Jan de Beur SM. Consumptive hypothyroidism caused by paraneoplastic production of type 3 iodothyronine deiodinase. *Thyroid : official journal of the American Thyroid Association*. 2005;15(12):1369-72.
 45. Dentice M, Luongo C, Huang S, Ambrosio R, Elefante A, Mirebeau-Prunier D, Zavacki AM, Fenzi G, Grachtchouk M, Hutchin M, et al. Sonic hedgehog-induced type 3 deiodinase blocks thyroid hormone action enhancing proliferation of normal and malignant keratinocytes. *Proceedings of the National Academy of Sciences of the United States of America*. 2007;104(36):14466-71.
 46. Markou A, Zavridou M, and Lianidou ES. miRNA-21 as a novel therapeutic target in lung cancer. *Lung Cancer (Auckl)*. 2016;7(19-27).
 47. Siomi H, and Siomi MC. Posttranscriptional regulation of microRNA biogenesis in animals. *Molecular cell*. 2010;38(3):323-32.
 48. Friedman RC, Farh KK, Burge CB, and Bartel DP. Most mammalian mRNAs are conserved targets of microRNAs. *Genome research*. 2009;19(1):92-105.
 49. Jansson MD, and Lund AH. MicroRNA and cancer. *Molecular oncology*. 2012;6(6):590-610.
 50. Iorio MV, Ferracin M, Liu CG, Veronese A, Spizzo R, Sabbioni S, Magri E, Pedriali M, Fabbri M, Campiglio M, et al. MicroRNA gene expression deregulation in human breast cancer. *Cancer research*. 2005;65(16):7065-70.
 51. Ciafre SA, Galardi S, Mangiola A, Ferracin M, Liu CG, Sabatino G, Negrini M, Maira G, Croce CM, and Farace MG. Extensive modulation of a set of microRNAs in primary glioblastoma. *Biochemical and biophysical research communications*. 2005;334(4):1351-8.
 52. Bloomston M, Frankel WL, Petrocca F, Volinia S, Alder H, Hagan JP, Liu CG, Bhatt D, Taccioli C, and Croce CM. MicroRNA expression patterns to differentiate pancreatic adenocarcinoma from normal pancreas and chronic pancreatitis. *Jama*. 2007;297(17):1901-8.
 53. Schetter AJ, Leung SY, Sohn JJ, Zanetti KA, Bowman ED, Yanaihara N, Yuen ST, Chan TL, Kwong DL, Au GK, et al. MicroRNA expression profiles associated with prognosis and therapeutic outcome in colon adenocarcinoma. *Jama*. 2008;299(4):425-36.
 54. Zhang BG, Li JF, Yu BQ, Zhu ZG, Liu BY, and Yan M. microRNA-21 promotes tumor proliferation and invasion in gastric cancer by targeting PTEN. *Oncology reports*. 2012;27(4):1019-26.
 55. Frankel LB, Christoffersen NR, Jacobsen A, Lindow M, Krogh A, and Lund AH. Programmed cell death 4 (PDCD4) is an important functional target of the microRNA miR-21 in breast cancer cells. *The Journal of biological chemistry*. 2008;283(2):1026-33.

56. Loffler D, Brocke-Heidrich K, Pfeifer G, Stocsits C, Hackermuller J, Kretzschmar AK, Burger R, Gramatzki M, Blumert C, Bauer K, et al. Interleukin-6 dependent survival of multiple myeloma cells involves the Stat3-mediated induction of microRNA-21 through a highly conserved enhancer. *Blood*. 2007;110(4):1330-3.
57. Meng F, Henson R, Wehbe-Janek H, Ghoshal K, Jacob ST, and Patel T. MicroRNA-21 regulates expression of the PTEN tumor suppressor gene in human hepatocellular cancer. *Gastroenterology*. 2007;133(2):647-58.
58. Morrisey EE. The magic and mystery of miR-21. *The Journal of clinical investigation*. 2010;120(11):3817-9.
59. Joyce CE, Zhou X, Xia J, Ryan C, Thrash B, Menter A, Zhang W, and Bowcock AM. Deep sequencing of small RNAs from human skin reveals major alterations in the psoriasis miRNAome. *Human molecular genetics*. 2011;20(20):4025-40.
60. Dziunycz P, Iotzova-Weiss G, Eloranta JJ, Lauchli S, Hafner J, French LE, and Hofbauer GF. Squamous cell carcinoma of the skin shows a distinct microRNA profile modulated by UV radiation. *The Journal of investigative dermatology*. 2010;130(11):2686-9.
61. Satzger I, Mattern A, Kuettler U, Weinspach D, Niebuhr M, Kapp A, and Gutzmer R. microRNA-21 is upregulated in malignant melanoma and influences apoptosis of melanocytic cells. *Experimental dermatology*. 2012;21(7):509-14.
62. Darido C, Georgy SR, Wilanowski T, Dworkin S, Auden A, Zhao Q, Rank G, Srivastava S, Finlay MJ, Papenfuss AT, et al. Targeting of the tumor suppressor GRHL3 by a miR-21-dependent proto-oncogenic network results in PTEN loss and tumorigenesis. *Cancer cell*. 2011;20(5):635-48.
63. Yu Z, Lin KK, Bhandari A, Spencer JA, Xu X, Wang N, Lu Z, Gill GN, Roop DR, Wertz P, et al. The Grainyhead-like epithelial transactivator Get-1/Grhl3 regulates epidermal terminal differentiation and interacts functionally with LMO4. *Developmental biology*. 2006;299(1):122-36.
64. Bhandari A, Gordon W, Dizon D, Hopkin AS, Gordon E, Yu Z, and Andersen B. The Grainyhead transcription factor Grhl3/Get1 suppresses miR-21 expression and tumorigenesis in skin: modulation of the miR-21 target MSH2 by RNA-binding protein DND1. *Oncogene*. 2013;32(12):1497-507.
65. Peyrard-Janvid M, Leslie EJ, Kousa YA, Smith TL, Dunnwald M, Magnusson M, Lentz BA, Unneberg P, Fransson I, Koillinen HK, et al. Dominant mutations in GRHL3 cause Van der Woude Syndrome and disrupt oral periderm development. *American journal of human genetics*. 2014;94(1):23-32.
66. Blanpain C, and Fuchs E. Stem cell plasticity. Plasticity of epithelial stem cells in tissue regeneration. *Science*. 2014;344(6189):1242281.
67. Alonso L, and Fuchs E. Stem cells of the skin epithelium. *Proceedings of the National Academy of Sciences of the United States of America*. 2003;100 Suppl 1(11830-5).
68. Taylor G, Lehrer MS, Jensen PJ, Sun TT, and Lavker RM. Involvement of follicular stem cells in forming not only the follicle but also the epidermis. *Cell*. 2000;102(4):451-61.

69. Beck B, and Blanpain C. Mechanisms regulating epidermal stem cells. *The EMBO journal*. 2012;31(9):2067-75.
70. Levy V, Lindon C, Harfe BD, and Morgan BA. Distinct stem cell populations regenerate the follicle and interfollicular epidermis. *Developmental cell*. 2005;9(6):855-61.
71. Jaks V, Barker N, Kasper M, van Es JH, Snippert HJ, Clevers H, and Toftgard R. Lgr5 marks cycling, yet long-lived, hair follicle stem cells. *Nature genetics*. 2008;40(11):1291-9.
72. Mascre G, Dekoninck S, Drogat B, Youssef KK, Brohee S, Sotiropoulou PA, Simons BD, and Blanpain C. Distinct contribution of stem and progenitor cells to epidermal maintenance. *Nature*. 2012;489(7415):257-62.
73. Ito M, Liu Y, Yang Z, Nguyen J, Liang F, Morris RJ, and Cotsarelis G. Stem cells in the hair follicle bulge contribute to wound repair but not to homeostasis of the epidermis. *Nature medicine*. 2005;11(12):1351-4.
74. Blanpain C, and Fuchs E. Epidermal homeostasis: a balancing act of stem cells in the skin. *Nature reviews Molecular cell biology*. 2009;10(3):207-17.
75. Pattabiraman DR, and Weinberg RA. Tackling the cancer stem cells - what challenges do they pose? *Nature reviews Drug discovery*. 2014;13(7):497-512.
76. Clarke MF, Dick JE, Dirks PB, Eaves CJ, Jamieson CH, Jones DL, Visvader J, Weissman IL, and Wahl GM. Cancer stem cells--perspectives on current status and future directions: AACR Workshop on cancer stem cells. *Cancer research*. 2006;66(19):9339-44.
77. Shackleton M, Quintana E, Fearon ER, and Morrison SJ. Heterogeneity in cancer: cancer stem cells versus clonal evolution. *Cell*. 2009;138(5):822-9.
78. Nguyen LV, Vanner R, Dirks P, and Eaves CJ. Cancer stem cells: an evolving concept. *Nature reviews Cancer*. 2012;12(2):133-43.
79. Lobo NA, Shimono Y, Qian D, and Clarke MF. The biology of cancer stem cells. *Annual review of cell and developmental biology*. 2007;23(675-99).
80. Bonnet D, and Dick JE. Human acute myeloid leukemia is organized as a hierarchy that originates from a primitive hematopoietic cell. *Nature medicine*. 1997;3(7):730-7.
81. Beck B, and Blanpain C. Unravelling cancer stem cell potential. *Nature reviews Cancer*. 2013;13(10):727-38.
82. Nassar D, and Blanpain C. Cancer Stem Cells: Basic Concepts and Therapeutic Implications. *Annual review of pathology*. 2016;11(47-76).
83. Li C, Heidt DG, Dalerba P, Burant CF, Zhang L, Adsay V, Wicha M, Clarke MF, and Simeone DM. Identification of pancreatic cancer stem cells. *Cancer research*. 2007;67(3):1030-7.
84. Prince ME, Sivanandan R, Kaczorowski A, Wolf GT, Kaplan MJ, Dalerba P, Weissman IL, Clarke MF, and Ailles LE. Identification of a subpopulation of cells with cancer stem cell properties in head and neck squamous cell carcinoma. *Proceedings of the National Academy of Sciences of the United States of America*. 2007;104(3):973-8.
85. Vermeulen L, Todaro M, de Sousa Mello F, Sprick MR, Kemper K, Perez Alea M, Richel DJ, Stassi G, and Medema JP. Single-cell cloning of colon cancer stem cells reveals a multi-lineage differentiation capacity. *Proceedings of the*

- National Academy of Sciences of the United States of America*. 2008;105(36):13427-32.
86. Schatton T, Murphy GF, Frank NY, Yamaura K, Waaga-Gasser AM, Gasser M, Zhan Q, Jordan S, Duncan LM, Weishaupt C, et al. Identification of cells initiating human melanomas. *Nature*. 2008;451(7176):345-9.
 87. Malanchi I, Peinado H, Kassen D, Hussenet T, Metzger D, Chambon P, Huber M, Hohl D, Cano A, Birchmeier W, et al. Cutaneous cancer stem cell maintenance is dependent on beta-catenin signalling. *Nature*. 2008;452(7187):650-3.
 88. Schober M, and Fuchs E. Tumor-initiating stem cells of squamous cell carcinomas and their control by TGF-beta and integrin/focal adhesion kinase (FAK) signaling. *Proceedings of the National Academy of Sciences of the United States of America*. 2011;108(26):10544-9.
 89. Lapouge G, Beck B, Nassar D, Dubois C, Dekoninck S, and Blanpain C. Skin squamous cell carcinoma propagating cells increase with tumour progression and invasiveness. *The EMBO journal*. 2012;31(24):4563-75.
 90. Owens DM, and Watt FM. Contribution of stem cells and differentiated cells to epidermal tumours. *Nature reviews Cancer*. 2003;3(6):444-51.
 91. Grachtchouk M, Pero J, Yang SH, Ermilov AN, Michael LE, Wang A, Wilbert D, Patel RM, Ferris J, Diener J, et al. Basal cell carcinomas in mice arise from hair follicle stem cells and multiple epithelial progenitor populations. *The Journal of clinical investigation*. 2011;121(5):1768-81.
 92. Youssef KK, Van Keymeulen A, Lapouge G, Beck B, Michaux C, Achouri Y, Sotiropoulou PA, and Blanpain C. Identification of the cell lineage at the origin of basal cell carcinoma. *Nature cell biology*. 2010;12(3):299-305.
 93. Wang GY, Wang J, Mancianti ML, and Epstein EH, Jr. Basal cell carcinomas arise from hair follicle stem cells in Ptch1(+/-) mice. *Cancer cell*. 2011;19(1):114-24.
 94. Thieu K, Ruiz ME, and Owens DM. Cells of origin and tumor-initiating cells for nonmelanoma skin cancers. *Cancer letters*. 2013;338(1):82-8.
 95. Larsimont JC, Youssef KK, Sanchez-Danes A, Sukumaran V, Defrance M, Delatte B, Liagre M, Baatsen P, Marine JC, Lippens S, et al. Sox9 Controls Self-Renewal of Oncogene Targeted Cells and Links Tumor Initiation and Invasion. *Cell stem cell*. 2015;17(1):60-73.
 96. Huang da W, Sherman BT, and Lempicki RA. Systematic and integrative analysis of large gene lists using DAVID bioinformatics resources. *Nature protocols*. 2009;4(1):44-57.
 97. Youssef KK, Lapouge G, Bouvree K, Rorive S, Brohee S, Appelstein O, Larsimont JC, Sukumaran V, Van de Sande B, Pucci D, et al. Adult interfollicular tumour-initiating cells are reprogrammed into an embryonic hair follicle progenitor-like fate during basal cell carcinoma initiation. *Nature cell biology*. 2012;14(12):1282-94.
 98. Weinberger C, Thompson CC, Ong ES, Lebo R, Gruol DJ, and Evans RM. The c-erb-A gene encodes a thyroid hormone receptor. *Nature*. 1986;324(6098):641-6.
 99. Xu LF, Wu ZP, Chen Y, Zhu QS, Hamidi S, and Navab R. MicroRNA-21 (miR-21) regulates cellular proliferation, invasion, migration, and apoptosis by

- targeting PTEN, RECK and Bcl-2 in lung squamous carcinoma, Gejiu City, China. *PLoS one*. 2014;9(8):e103698.
100. Chan JA, Krichevsky AM, and Kosik KS. MicroRNA-21 is an antiapoptotic factor in human glioblastoma cells. *Cancer research*. 2005;65(14):6029-33.
 101. Martin del Campo SE, Latchana N, Levine KM, Grignol VP, Fairchild ET, Jaime-Ramirez AC, Dao TV, Karpa VI, Carson M, Ganju A, et al. MiR-21 enhances melanoma invasiveness via inhibition of tissue inhibitor of metalloproteinases 3 expression: in vivo effects of MiR-21 inhibitor. *PLoS one*. 2015;10(1):e0115919.
 102. Guinea-Viniegra J, Jimenez M, Schonthaler HB, Navarro R, Delgado Y, Concha-Garzon MJ, Tschachler E, Obad S, Dauden E, and Wagner EF. Targeting miR-21 to treat psoriasis. *Science translational medicine*. 2014;6(225):225re1.
 103. Wang T, Feng Y, Sun H, Zhang L, Hao L, Shi C, Wang J, Li R, Ran X, Su Y, et al. miR-21 regulates skin wound healing by targeting multiple aspects of the healing process. *The American journal of pathology*. 2012;181(6):1911-20.
 104. Gordon WM, Zeller MD, Klein RH, Swindell WR, Ho H, Espetia F, Gudjonsson JE, Baldi PF, and Andersen B. A GRHL3-regulated repair pathway suppresses immune-mediated epidermal hyperplasia. *The Journal of clinical investigation*. 2014;124(12):5205-18.
 105. Ting SB, Caddy J, Wilanowski T, Auden A, Cunningham JM, Elias PM, Holleran WM, and Jane SM. The epidermis of grhl3-null mice displays altered lipid processing and cellular hyperproliferation. *Organogenesis*. 2005;2(2):33-5.
 106. Antonini D, Sibilio A, Dentice M, and Missero C. An Intimate Relationship between Thyroid Hormone and Skin: Regulation of Gene Expression. *Frontiers in endocrinology*. 2013;4(104).
 107. van Rooij E, Sutherland LB, Liu N, Williams AH, McAnally J, Gerard RD, Richardson JA, and Olson EN. A signature pattern of stress-responsive microRNAs that can evoke cardiac hypertrophy and heart failure. *Proceedings of the National Academy of Sciences of the United States of America*. 2006;103(48):18255-60.
 108. Lu TX, Munitz A, and Rothenberg ME. MicroRNA-21 is up-regulated in allergic airway inflammation and regulates IL-12p35 expression. *J Immunol*. 2009;182(8):4994-5002.
 109. Jo A, Denduluri S, Zhang B, Wang Z, Yin L, Yan Z, Kang R, Shi LL, Mok J, Lee MJ, et al. The versatile functions of Sox9 in development, stem cells, and human diseases. *Genes & diseases*. 2014;1(2):149-61.
 110. Matheu A, Collado M, Wise C, Manterola L, Cekaite L, Tye AJ, Canamero M, Bujanda L, Schedl A, Cheah KS, et al. Oncogenicity of the developmental transcription factor Sox9. *Cancer research*. 2012;72(5):1301-15.
 111. Wang H, McKnight NC, Zhang T, Lu ML, Balk SP, and Yuan X. SOX9 is expressed in normal prostate basal cells and regulates androgen receptor expression in prostate cancer cells. *Cancer research*. 2007;67(2):528-36.
 112. Nowak JA, Polak L, Pasolli HA, and Fuchs E. Hair follicle stem cells are specified and function in early skin morphogenesis. *Cell stem cell*. 2008;3(1):33-43.

113. Shi G, Sohn KC, Li Z, Choi DK, Park YM, Kim JH, Fan YM, Nam YH, Kim S, Im M, et al. Expression and functional role of Sox9 in human epidermal keratinocytes. *PloS one*. 2013;8(1):e54355.
114. Larsimont JC, and Blanpain C. Single stem cell gene therapy for genetic skin disease. *EMBO molecular medicine*. 2015;7(4):366-7.
115. Catalano V, Dentice M, Ambrosio R, Luongo C, Carollo R, Benfante A, Todaro M, Stassi G, and Salvatore D. Activated Thyroid Hormone Promotes Differentiation and Chemotherapeutic Sensitization of Colorectal Cancer Stem Cells by Regulating Wnt and BMP4 Signaling. *Cancer research*. 2016;76(5):1237-44.
116. Wang T, Lu XJ, Chi JC, Ding M, Zhang Y, Tang XY, Li P, Zhang L, Zhang XY, and Zhai B. Microwave ablation of hepatocellular carcinoma as first-line treatment: long term outcomes and prognostic factors in 221 patients. *Scientific reports*. 2016;6(32728).
117. Trempus CS, Morris RJ, Bortner CD, Cotsarelis G, Faircloth RS, Reece JM, and Tennant RW. Enrichment for living murine keratinocytes from the hair follicle bulge with the cell surface marker CD34. *The Journal of investigative dermatology*. 2003;120(4):501-11.
118. Trempus CS, Morris RJ, Ehinger M, Elmore A, Bortner CD, Ito M, Cotsarelis G, Nijhof JG, Peckham J, Flagler N, et al. CD34 expression by hair follicle stem cells is required for skin tumor development in mice. *Cancer research*. 2007;67(9):4173-81.
119. Grachtchouk M, Rong M, Yu S, Zhang XY, Sasaki H, Hui CC, and Dlugosz AA. Basal cell carcinomas in mice overexpressing Gli2 in skin. *Nature genetics*. 2000;24(3):216-7.

Reciprocal interplay between thyroid hormone and microRNA-21 regulates hedgehog pathway–driven skin tumorigenesis

Daniela Di Girolamo,¹ Raffaele Ambrosio,² Maria A. De Stefano,¹ Giuseppina Mancino,¹ Tommaso Porcelli,¹ Cristina Luongo,¹ Emery Di Cicco,¹ Giulia Scalia,³ Luigi Del Vecchio,³ Annamaria Colao,¹ Andrzej A. Dlugosz,⁴ Caterina Missero,^{3,5} Domenico Salvatore,^{1,3} and Monica Dentice¹

¹Department of Clinical Medicine and Surgery, University of Naples "Federico II," Naples, Italy. ²Istituto Di Ricovero e Cura a Carattere Scientifico SDN, Naples, Italy. ³CEINGE-Biotecnologie Avanzate, Naples, Italy. ⁴Department of Dermatology and Comprehensive Cancer Center, University of Michigan, Ann Arbor, Michigan, USA. ⁵Department of Biology, University of Naples "Federico II," Naples, Italy.

The thyroid hormone–inactivating (TH-inactivating) enzyme type 3 iodothyronine deiodinase (D3) is an oncofetal protein that is rarely expressed in adult life but has been shown to be reactivated in the context of proliferation and neoplasms. D3 terminates TH action within the tumor microenvironment, thereby enhancing cancer cell proliferation. However, the pathological role of D3 and the contribution of TH metabolism in cancer have yet to be fully explored. Here, we describe a reciprocal regulation between TH action and the cancer-associated microRNA-21 (miR21) in basal cell carcinoma (BCC) skin tumors. We found that, besides being negatively regulated by TH at the transcriptional level, miR21 attenuates the TH signal by increasing D3 levels. The ability of miR21 to positively regulate D3 was mediated by the tumor suppressor gene *GRHL3*, a hitherto unrecognized D3 transcriptional inhibitor. Finally, in a BCC mouse model, keratinocyte-specific D3 depletion markedly reduced tumor growth. Together, our results establish TH action as a critical hub of multiple oncogenic pathways and provide functional and mechanistic evidence of the involvement of TH metabolism in BCC tumorigenesis. Moreover, our results identify a miR21/*GRHL3*/D3 axis that reduces TH in the tumor microenvironment and has potential to be targeted as a therapeutic approach to BCC.

Introduction

Basal cell carcinoma (BCC) is the most frequently diagnosed human cancer and accounts for approximately 80% of all nonmelanoma skin cancers. BCC formation is based on a combination of inherited and environmental factors, mainly UV irradiation and long-term sun exposure. Proliferation and survival of BCC cells is physiologically regulated by the hedgehog (Hh) pathway, which plays a pivotal role in embryogenic development and tumorigenesis (1–4). Sporadic BCCs in humans are predominantly due to inactivation of *PTCH1*, an inhibitor of Hh signaling, and the consequent activation of Gli transcription factors (5, 6). Therapeutics targeting Sonic hedgehog (SHH) signaling are now being used in patients and represent an important nonsurgical approach to interfere with BCC occurrence and growth (7).

Type 3 iodothyronine deiodinase (D3, encoded by the *DIO3* gene) is an oncofetal protein commonly deregulated in a wide range of adult tissues and re-expressed in cancer (8). D3 belongs to the deiodinase family of enzymes, which regulate thyroid hormone (TH) availability in target cells, thereby allowing the intracellular adaptation of the TH signal (9). The major product of the thyroid gland is T4, while the only active TH (T3) derives from the conversion of T4 into T3 catalyzed by the deiodinases D1 and D2. D3

degrades T4 and T3 into inactive metabolites and is thus the major physiological inactivator of TH (9). D3 is overexpressed in BCCs of both mouse and human origin, and is under the control of SHH, which increases D3 expression by acting via a conserved *GLI2* binding site on the human *DIO3* promoter (10). By decreasing TH action in the BCC microenvironment, D3 promotes BCC tumorigenesis. In addition, *GLI2* and the SHH pathway are negative targets of TH, which thus attenuates cancer formation (11).

Among all cancer-related microRNAs (miRNAs), miR21 has been related to the pathogenesis of various malignant tumors, including prostate, gastric, colon, breast, and lung cancer (12–20). Apart from being involved in cancerogenesis, miR21 plays a crucial role in a plethora of biological functions and diseases, namely development, cardiovascular diseases, and inflammation (21). miR21 is also expressed in skin (22–24), and its potential role as a regulator of skin homeostasis is demonstrated by its upregulation in such diseases as psoriasis, atopic dermatitis (25, 26), melanoma, and squamous cell carcinoma (SCC) (27–29). However, nothing is known about miR21 expression in BCC.

GRHL3 is a transcription factor expressed in the skin in the differentiated suprabasal layers, and is essential for epidermal differentiation and barrier formation at the end of mouse embryogenesis (30–33). *Grhl3* KO mice exhibit impaired epidermal differentiation and decreased expression of several genes involved in barrier formation (32). Accordingly, in humans, dominant-negative *GRHL3* mutations are associated with defective periderm

Conflict of interest: The authors have declared that no conflict of interest exists.

Submitted: September 9, 2015; **Accepted:** March 11, 2016.

Reference information: *J Clin Invest*. doi:10.1172/JCI84465.

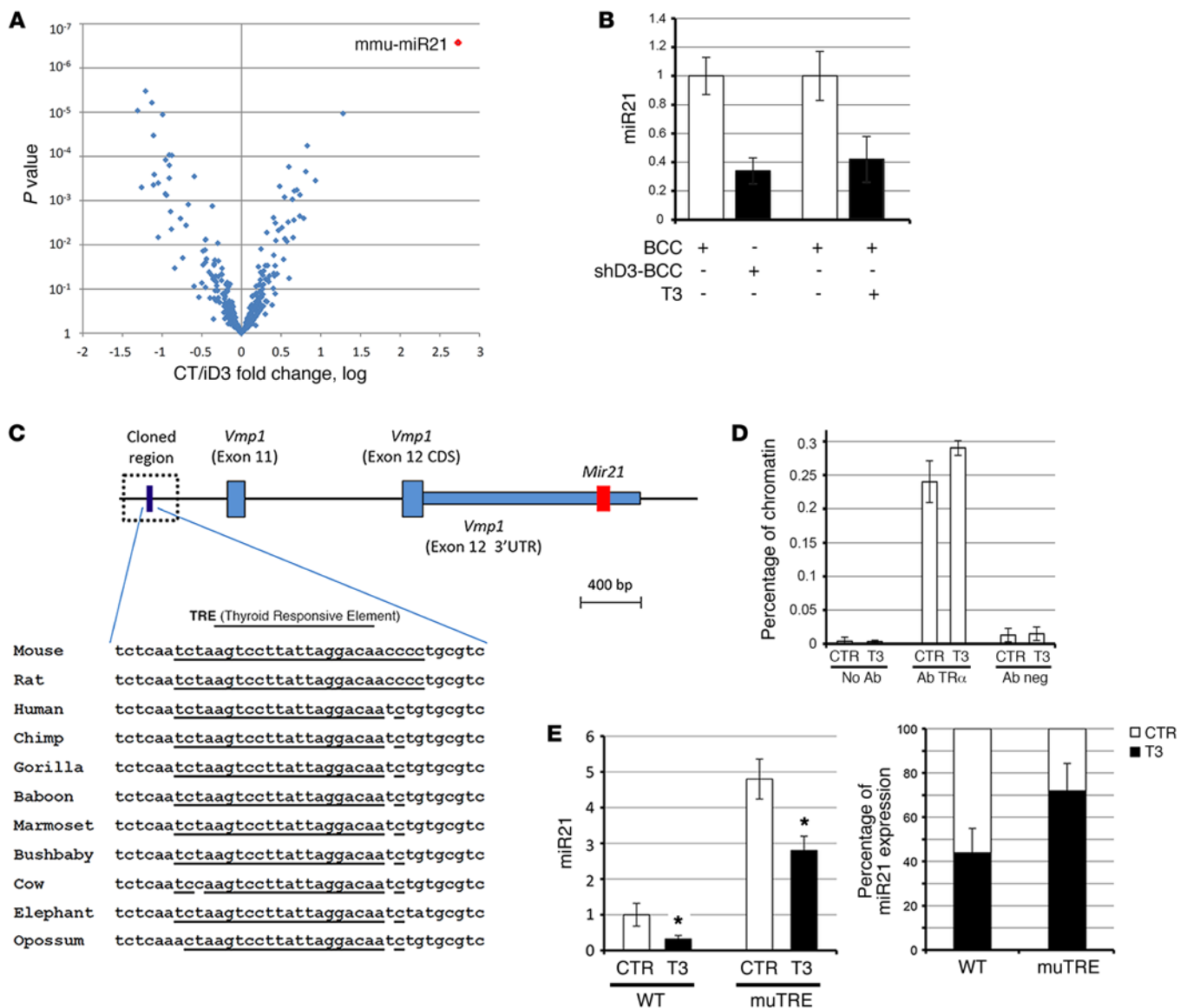


Figure 1. TH represses miR21 in mouse and human BCC. (A) Genome-wide miRNA expression analysis in D3-depleted and control BCC cells. All the deregulated miRNAs in shD3 relative to control cells are plotted against the *P* value. mmu-miR21, murine miR-21. (B) miR21 expression was measured by TaqMan real-time PCR in cDNAs from control BCC, shD3, and BCC cells treated with 30 nM T3 for 48 hours. (C) Schematic structural organization of the miR21 gene (red) and the miR21 enhancer region. The expression of the thyroid hormone-responsive element (TRE) and its comparison between species are indicated below. (D) ChIP analysis of the interaction between TR α and the miR21 enhancer region. Chromatin extracted from BCC cells was immunoprecipitated using the indicated antibodies. (E) miR21 expression was measured by TaqMan PCR in BCC cells carrying a mutated TRE element in the miR21 region (mut-TRE) and control BCC cells (WT) treated or not with 30 nM T3 for 48 hours. Right: Reduction of miR21 in T3-treated cells versus nontreated cells in WT cells and CRISPR/Cas9-mediated TRE-mutated cells. **P* < 0.05. Data represent the mean of at least 3 independent experiments in duplicate. SDs are indicated. Differences between samples were assessed by Student's 2-tailed *t* test for independent samples.

development in Van der Woude syndrome (34). Moreover, GRHL3 was found to be a potent tumor suppressor in mouse and human SCC, and an upstream regulator of PTEN (31).

In this study we demonstrate that miR21 is a negative TH target. Moreover, besides being regulated by TH, miR21 also modulates TH metabolism by inducing D3 expression. Importantly, we found that a miR21 target gene, *GRHL3*, which is essential for keratinocyte differentiation, is a novel suppressor of D3 to our knowledge and accounts for the positive regulation of miR21 on D3 levels.

Our data demonstrate the existence of a miR21/GRHL3/D3 regulatory circuit that leads to a reduction of the TH signal

in the tumor microenvironment. Disruption of this regulation in vivo drastically attenuates the oncogenic potential of BCC cells. Indeed, targeted mutagenesis of D3 potently reduces the tumorigenic ability of BCC cells and of miR21-overexpressing BCC cells in a xenograft mouse model. Furthermore, genetic D3 depletion in the keratinocyte compartment drastically reduced formation of BCC-like tumors in a GLI2-driven mouse model.

Together, our results provide what we believe to be novel insight into the function of TH in regulating the skin tumorigenic program and reveal a general mode of TH downregulation by oncogenic signals.

Results

TH regulates the expression of multiple miRNAs and, in particular, downregulates miR21 in BCC. We previously showed that TH regulates the proliferative potential of BCC cells in vitro and in vivo (10, 11). To explore whether TH action in BCC involves the regulation of miRNAs, we analyzed the differential expression of mature miRNAs (miChip) in D3-silenced mouse BCC cells. We used a microarray platform of miRNA, the Exiqon platform (miRCURY LNA Arrays; Exiqon, Denmark), to compare the expression of miRNAs in BCC cells transfected with a control scrambled shRNA oligo versus the D3-targeting shRNA oligo (10). This analysis showed that 46 miRNAs were differentially expressed (Supplemental Table 1; supplemental material available online with this article; doi:10.1172/JCI84465DS1). Among them, we selected miR21 for further studies, since it is overexpressed in a wide variety of cancers and has been causally linked to cell proliferation, apoptosis, and migration (12, 13), and, importantly, it is the most sensitive target upon D3 depletion (variation of 6.62-fold; Figure 1A and Supplemental Table 1).

We validated miR21 as a negative TH target gene by measuring the mature miR21 transcript by TaqMan RT-PCR and by Northern blotting of BCC cells treated with TH (30 nM T3), and in D3-depleted BCC cells (shD3) (10), in which the TH signal was amplified (Figure 1B and Supplemental Figure 1A). Accordingly, while repressed by TH treatment and D3 depletion, miR21 was upregulated by D3 overexpression and by TH deprivation in serum (Supplemental Figure 1, B and C). To explore the possibility that TH directly inhibits miR21 transcription, we analyzed the sequence of the miR21 enhancer region (35). In silico analysis revealed a conserved thyroid hormone-responsive element-binding (TRE-binding) site within the enhancer (Figure 1C). We cloned 389 bp of the enhancer within the pGL3-basic vector to perform functional studies in the human embryonic kidney (HEK) 293 cell line and in mouse BCC cells. As shown in Supplemental Figure 2, A and B, the miR21 enhancer was efficiently downregulated by TH and by double thyroid receptor transfection/TH treatment in both cell lines, thus demonstrating that TH represses the transcription of the pre-miR21. ChIP analysis revealed that the thyroid receptor (TR) physically binds to the newly identified TRE (Figure 1D). Furthermore, we mutagenized the core motif of the TRE within the miR21 enhancer region using CRISPR/Cas9 technology in the BCC cells. Effective mutagenesis was confirmed by sequencing of the DNA of clones containing the mutated TRE. One of the positive clones was treated with T3, and miR21 expression was measured using TaqMan PCR. As shown in Figure 1E, the endogenous miR21 was expressed at higher levels in cells with mutated TRE when compared with the control, WT BCC cells. Furthermore, the repression of miR21 by T3 was partially reduced in cells with mutated TRE, which demonstrates that mutation of the TRE attenuates the effect of T3 on miR21 (Figure 1E, right). The fact that TRE mutation does not completely abolish the regulation of T3 on miR21 suggests the existence of multiple TREs in other parts of the miR21 regulatory elements. Together, these results point to a negative regulation of T3 on the miR21 transcription via a direct T3-TR binding to the miR21 enhancer.

miR21 positively regulates D3 expression. Next, we explored the potential of miR21 to modulate the TH signal in BCC cells. To this aim, we measured the expression of deiodinases D2 and D3 and

other TH signaling modulators (TR α and TR β , MCT8 and MCT10) in BCC cells and in BCC cells transiently overexpressing miR21. While *DIO2* mRNA, the TH receptors, and the transporters were not modified by miR21 expression (Supplemental Figure 3), overexpression of miR21 strongly over induced D3 levels in a time-dependent manner (Figure 2A and Supplemental Figure 3).

We then inhibited miR21 in BCC cells by transfecting the LNA oligonucleotide complementary to miR21 (anti-miR21). In accordance with its role as an inducer of D3 expression, miR21 inhibition potently reduced D3 expression at the mRNA and protein levels (Figure 2B). Importantly, overexpression of miR21 also attenuated intracellular TH action as indicated by the cotransfection of increasing amounts of miR21 together with an artificial T3-responsive promoter (Figure 2C).

miR21 induces D3 expression by targeting the tumor suppressor GRHL3. miRNAs often inhibit mRNA expression at the post-transcriptional level. Since D3 is induced by miR21, we tested the hypothesis that a direct miR21 target, and putative suppressor of D3, might mediate this effect. To this aim, we searched for miR21 downstream targets that could potentially inhibit D3 expression. By using the computational algorithm TargetScan (<http://www.targetscan.org/>) together with published and/or validated miR21 target genes, we obtained a list of genes potentially controlled by miR21 (Supplemental Table 2). This list was further analyzed with the DAVID program for functional classification (36). By selecting the categories of "Regulation of transcription," "Epidermal development," and "Tumor suppressor," we found only a few genes that were present in all these 3 categories (Figure 2D). We tested the ability of 3 different genes belonging to these categories, *TP63*, *KLF5*, and *GRHL3*, to affect D3 expression. Among these, only 1 gene repressed D3 expression, namely *GRHL3* (Figure 2E and Supplemental Figure 4).

GRHL3 is a tumor suppressor functionally related to SCC formation (31, 33). We first evaluated the expression of *GRHL3* in BCC and normal skin, and, as shown in Supplemental Figure 5A, we observed that *GRHL3* is highly expressed in normal skin and in WT keratinocytes, while it is repressed in BCC tissues and cells. We also tested whether *GRHL3* is a miR21 downstream target in the BCC cells, as already demonstrated in other cell contexts (31). BCC cells transfected with miR21 or with anti-miR21 LNA (shown in Figure 2, A and B) were analyzed for *GRHL3* mRNA and protein expression. miR21 overexpression reduced *GRHL3*, while miR21 silencing increased *GRHL3* levels, thus validating *GRHL3* as a miR21 target in the BCC cell context (Supplemental Figure 6). Importantly, the same effects were observed in primary cultures of keratinocytes, in which, thanks to the very low level of endogenous miR21, overexpression of miR21 changed *DIO3* and *GRHL3* to a much greater extent than it did in BCC cells (Figure 2F).

To determine whether *GRHL3* indeed negatively regulates D3, we knocked down the endogenous protein using 2 different siRNA oligos (siGRHL3-1 and siGRHL3-2). D3 levels were significantly higher in BCC cells transfected with 1 or more siGRHL3 oligos than in BCC cells transfected with scrambled oligos (siCTR). This result confirms that *GRHL3* is a repressor of D3 expression (Figure 2G and Supplemental Figure 5B).

We next tested whether *GRHL3* directly binds to the *Dio3* promoter. In silico analysis revealed a putative *GRHL3* binding site within the promoter region of the *Dio3* gene (G1: GCGAAC-

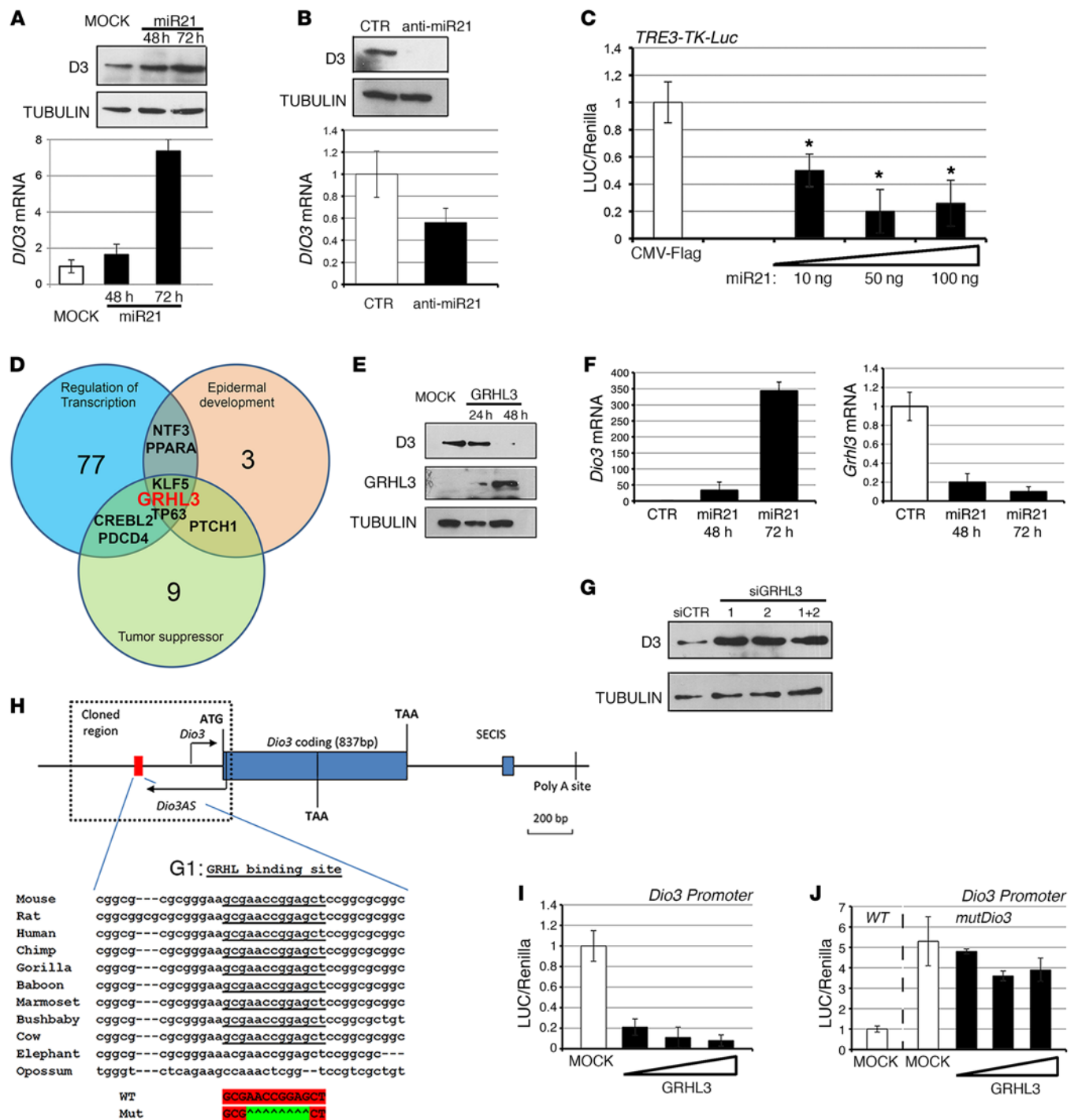


Figure 2. miR21 upregulates D3 expression by targeting GRHL3. (A) BCC cells were transiently transfected with miR21 expression plasmid, and cells were collected at the indicated times. D3 mRNA and protein were measured by real-time PCR and Western blot (see complete unedited blots in the supplemental material). (B) LNA anti-miR21 or a control LNA-scrambled oligo was transfected in BCC cells, and D3 mRNA and protein were measured as in A. (C) BCC cells transfected with the artificial T3-responsive promoter TRE3-TK-Luc and CMV-renilla as internal control. Increasing amounts of miR21 were cotransfected, and cells were analyzed for luciferase activity. The results are shown as means \pm SD of the luciferase/renilla (LUC/Renilla) ratios from at least 3 separate experiments, performed in duplicate. (D) miR21 target genes were classified for functional classification with the DAVID program (36). (E) D3 protein levels were measured by Western blot in BCC cells transfected with Flag-GRHL3 and harvested at the indicated times. GRHL3 (anti-Flag) and tubulin levels were measured as control. (F) Primary cultures of keratinocytes were transfected with miR21, and cells were harvested at 48 and 72 hours. *Dio3* and *Grhl3* mRNAs were measured by real-time PCR. (G) BCC cells were transfected with 2 different siRNAs targeting endogenous *Grhl3* oligos or a combination of them, and D3 protein was measured by Western blot analysis. (H) Schematic representation of the *Dio3* locus, the *Dio3* promoter, and the G1 site (red) responsive to GRHL. (I and J) BCC cells were transiently transfected with *Dio3*-Luc promoter (I) or *Dio3*-Luc and *mutDio3*-Luc promoters (J) and with increasing amounts of the GRHL3 plasmid. Cells were harvested 48 hours after transfection and analyzed for luciferase activity. CMV-renilla was cotransfected as internal control. The results are shown as means \pm SD of the LUC/renilla ratios from at least 3 separate experiments, performed in duplicate. * $P < 0.05$.

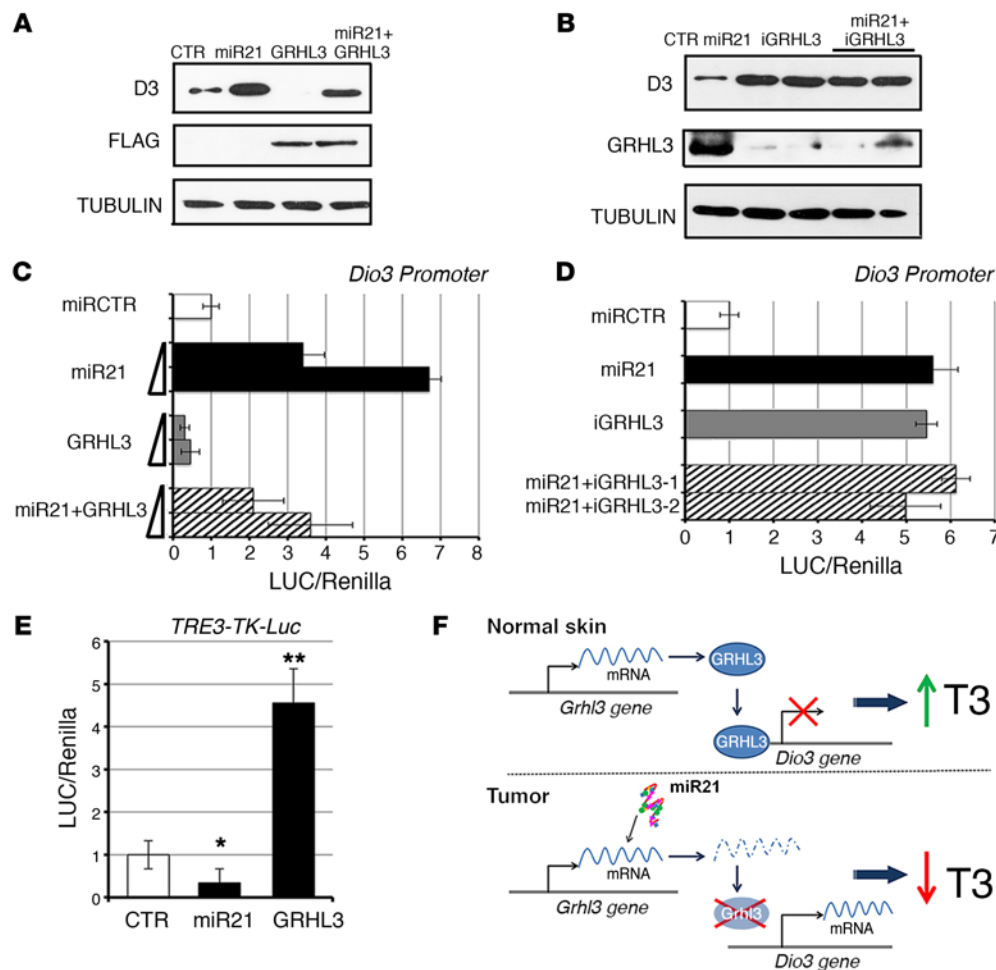


Figure 3. The miR21/GRHL3 axis regulates D3 expression and TH intracellular concentration. (A) D3 protein levels were measured by Western blot from BCC cells transfected with miR21, GRHL3, and the 2 expression plasmids together. Lysates were also probed with anti-Flag antibody as control of Flag-GRHL3 transfection efficiency. (B) BCC cells were transfected with miR21 and miR21 plus 2 different siRNAs for GRHL3 knockdown. Anti-GRHL3 antibody was used as internal control of GRHL3 knockdown. (C and D) The *Dio3* promoter was cotransfected with the indicated constructs together with CMV-renilla as internal control. Luciferase activity was measured and reported as means \pm SD of the LUC/renilla ratios from at least 3 separate experiments, performed in duplicate. (E) The T3-responsive promoter TRE3-TK-Luc was cotransfected in BCC cells with the indicated plasmids. Luciferase activity was measured as in C and D. $*P < 0.05$, $**P < 0.01$. (F) The miR21/GRHL3/D3 axis regulates intracellular T3 availability.

CGGAGCT), which is highly conserved, and located 436 bp from the ATG codon (Figure 2H). Functional studies demonstrated that GRHL3 binds to the G1 site and represses the activity of the *Dio3* promoter. Indeed, cotransfection of the mouse *Dio3* promoter (pmD3Luc) with increasing amounts of GRHL3 showed that the *Dio3* promoter is potently inhibited by GRHL3 (Figure 2I). Mutation of the G1 site within the *Dio3* promoter revealed that, while the basal activity of the mutated promoter was increased as expected, the GRHL3-induced repression was abolished (Figure 2, I and J, and Supplemental Figure 6D). These data indicate that the tumor suppressor GRHL3 is a direct repressor of D3.

To assess the contribution of GRHL3 to the miR21-dependent D3 upregulation, we transfected miR21 or GRHL3 or both in BCC cells (Figure 3A). The forced expression of GRHL3 downregulated D3 expression and, most importantly, abolished the miR21-mediated induction of D3 (Figure 3A). This observation was confirmed by a different approach, cotransfection of the *Dio3* promoter with miR21 alone and with miR21 plus GRHL3. Also in this context, GRHL3 antagonized the effects induced by miR21 on D3 (Figure 3C). Interestingly, concomitant miR21 overexpression and GRHL3 downregulation by siRNA did not result in synergistic D3 upregulation, which reinforces the concept that suppression of GRHL3 is the mechanism by which miR21 enhances D3 (Figure 3, B and D). Notably, miR21 and GRHL3 expression ultimately decreased and increased, respectively, the effect of TH in the nucleus (Figure 3E).

Furthermore, when the G1 site in the *Dio3* promoter was mutated, miR21 failed to regulate D3 expression, thus reinforcing the finding that GRHL3 is the only gene mediating miR21-dependent D3 regulation (Supplemental Figure 6D). The picture that emerges from these results is that miR21 upregulates D3 expression by inhibiting the D3 repressor GRHL3.

Since TH negatively regulates miR21, we tested the possibility that TH treatment could in turn increase GRHL3 expression. Indeed, we observed that T3 treatment positively regulates GRHL3 and that this effect is mediated by miR21, as demonstrated by the results of T3 treatment and miR21 silencing shown in Supplemental Figure 7.

The identified miR21/GRHL3/D3 axis and its ability to modulate TH activity are depicted in Figure 3F.

BCC tumorigenesis requires an intact miR21/GRHL3/D3 axis. To assess the functional role of the newly identified network, we sought to disrupt the miR21/D3 axis by depleting D3 or by inducing miR21 in a genetic *Dio3*-null background in vitro and in vivo. We used the CRISPR/Cas9 technology to genetically deplete D3 in BCC cells (D3KO clones). We also stably overexpressed miR21 in BCC cells (miR cells). One representative D3KO clone was subsequently stably transfected with the miR21 plasmid, and double D3KO-miR21-overexpressing cells were selected (D3KO-miR cells). We first confirmed D3 depletion in D3KO clones (Supplemental Figure 8, A–C), and miR21 and D3 expression in miR cells (Supplemental Figure 8, D and E) and in double D3KO-miR cells (Supplemental Figure 8, F and G).

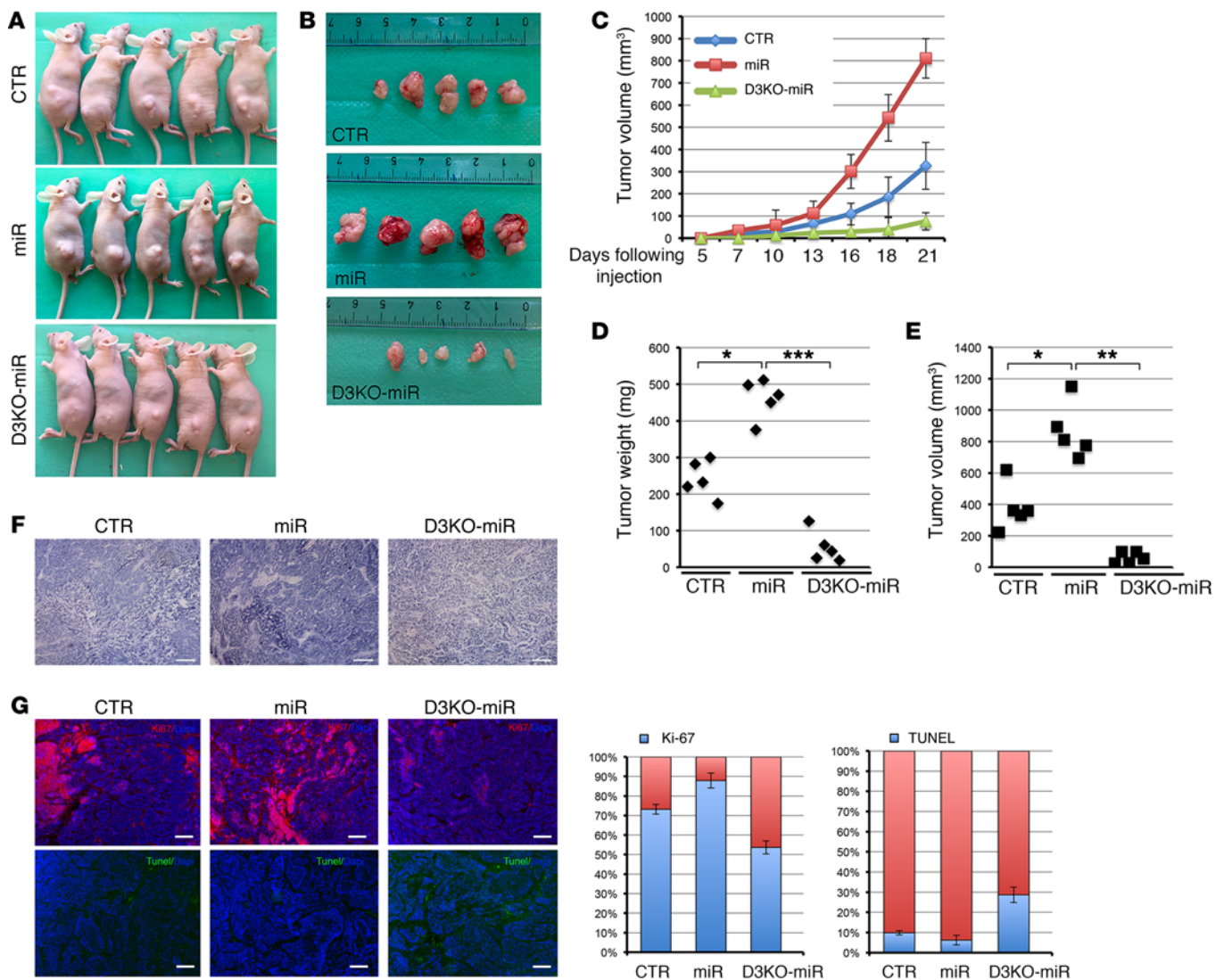


Figure 4. Targeted D3 depletion drastically reduces the tumorigenic potential of BCC cells in nude mice. (A and B) 1×10^6 per $100 \mu\text{l}$ of control CRISPR-CTR cells (CTR), stable miR21-overexpressing (miR) BCC cells, CRISPR/Cas9-D3KO cells (D3KO), and double D3KO-miR cells were injected s.c. into the flanks of nude mice. Mice were collected 3 weeks after injection, and tumors were measured as indicated in Methods. (C) Tumor volume was measured with a caliper for 3 weeks in CTR, miR, and D3KO-miR cells deriving tumors. (D and E) Tumor weight and volume measured 3 weeks after cell injection. (F and G) Tumor sections were analyzed by H&E staining and by immunofluorescence for Ki-67 and TUNEL expression in the indicated tumors. Scale bars: $100 \mu\text{m}$. Right: Percentage of Ki-67-positive and TUNEL-positive cells. * $P < 0.05$, ** $P < 0.01$, *** $P < 0.001$.

Because the level of miR21 was higher in BCC tissue than in normal skin (Figure 1, F and G), we tested whether the increase of miR21 exceeded its basal levels of transcription. Indeed, we observed that miR21 is 10-fold overexpressed in miR clones versus control BCC cells (Supplemental Figure 8D). GRHL3 expression was very low in all generated cells and was further suppressed by miR21 overexpression (Supplemental Figure 8, H and I).

We next subcutaneously injected the cells generated into athymic (nude) mice and examined the weight and morphology of the resulting subcutaneous xenograft tumors. Tumors originating from miR cells grew rapidly, and were palpable 2 weeks after injection (Figure 4, A and B). D3KO-miR cells generated much smaller tumors, which become palpable 3 weeks after injection, while D3KO cells did not generate tumors (Figure 4, A–C). Importantly, miR21 overexpression exacerbated tumorigenesis versus control BCC cells (Figure 4,

A–C). On the contrary, D3 ablation almost completely abolished the tumorigenic advantage acquired upon miR21 overexpression; consequently, D3 depletion results in a potent antitumoral effect even in the presence of an excess of miR21. We found a 3.54-fold reduction (D3KO-miR) and a 2.04-fold increase (miR21) in tumor weight, and a 4.2-fold reduction (D3KO-miR) and a 2.2-fold increase (miR21) in tumor volume, compared with control cell-generated tumors (Figure 4, D and E). Accordingly, H&E, Ki-67, and TUNEL staining showed that control and miR-derived tumors have a high mitotic grade, while D3KO-miR-derived tumors showed multiple areas of cell death (Figure 4, F and G). Consistent with increased D3 expression in miR cells versus control cells, D3 mRNA and protein were upregulated in tumors overexpressing miR21 (Supplemental Figure 9). Furthermore, none of the generated tumors expressed GRHL3, thus confirming the tumor-suppressor role of this transcriptional factor (Supplemental Figure 10).

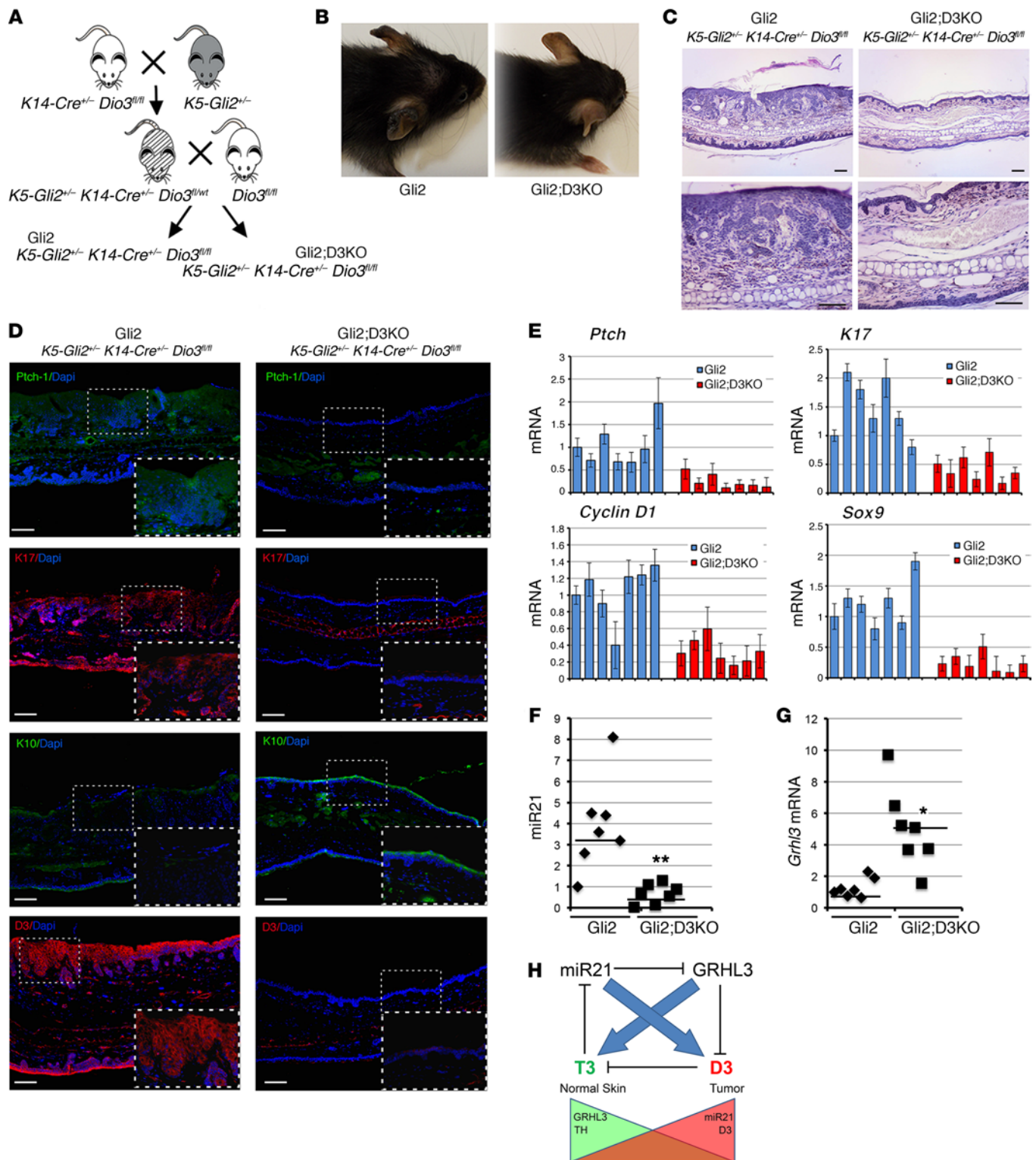


Figure 5. Epidermal D3 depletion significantly reduces Gli2-driven BCC-like tumor formation and inhibits miR21 expression. (A) Genetic D3 depletion was specifically induced in keratinocytes by crossing of *K5-Gli2* *K14-Cre*^{+/+} with *Dio3*^{fl/fl} mice. (B) Mice were analyzed at 6 months of age when BCC-like formations were abundant and readily visible on the ears of control (Gli2) mice ($n = 11$). (C) Histological analysis of ears from Gli2 and Gli2;D3KO mice. H&E stainings were performed on sections of ears from Gli2 and Gli2;D3KO mice. Scale bars: 100 μm . (D) Immunofluorescent staining for PTCH1, K17, K10, and D3 expression. Scale bars: 100 μm . (E) Real-time PCR analysis to measure the expression of the indicated genes in Gli2 versus Gli2;D3KO mice ($n = 7$). (F and G) miR21 and *Grhl3* expression was measured in the ears from Gli2 and Gli2;D3KO mice ($n = 7$). (H) Schematic representation of the mutual, negative-feedback loop by which TH regulates miR21 and miR21 controls intracellular TH through GRHL3. * $P < 0.05$, ** $P < 0.01$.

Genetic D3 depletion potently reduces BCC-like tumor growth in vivo. Having shown that D3 depletion drastically attenuates BCC tumorigenesis and miR21 oncogenic potential in xenografts, we evaluated the role of D3 depletion in genetically induced BCC tumors in vivo. To this aim, we generated a keratinocyte-specific conditional D3-null mouse (*K14-Cre^{+/+} Dio3^{fl/fl}*) in a mouse model developing BCC-like tumors (*K5-Gli2*) (37), thereby generating a spontaneously forming mouse BCC-like model in an epidermal-specific D3-null background, namely, *K5-Gli2 K14-Cre^{+/+} Dio3^{fl/fl}*, henceforth referred to as “Gli2;D3KO” (Figure 5A), while *K5-Gli2 K14-Cre^{-/-} Dio3^{fl/fl}* mice (referred to as “Gli2”) served as controls. Constitutive activation of GLI2 in keratinocytes of Gli2 mice resulted in epidermal hyperplasia, BCC, and basaloid follicular hematoma with conspicuous down-growth, arising mostly on the ears of mice at 6 months of age (Figure 5, B and C, and Supplemental Figure 6). Strikingly, *Dio3* deletion in Gli2;D3KO mice reduced the number and size of tumors (Figure 5, B and C, and Supplemental Figure 6). The few lesions that developed on the ears of Gli2;D3KO mice were much smaller than those found in Gli2 mice. Expression of the BCC markers K17 and PTCH1 and SOX9 was drastically reduced in D3-depleted mice as measured by immunofluorescence and RT-PCR (Figure 5, D and E). Additionally, K10, a marker of the differentiating layers of the epidermis, was significantly downregulated in Gli2 mice, while it was well preserved in Gli2;D3KO mice (Figure 5D).

We next evaluated whether, by enhancing TH levels, D3 ablation in skin could affect the expression of miR21 and GRHL3 in the tumor. As shown in Figure 5, F and G, miR21 was drastically reduced upon D3 depletion, while GRHL3 was upregulated in the absence of D3.

The data reported in this section indicate a functional requirement of D3 for growth in Hh pathway-driven skin tumors. These data also suggest that effective D3 loss and consequent TH activation lead to a remarkable attenuation of miR21 expression in vivo in BCC and a corresponding increase in the miR target GRHL3, and functionally validate our model of a reciprocal regulation of TH on miR21 and miR21 over TH metabolism in skin. The TH-miR21 interplay is schematically represented in Figure 5H.

The miR21/GRHL3/D3 axis is recapitulated in human BCC. Lastly, we sought to address whether the regulation of T3 on miR21 and GRHL3 is recapitulated also in human BCC. To this aim, we evaluated miR21 levels in 16 human BCC tissues versus samples of healthy skin from the same patients by TaqMan real-time RT-PCR. In accordance with the concept that miR21 is a marker of tumorigenesis, miR21 was expressed at significantly higher levels in BCC tissue than in the healthy skin samples (12.05-fold, $P = 6.2 \times 10^{-8}$; Figure 6A). Similar miR21 overexpression in tumors occurred in mouse BCC cells and tumors (Supplemental Figure 11). We also measured *GRHL3* and *DIO3* expression in the human samples (Figure 6, B and C). As expected, *GRHL3* was highly expressed in normal skin and drastically repressed in most of the BCC samples. D3 expression correlated with miR21 expression (Figure 6C).

Considering that miR21 and D3 are upregulated in human BCC, and GRHL3 is remarkably lower in BCC than in nontumor tissues, we performed a correlation analysis between miR21/GRHL3, miR21/D3, and GRHL3/D3 expression in BCC tissues. Using Pearson's correlation analysis, we observed a significant

inverse correlation between miR21 and GRHL3 and between D3 and GRHL3; conversely, miR21 expression and D3 expression were linked by a positive correlation (Figure 6, D–F; miR21 vs. GRHL3: $R = -0.35$, $P = 0.048$; miR21 vs. D3: $R = 0.5$, $P = 0.0049$; GRHL3 vs. D3: $R = -0.35$, $P = 0.048$). The inverse correlation between miR21 and GRHL3 is in line with the demonstration by Bhandari et al. that miR21 negatively regulates GRHL3 in skin (33). Taken together, these results confirm the model established in our study and suggest that targeting D3 and increasing the TH signal might represent a therapeutic approach to BCC.

Discussion

Here we describe what we believe to be a novel network by which TH signaling, by modulating miRNA expression, interacts with oncogenic pathways to regulate the growth of BCC tumors. T3 suppresses miR21 expression, thus attenuating BCC, and is contextually regulated by miR21 through the control of the TH-inactivating enzyme D3. These conclusions are supported by genome-wide, biochemical, and expression data coupled with functional studies in vivo in xenografts and in a BCC mouse model.

TH deregulation is frequent in human tumors, but it is not known whether it is a bystander event or whether it might drive or control cancer growth in vivo. Notably, the TH-inactivating enzyme D3 is upregulated in many human tumors and cancer cell lines (8). Determining the role of TH in cancer is challenging, mostly because TH plays pleiotropic roles in the body and it has been shown to trigger distinct, even opposing, functions in different cellular districts. On the basis of in vitro findings and studies conducted with a xenograft model, we previously reported that TH induces apoptosis and inhibits cell-cycle progression in BCC (10, 11). Our present findings complement these previous reports and extend the function of TH in BCC to the control of miR21-dependent oncogenic action. Importantly, using a unique skin-specific *Dio3* KO mouse model, we provide the first in vivo genetic evidence that D3 depletion, which is equivalent to TH treatment, drastically reduces BCC formation.

TH signaling, miR21, and cancer. The classical mode of TH action is mainly mediated by nuclear receptors, the TRs, which are ligand-dependent transcription factors that bind to TREs in the promoter of target genes. In the absence of the ligand, TRs are associated with corepressors and with histone deacetylases, thereby preventing transcription. Upon T3 binding, the repressive complex is destabilized and corepressors are replaced by coactivators that ultimately recruit RNA polymerase II in transcription of target genes (38). Many cell cycle-related and proliferation-controlling genes are TH targets, and, as such, TH positively or negatively controls cell proliferation and differentiation in various contexts (8). Moreover, TH signaling is often compromised in carcinogenesis as demonstrated by the reduced expression or deletion of TR genes in human cancers, which suggests that TRs could function as tumor suppressors. The inverse association between TH and cancer was confirmed by the findings that the *v-erb-a* oncogene, which is the avian erythroblastosis gene, is a mutated form of the *THRA* gene (coding for the TR α protein) (39), and that *v-erb-a* antagonizes T3 function in avian erythroblastosis virus-transformed erythroleukemic cells, thereby blocking T3-dependent cell differentiation (40).

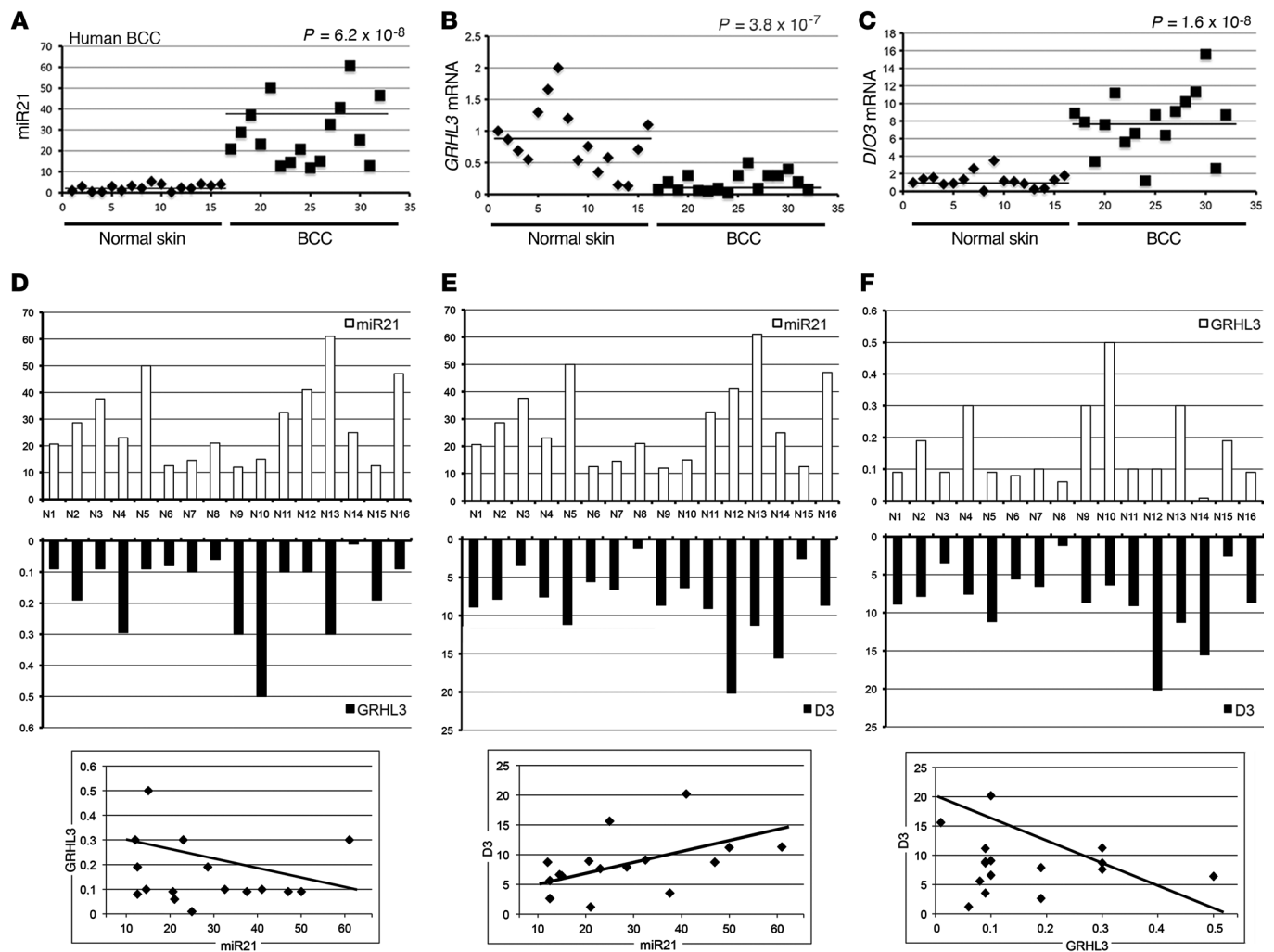


Figure 6. miR21 inversely correlates with GRHL3 and is positively correlated with D3 in human BCCs. (A–C) The expression of miR21, *GRHL3*, and *DIO3* was measured in 16 human BCC tumors compared with normal skin counterparts. All samples were run in triplicate and referred to normal skin in sample 1 set arbitrarily as 1. *P* values were calculated by 1-way ANOVA, $*P < 0.05$. (D–F) The same data as in A–C were reported as scale bars, and correlations between miR21/*GRHL3*, miR21/*D3*, and *D3*/*GRHL3* were calculated by Pearson's correlation analysis (bottom).

In this perspective, our finding that TH exerts negative control over miR21 expression is particularly relevant. miR21 is one of a handful of key miRNAs that promote human and mouse oncogenesis (12–20). Here, we provide what is to our knowledge the first evidence that miR21 is overexpressed in human and mouse BCC, while it is barely detectable in normal skin (Figure 6 and Supplemental Figure 11). Our data demonstrate that miR21 is suppressed by TH at the transcriptional level by directly binding to a TRE located within the miR21 enhancer region. Decreased expression of D3 or TH treatment of BCC cells contributes to downregulation of miR21 levels (Figure 1 and Supplemental Figure 1). Furthermore, our finding that miR21 is also an upstream regulator of D3 (Figure 2) highlights the existence of a reciprocal TH–miR21 interplay, which regulates skin tumorigenesis.

Besides in cancer, there are many other contexts in which miR21 functions, D3 expression, and TH metabolism are linked. For instance, miR21 is implicated in many types of cardiac stress, including the myocardial remodeling that occurs after infarction, in which both D3 and miR21 are induced (41, 42). Moreover,

miR21 is induced during immune cell activation (21, 43). The analogy of miR21 with D3 expression in multiple settings suggests that the miR21/*D3* axis is a potential therapeutic target.

Although thyroid dysfunctions affect the skin phenotype and many people with hypothyroidism and hyperthyroidism have skin-related conditions (44), there is no evidence of an association between thyroid dysfunctions and BCC formation. This apparent lack of an association may be explained in 1 of 2 ways. Firstly, BCCs grow very slowly, while alterations of TH circulation at plasma levels are acute conditions that generally do not become chronic. Secondly, the deiodinase family represents a potent homeostatic mechanism when thyroid dysfunction induces a minimal variation of TH, and is thus able to preserve intracellular “normal” T3 concentrations even in the presence of altered thyroid status at plasma level. Conversely, D3 upregulation in the BCC might not alter circulating TH concentrations.

The tumor suppressor GRHL3 is an inhibitor of D3. Our data demonstrate that the developmental factor and tumor suppressor GRHL3 represses *DIO3* transcription and mediates the positive

regulation of D3 expression by miR21. Although *GRHL3* has been shown to be a miR21 target gene in SCCs (31, 33), this regulation appears to be context-dependent, since it was not among the miR21 targets in tissues in which miR21 was modified (45). Here we demonstrate that *GRHL3* is downregulated by miR21 in BCC (Figures 2 and 3). Accordingly, *GRHL3* inhibition increases the expression of D3 in BCC cells. This is consistent with the poor expression of D3 in adult tissues and its reactivation in many tumoral contexts (8). Remarkably, forced *GRHL3* expression prevents miR21-dependent D3 transcription, thus providing genetic evidence for a miR21/*GRHL3*/D3 epistatic cascade (Figure 3, A–D).

The discovery of a miR21/*GRHL3*/D3 axis prompts some considerations regarding the role of TH metabolism in the skin. First, both miR21 and *GRHL3* (which are functionally related to D3 expression) play critical roles in different skin cancer subtypes (33, 46). These observations reinforce the concept that D3 expression and TH metabolism play a critical role in skin cancer. Second, we previously demonstrated that D3 overexpression amplifies keratinocyte proliferation (10), and while its expression is very low in adult tissues, D3 is re-expressed in many hyperproliferative conditions (8). The inverse correlation between D3 and *GRHL3* in BCC emphasizes the opposite roles played by the 2 genes in BCC tumorigenesis and, most importantly, suggests that the negative control exerted by *GRHL3* on D3 expression might be extended to such other pathological conditions as psoriasis and wound healing in which *GRHL3* plays a regulatory role (47, 48). Third, *GRHL3* is critical for keratinocyte differentiation and skin barrier formation, and *Grhl3*^{-/-} mice exhibit impaired epidermal differentiation and decreased expression of multiple differentiation genes (47). This implies that D3 suppression and increased TH signaling are also part of the differentiation program of keratinocytes. Should this be the case, it would be clinically relevant, since alterations of TH levels in patients are associated with cutaneous manifestations, and generalized myxedema (increased glycosaminoglycan deposition in skin, which appears cold, dry, and pale, with abundant hair loss) is the classical clinical sign of hypothyroid patients (44). Further studies are needed to determine whether T3 directly affects skin barrier formation and hair follicle cycle regulation.

D3 depletion drastically reduces BCC tumorigenesis. To assess the pathological role of the newly identified circuit *in vivo*, we inhibited D3 by CRISPR/Cas9 technology in BCC cells and in miR21-overexpressing BCC cells. These experiments demonstrated that blockade of D3 potentially attenuates BCC cell proliferation and *in vivo* xenograft tumorigenesis. miR21 overexpression stimulated the oncogenic potential of BCC cells to a greater extent than control cells (Figure 4). Notably, although BCC cells were transduced with miR21, their ability to form tumors was significantly hampered by D3 ablation, which strongly supports the concept that the TH inactivation pathway plays a pivotal role in tumor growth.

Intracellular TH regulation by D3 appears to be critical for tumorigenic potential in an *in vivo* model of BCC-like tumor formation. Indeed, we demonstrate that skin-specific D3 depletion drastically reduces tumor occurrence in mice with spontaneously forming BCC tumors, and prevents miR21 overexpression in these tumors. Thus, our data demonstrate that blocking TH degradation at the cellular level is a new modality with which to interfere with skin tumorigenesis. The few tumors that developed

in our D3-depleted mice contained very low levels of miR21, but substantially increased *GRHL3* expression. D3 depletion potentially attenuates BCC growth driven by the Shh/Gli2 pathway and by miR21 overexpression. However, although in a drastically attenuated fashion, BCC cells still generate tumors when miR21 is overexpressed and D3 is depleted, thus suggesting that increasing the intracellular TH signaling is not sufficient to eradicate BCC tumorigenesis. Collectively, these data are consistent with a strong link between miR21 expression and D3 overexpression, and an inverse correlation between D3 and *GRHL3*. Moreover, they suggest the existence of a common route by which tumor cells attenuate the TH signal in the tumor microenvironment (Figure 5H).

In conclusion, our findings demonstrate that TH functions as a suppressor of BCC tumors by regulating multiple pathways, irrespective of miR21, and identify the TH-inactivating enzyme D3 as a potential target of anticancer therapy for human BCC.

Methods

Cell cultures and transfections. BCC cells were derived from transgenic mice expressing a constitutively active form of *Gli2* under the control of the keratin 5 promoter, as previously described (49). BCC cells were cultured under low-calcium conditions with 8% Ca²⁺-chelated fetal bovine serum (FBS) and keratinocyte growth factor (Sigma-Aldrich). HEK-293 cells were cultured in DMEM with 10% FBS, 2 mM L-glutamine, and 10 U/ml penicillin/streptomycin. All transient transfections for BCC cells were performed using Lipofectamine 2000 (Life Technologies) according to the manufacturer's instructions. HEK-293 cells were transfected using IBAfect reagent (IBA BioTAGnology). Mouse primary keratinocytes were isolated from C57BL/6 newborn mice and cultured under low-calcium conditions (0.05 mM) in the presence of 4% calcium-chelated FBS (Invitrogen) and EGF (Invitrogen) as previously described (50).

Plasmids, siRNA, and reagents. Two luciferase-driving constructs (pmD3Luc and miR21-Enhancer-Luc) were generated as follows: For the pmD3Luc (*Dio3* promoter) a genomic mouse DNA was used as a PCR template; the oligonucleotides pmD3U and pmD3L (Supplemental Table 3) generated a 750-bp fragment containing the mouse *Dio3* 5' flanking region. For the miR21-Enhancer-Luc plasmid, we used the oligos mMiR21U and mMiR21L to amplify 389 bp of the miR21 5' flanking region (35). The amplified regions were cloned into the NheI/BglII (pmD3Luc) or SacI/XhoI (miR21-Enhancer-Luc) sites of a pGL3-basic vector (Promega Corp.). The mutated plasmid pmD3Luc-del was obtained from the pmD3Luc by recombinant PCR with 2 sets of oligonucleotides. Briefly, the 2 PCR products, pmD3U/pmD3mGRHL2 and pmD3mGRHLU/pmD3L to obtain pmD3Luc-del, were combined by PCR using outside oligonucleotides, and the final PCR products were reinserted into the pGL3-basic vector (Promega Corp.). The Flag-*GRHL3* plasmid was generated by PCR on mouse normal skin cDNA; the coding sequence of mouse *Grhl3* was amplified by PCR with specific oligonucleotides (mGRHL3clonU and mGRHL3clonL); the PCR product was inserted into the HindIII/EcoRI sites of the pFLAG-CMV-2 vector (Sigma-Aldrich). *GRHL3* silencing was performed with siRNA technology: 2 siRNAs targeting *GRHL3* were purchased from Life Technologies (catalog s106644, s106646). Stealth RNAi negative control duplex (Invitrogen) served as control. Effective *GRHL3* silencing was confirmed by measurement of *GRHL3* protein levels in transfected cells (Supplemental Figure 4B). The primer sequence is reported in Supplemental Table 3. The miR21-overexpressing plasmid

was provided by G. De Vita (University of Naples Federico II, Naples, Italy). Knockdown of miR21 was performed by transient transfection of anti-miR21 LNA (ID mh10206; Ambion). LNA-scrambled CTR served as control. Western blot analysis was performed with the following antibodies: anti-D3 (D3-718; ref. 51), anti-cyclin D1 (sc-246; Santa Cruz Biotechnology Inc.), and anti-tubulin (sc-8035; Santa Cruz Biotechnology Inc.). Anti-K17 (NCL-CK17; Novocastra), anti-K10 (PRB-159P), anti-Sox9 (ab26414; Abcam), and anti-PTCH1 (2113; Novus Biologicals) antibodies were used for immunofluorescence experiments.

Genome editing of the *Dio3* locus using the CRISPR/Cas9 system. Targeted depletion of D3 in mouse BCC cells was obtained with CRISPR/Cas9 technology using the CRISPR/Cas9 system from Santa Cruz Biotechnology Inc. (*Dio3* CRISPR/Cas9 KO Plasmid, catalog sc-430733) and control plasmid (Control CRISPR/Cas9 Plasmid, catalog sc-418922). The D3 CRISPR/Cas9 KO plasmid consists of a pool of 3 plasmids, each encoding the Cas9 nuclease and a target-specific 20-nucleotide guide RNA. CRISPR/Cas9-guided mutagenesis in this case resulted in a deletion in the *Dio3* coding region. Briefly, BCC cells were transfected with 500 ng of the D3 CRISPR/Cas9 KO plasmid or control plasmid with Lipofectamine 2000 (Life Technologies). Three days after transfection, the cells were FACS-sorted for GFP expression, and single clones were selected and analyzed by PCR to verify D3 coding sequence integrity using specific oligonucleotides (gdio3U: CGACCCAAGATTCTCTGGGGCA; and gdio3L: AGCAGAGTCTCAAGTTAGCCAGAC; Supplemental Figure 4). Effective D3 depletion was confirmed by Western blot analysis (Supplemental Figure 4).

Genome editing of the TRE in the miR21 enhancer using the CRISPR/Cas9 system. Targeted mutagenesis of the TRE site within the miR21 enhancer region was performed with CRISPR/Cas9 technology and the CRISPR/Cas9 system from ADDGENE [pSpCas9(BB)-2A-GFP]. We used 2 custom-designed synthetic single guide RNAs (sgRNAs) targeting the genomic region flanking the TRE site. Each sgRNA was cloned into the pX458 [pSpCas9(BB)-2A-GFP] vector, which also encodes the Cas9 nuclease (52). To obtain the mutated template, recombinant PCR was performed on the genomic mouse DNA (Supplemental Figure 2) using 2 sets of oligos (mHmir21dU and mMIR21mutL; mMIR21mutU and mHmir21dL), which generated a 2-kb fragment containing the mutation TCCTAATAAGGA to TtTAATAAaaA. The vector and the TRE-mutated sequence were transfected into BCC cells, and cells expressing GFP were sorted by FACS into individual wells of 96-well plates and expanded in culture. Successful homology directed repair-mediated mutation was assessed by PCR and Sanger sequencing.

Luciferase assays. The Luc plasmids (pmD3Luc, miR21-Enhancer-Luc, or TRE3-TK-Luc) and CMV-renilla reporters were cotransfected into BCC and HEK-293 cells, and treated with 30 nM T3 as indicated. Luciferase activities were measured 48 hours after transfection using the Dual Luciferase Reporter Assay System (Promega Corp.), and differences in transfection efficiency were corrected relative to the level of renilla activity. Each construct was studied in triplicate in at least 3 separate transfection experiments.

Western blot analysis. Total protein extracts from BCC cells were run on a 10% SDS-PAGE gel and transferred on Immobilon-P transfer membrane (Millipore). The membrane was then blocked with 5% non-fat dry milk in PBS, probed with anti-D3 polyclonal antibodies (1:500), anti-Flag (1:1,000, M2; Sigma-Aldrich), or GRHL3 antibody (1:500, sc-398839; Santa Cruz Biotechnology Inc.) for 2 hours, washed and

incubated with HRP-conjugated donkey anti-rabbit IgG secondary antibody (1:3,000), and detected by chemiluminescence (Millipore). After extensive washing, the membrane was incubated with anti-tubulin-specific antibodies (sc-8035, 1:10,000; Santa Cruz Biotechnology Inc.) as loading control. All Western blots were run in triplicate, and bands were quantitated in 1 representative gel.

miRNA Northern blot. Total RNA was isolated from BCC cells treated or not with T3, using TRIzol (Invitrogen) and quantitated at 260 nm using a standard spectrometry. Ten micrograms of total RNA was resuspended in 2' Tris/borate/EDTA (TBE) urea sample buffer (Invitrogen) to a final volume of 10 μ l. Samples were heated at 70°C for 5 minutes and loaded onto a 15% polyacrylamide gel containing TBE urea. Electrophoresis was performed in 1' TBE running buffer at 120 V with a run time between 60 and 90 minutes. After electrophoresis, the gel was rinsed in deionized water, followed by a 5-minute wash in 1' TBE. RNA was transferred onto a Hybond-N+ membrane for 30 minutes at 20 V using a Bio-Rad Miniprotein II apparatus. The nylon membrane was placed in the Stratagene UV Crosslinker and RNA cross-linked at 1,200 kJ. As miR21 probe, we designed the oligonucleotide Mir21probe (Supplemental Table 3) containing the mature miRNA sequence. The oligo was hybridized to the OprobAAA: 5'-TTTTTTTTTCTCTGTGCC-3', and elongated with Klenow exo⁻ (Life Technologies) and ATP α -³²P (PerkinElmer Inc.) to generate a tail of radioactive adenine. To normalize the RNA, we used the 5S subunit of rRNA (Supplemental Table 3), which was also hybridized to the OprobAAA and radiolabeled.

Animals, histology, and immunostaining. *K5-Gli2 K14-Cre^{+/+} Dio3^{fl/fl}* (Gli2;D3KO) mice were obtained by crossing of a keratinocyte-specific conditional D3-null mouse (*K14-Cre^{+/+} D3^{fl/fl}*) with the mouse model *K5-Gli2* (37). Female 5-week-old BALB/c (nude) mice were purchased from Charles River Laboratories. All animal experiments and mouse husbandry were done in the animal facility at CEINGE-Biotecnologie Avanzate, Naples, Italy, in accordance with institutional guidelines. For immunofluorescence and histology, ears from Gli2;D3KO and control xenograft tumors of mice at 6 months of age were embedded in paraffin, cut into 7- μ m sections, and H&E-stained. Slides were baked at 60°C, deparaffinized by xylenes, dehydrated with ethanol, rehydrated in PBS, and permeabilized by 0.5% Triton X-100 in PBS. Antigen retrieval was performed by incubation in 0.01 M citrate buffer (pH 6.0) or 0.5 M Tris buffer (pH 8.0) at 95°C for 15 minutes. Sections were blocked in 1% BSA/0.05% Tween/PBS for 30 minutes at 37°C. Primary antibody incubation was carried out overnight at 4°C in blocking buffer followed by washing in 0.2% Tween/PBS. Secondary antibody incubation was carried out at room temperature for 1 hour, followed by washing in 0.2% Tween/PBS. Images were acquired with an IX51 Olympus microscope and the Cell*F Olympus Imaging Software.

Real-time RT-PCR. mRNAs were extracted with TRIzol reagent (Life Technologies). cDNAs were prepared with SuperScript VILO Master Mix (Life Technologies) as indicated by the manufacturer. The cDNAs were amplified by PCR in an iQ5 Multicolor Real-Time Detector System (Bio-Rad) with the fluorescent double-stranded DNA-binding dye SYBR Green (Applied Biosystems). Specific primers for each gene were designed to work under the same cycling conditions (95°C for 10 minutes followed by 40 cycles at 95°C for 15 seconds and 60°C for 1 minute), generating products of comparable sizes (~200 bp for each amplification). Primer combinations were positioned whenever possible to span an exon-exon junction and the RNA digested with

deoxyribonuclease to avoid genomic DNA interference. For each reaction, standard curves for reference genes were constructed based on six 4-fold serial dilutions of cDNA. All samples were run in triplicate. The template concentration was calculated from the cycle number when the amount of PCR product passed a threshold established in the exponential phase of the PCR. The relative amounts of gene expression were calculated with cyclophilin A expression as an internal standard (calibrator). The results, expressed as *n*-fold differences in target gene expression, were determined as follows: $n \times \text{target} = 2^{(\Delta C_{t\text{sample}} - \Delta C_{t\text{calibrator}})}$.

miRNA microarray analysis. miRNA microarray analysis was performed in BCC cells transfected with shD3 or shCTR stealth oligos. Briefly, total RNA was harvested using the TRIzol reagent (Invitrogen) according to the manufacturer's instructions. The samples were hybridized to the miRCURY LNA Array (version 9.2; Exiqon). Data have been submitted to the Gene Expression Omnibus database (GEO GSE78265).

TaqMan miRNA assay. miR21, RNU6B, and Sno234 were analyzed using 2-step real-time PCR protocols with TaqMan MicroRNA Assays: hsa-miR-21 catalog 000397; RNU6B catalog 001093; SnoRNA234 catalog 001234 (Applied Biosystems). Reverse transcriptase reactions were performed using the TaqMan MicroRNA Reverse Transcription Kit (Applied Biosystems) in a reaction mix of 15 μ l total volume with 7 μ l of Master Mix containing 1' RT buffer, 1.0 mM of total dNTPs, 50 U MultiScribe Reverse Transcriptase Enzyme, and 0.25 U of RNase inhibitor; 3 μ l of RT primers (Applied Biosystems); and 5 μ l of RNA sample. The amplification conditions were as follows: annealing at 16°C for 30 minutes, extension at 42°C for 30 minutes, and RT inactivation at 85°C for 10 minutes. Quantitative PCRs (qPCRs) were performed on Applied Biosystems Step One Plus Real-Time PCR System with a mixture of 20 μ l final volume containing 1' TaqMan Universal PCR Master Mix (Applied Biosystems), 1 MicroRNA Assay (Applied Biosystems), and 3 μ l cDNA (RT product diluted 1:5). Thermal cycling conditions were 10 minutes at 95°C followed by 40 cycles of 15 seconds at 95°C and 1 minute at 60°C. The end point of qPCR data is the threshold cycle (Ct), which represents the fractional cycle number at which the fluorescence reaches the fixed threshold. All qPCR reactions were run in duplicate. The relative quantification of miRNA expression was analyzed using the $2^{-\Delta\Delta C_t}$ method.

Tumor xenografts. To evaluate in vivo tumorigenesis, a BCC xenografting mouse model was established. After resuspension in PBS, 1×10^6 in 100 μ l of CRISPR-CTR BCC cells (control), 1 D3KO clone (D3KO n.12, Supplemental Figure 4), and miR21 and D3KO-miR21 cells were injected s.c. into the flanks of 5-week-old female BALB/c-nu mice. Mice were examined twice a week, and the tumor was measured with a caliper and then weighed 3 weeks after injection. All animals were maintained in a sterile environment on a daily 12-hour light/12-

hour dark cycle. Tumor volume was calculated according to the formula: volume (mm^3) = $4/3 \times \pi \times (\text{length}/2) \times (\text{width}/2) \times (\text{height}/2)$. Tumor xenografts were harvested, weighed, and snap-frozen for immunofluorescence analysis.

Human samples. Human BCC samples were collected at the Istituto Nazionale Tumori Ospedale Pascale in Naples.

Statistics. The results are shown as means \pm SD throughout. Differences between samples were assessed by Student's 2-tailed *t* test for independent samples. In all experiments, differences were considered significant when *P* was less than 0.05. Asterisks indicate significance at **P* < 0.05, ***P* < 0.01, and ****P* < 0.001 throughout. Differences of mRNA levels in human BCC samples versus normal skin samples were analyzed using a 1-way ANOVA, and *P* less than 0.05 was considered significant. Relative mRNA levels (in which the control sample was arbitrarily set as 1) are reported as results of real-time PCR, in which expression of cyclophilin A was used as a housekeeping gene. The relationship between miR21/GRHL3, miR21/D3, and GRHL3/D3 expression was analyzed using Pearson's correlation.

Study approval. This work was approved by the appropriately constituted research ethics committee of the University of Naples Federico II.

Author contributions

DDG, GM, TP, CL, and EDC performed the in vitro and in vivo experiments and prepared the figures. RA generated plasmids and mouse models. MADS performed histochemistry and immunofluorescence. GS performed FACS sorting studies. DS, CM, LDV, AC, and AAD provided observations and scientific interpretations. DS contributed to experiment supervision and interpretation. MD designed the overall study, supervised the experiments, analyzed the results, and wrote the paper. All authors discussed the results and provided input on the manuscript.

Acknowledgments

This work was supported by grants from the European Research Council under the European Union's Horizon 2020 Programme-ERC-StG-2014 (STARS-639548) and by Italian Association for Cancer Research grants to M. Dentice (IG 13065), D. Salvatore (IG 11362), and C. Missero (IG 17079). We thank Jean Ann Gilder (Scientific Communication Srl., Naples, Italy) for writing assistance.

Address correspondence to: Monica Dentice, Department of Clinical Medicine and Surgery, University of Naples "Federico II," Via S. Pansini 5, 80131 Naples, Italy. Phone: 39.081.7463848; E-mail: monica.dentice@unina.it.

- Gailani MR, et al. The role of the human homologue of *Drosophila* patched in sporadic basal cell carcinomas. *Nat Genet.* 1996;14(1):78-81.
- Kasper M, Jaks V, Hohl D, Toftgard R. Basal cell carcinoma — molecular biology and potential new therapies. *J Clin Invest.* 2012;122(2):455-463.
- Oro AE, Higgins KM, Hu Z, Bonifas JM, Epstein EH Jr, Scott MP. Basal cell carcinomas in mice overexpressing sonic hedgehog. *Science.* 1997;276(5313):817-821.
- Xie J, et al. Activating Smoothed mutations in sporadic basal-cell carcinoma. *Nature.* 1998;391(6662):90-92.
- Johnson RL, et al. Human homolog of patched, a candidate gene for the basal cell nevus syndrome. *Science.* 1996;272(5268):1668-1671.
- Hahn H, et al. Mutations of the human homologue of *Drosophila* patched in the nevoid basal cell carcinoma syndrome. *Cell.* 1996;85(6):841-851.
- Wong SY, Dlugosz AA. Basal cell carcinoma, Hedgehog signaling, and targeted therapeutics: the long and winding road. *J Invest Dermatol.* 2014;134(e1):E18-E22.
- Dentice M, Antonini D, Salvatore D. Type 3 deiodinase and solid tumors: an intriguing pair. *Expert Opin Ther Targets.* 2013;17(11):1369-1379.
- Gereben B, et al. Cellular and molecular basis of deiodinase-regulated thyroid hormone signaling. *Endocr Rev.* 2008;29(7):898-938.
- Dentice M, et al. Sonic hedgehog-induced type 3 deiodinase blocks thyroid hormone action enhancing proliferation of normal and malignant keratinocytes. *Proc Natl Acad Sci U S A.* 2007;104(36):14466-14471.
- Luongo C, Ambrosio R, Salzano S, Dlugosz AA, Missero C, Dentice M. The sonic hedgehog-induced type 3 deiodinase facilitates tumorigenesis of basal cell carcinoma by reducing Gli2 inactivation. *Endocrinology.* 2014;155(6):2077-2088.

12. Volinia S, et al. A microRNA expression signature of human solid tumors defines cancer gene targets. *Proc Natl Acad Sci U S A*. 2006;103(7):2257–2261.
13. Chan JA, Krichevsky AM, Kosik KS. MicroRNA-21 is an antiapoptotic factor in human glioblastoma cells. *Cancer Res*. 2005;65(14):6029–6033.
14. Xu LF, Wu ZP, Chen Y, Zhu QS, Hamidi S, Navab R. MicroRNA-21 (miR-21) regulates cellular proliferation, invasion, migration, and apoptosis by targeting PTEN, RECK and Bcl-2 in lung squamous carcinoma, Gejiu City, China. *PLoS One*. 2014;9(8):e103698.
15. Lv L, et al. MicroRNA-21 is overexpressed in renal cell carcinoma. *Int J Biol Markers*. 2013;28(2):201–207.
16. Hiyoshi Y, et al. MicroRNA-21 regulates the proliferation and invasion in esophageal squamous cell carcinoma. *Clin Cancer Res*. 2009;15(6):1915–1922.
17. Li X, Huang K, Yu J. Inhibition of microRNA-21 upregulates the expression of programmed cell death 4 and phosphatase tensin homologue in the A431 squamous cell carcinoma cell line. *Oncol Lett*. 2014;8(1):203–207.
18. Ren W, et al. MiR-21 modulates chemosensitivity of tongue squamous cell carcinoma cells to cisplatin by targeting PDCD4. *Mol Cell Biochem*. 2014;390(1–2):253–262.
19. Asangani IA, et al. MicroRNA-21 (miR-21) post-transcriptionally downregulates tumor suppressor Pcdcd4 and stimulates invasion, intravasation and metastasis in colorectal cancer. *Oncogene*. 2008;27(15):2128–2136.
20. Cao Z, Yoon JH, Nam SW, Lee JY, Park WS. PDCD4 expression inversely correlated with miR-21 levels in gastric cancers. *J Cancer Res Clin Oncol*. 2012;138(4):611–619.
21. Morrissey EE. The magic and mystery of miR-21. *J Clin Invest*. 2010;120(11):3817–3819.
22. Hildebrand J, et al. A comprehensive analysis of microRNA expression during human keratinocyte differentiation in vitro and in vivo. *J Invest Dermatol*. 2011;131(1):20–29.
23. Yi R, et al. Morphogenesis in skin is governed by discrete sets of differentially expressed microRNAs. *Nat Genet*. 2006;38(3):356–362.
24. Ahmed MI, Mardaryev AN, Lewis CJ, Sharov AA, Botchkareva NV. MicroRNA-21 is an important downstream component of BMP signalling in epidermal keratinocytes. *J Cell Sci*. 2011; 124(pt 20):3399–3404.
25. Joyce CE, et al. Deep sequencing of small RNAs from human skin reveals major alterations in the psoriasis miRNAome. *Hum Mol Genet*. 2011;20(20):4025–4040.
26. Zibert JR, Lovendorf MB, Litman T, Olsen J, Kaczkowski B, Skov L. MicroRNAs and potential target interactions in psoriasis. *J Dermatol Sci*. 2010;58(3):177–185.
27. Dziunycz P, et al. Squamous cell carcinoma of the skin shows a distinct microRNA profile modulated by UV radiation. *J Invest Dermatol*. 2010;130(11):2686–2689.
28. Akagi I, et al. Relationship between altered expression levels of MIR21, MIR143, MIR145, and MIR205 and clinicopathologic features of esophageal squamous cell carcinoma. *Dis Esophagus*. 2011;24(7):523–530.
29. Satzger I, et al. microRNA-21 is upregulated in malignant melanoma and influences apoptosis of melanocytic cells. *Exp Dermatol*. 2012;21(7):509–514.
30. Stramer B, Martin P. Cell biology: master regulators of sealing and healing. *Curr Biol*. 2005;15(11):R425–R427.
31. Darido C, et al. Targeting of the tumor suppressor GRHL3 by a miR-21-dependent proto-oncogenic network results in PTEN loss and tumorigenesis. *Cancer Cell*. 2011;20(5):635–648.
32. Yu Z, et al. The Grainyhead-like epithelial transactivator Get-1/Grhl3 regulates epidermal terminal differentiation and interacts functionally with LMO4. *Dev Biol*. 2006;299(1):122–136.
33. Bhandari A, et al. The Grainyhead transcription factor Grhl3/Get1 suppresses miR-21 expression and tumorigenesis in skin: modulation of the miR-21 target MSH2 by RNA-binding protein DND1. *Oncogene*. 2013;32(12):1497–1507.
34. Peyrard-Janvid M, et al. Dominant mutations in GRHL3 cause Van der Woude Syndrome and disrupt oral periderm development. *Am J Hum Genet*. 2014;94(1):23–32.
35. Fujita S, et al. miR-21 Gene expression triggered by AP-1 is sustained through a double-negative feedback mechanism. *J Mol Biol*. 2008;378(3):492–504.
36. Huang da W, Sherman BT, Lempicki RA. Systematic and integrative analysis of large gene lists using DAVID bioinformatics resources. *Nat Protoc*. 2009;4(1):44–57.
37. Grachtchouk M, et al. Basal cell carcinomas in mice overexpressing Gli2 in skin. *Nat Genet*. 2000;24(3):216–217.
38. Ortega-Carvalho TM, Sidhaye AR, Wondisford FE. Thyroid hormone receptors and resistance to thyroid hormone disorders. *Nat Rev Endocrinol*. 2014;10(10):582–591.
39. Weinberger C, Thompson CC, Ong ES, Lebo R, Gruol DJ, Evans RM. The c-erbA gene encodes a thyroid hormone receptor. *Nature*. 1986;324(6098):641–646.
40. Gandrillon O, Ferrand N, Michaille JJ, Roze L, Zile MH, Samarut J. c-erbA alpha/T3R and RARs control commitment of hematopoietic self-renewing progenitor cells to apoptosis or differentiation and are antagonized by the v-erbA oncogene. *Oncogene*. 1994;9(3):749–758.
41. van Rooij E, et al. A signature pattern of stress-responsive microRNAs that can evoke cardiac hypertrophy and heart failure. *Proc Natl Acad Sci U S A*. 2006;103(48):18255–18260.
42. Tatsuguchi M, et al. Expression of microRNAs is dynamically regulated during cardiomyocyte hypertrophy. *J Mol Cell Cardiol*. 2007;42(6):1137–1141.
43. Lu TX, Munitz A, Rothenberg ME. MicroRNA-21 is up-regulated in allergic airway inflammation and regulates IL-12p35 expression. *J Immunol*. 2009;182(8):4994–5002.
44. Antonini D, Sibillio A, Dentiche M, Missero C. An intimate relationship between thyroid hormone and skin: regulation of gene expression. *Front Endocrinol (Lausanne)*. 2013;4:104.
45. Ma X, et al. Loss of the miR-21 allele elevates the expression of its target genes and reduces tumorigenesis. *Proc Natl Acad Sci U S A*. 2011;108(25):10144–10149.
46. Medina PP, Nolde M, Slack FJ. OncomiR addiction in an in vivo model of microRNA-21-induced pre-B-cell lymphoma. *Nature*. 2010;467(7311):86–90.
47. Ting SB, et al. A homolog of *Drosophila* grainy head is essential for epidermal integrity in mice. *Science*. 2005;308(5720):411–413.
48. Gordon WM, et al. A GRHL3-regulated repair pathway suppresses immune-mediated epidermal hyperplasia. *J Clin Invest*. 2014;124(12):5205–5218.
49. Sheng H, et al. Dissecting the oncogenic potential of Gli2: deletion of an NH(2)-terminal fragment alters skin tumor phenotype. *Cancer Res*. 2002;62(18):5308–5316.
50. Antonini D, et al. An autoregulatory loop directs the tissue-specific expression of p63 through a long-range evolutionarily conserved enhancer. *Mol Cell Biol*. 2006;26(8):3308–3318.
51. Huang SA, et al. Transforming growth factor-beta promotes inactivation of extracellular thyroid hormones via transcriptional stimulation of type 3 iodothyronine deiodinase. *Mol Endocrinol*. 2005;19(12):3126–3136.
52. Ran FA, Hsu PD, Wright J, Agarwala V, Scott DA, Zhang F. Genome engineering using the CRISPR-Cas9 system. *Nat Protoc*. 2013;8(11):2281–2308.

The Concerted Action of Type 2 and Type 3 Deiodinases Regulates the Cell Cycle and Survival of Basal Cell Carcinoma Cells

AU1 ▶ Caterina Miro,¹ Raffaele Ambrosio,² Maria Angela De Stefano,¹ Daniela Di Girolamo,¹ Emery Di Cicco,¹
AU2 ▶ Annunziata Gaetana Cicatiello,¹ Giuseppina Mancino,¹ Tommaso Porcelli,¹ Maddalena Raia,³
Luigi Del Vecchio,³ Domenico Salvatore,^{1,3,*} and Monica Dentice^{1, 3,*}

Background: Thyroid hormones (THs) mediate pleiotropic cellular processes involved in metabolism, cellular proliferation, and differentiation. The intracellular hormonal environment can be tailored by the type 1 and 2 deiodinase enzymes D2 and D3, which catalyze TH activation and inactivation respectively. In many cellular systems, THs exert well-documented stimulatory or inhibitory effects on cell proliferation; however, the molecular mechanisms by which they control rates of cell cycle progression have not yet been entirely clarified. We previously showed that D3 depletion or TH treatment influences the proliferation and survival of basal cell carcinoma (BCC) cells. Surprisingly, we also found that BCC cells express not only sustained levels of D3 but also robust levels of D2. The aim of the present study was to dissect the contribution of D2 to TH metabolism in the BCC context, and to identify the molecular changes associated with cell proliferation and survival induced by TH and mediated by D2 and D3.

Methods: We used the CRISPR/Cas9 technology to genetically deplete D2 and D3 in BCC cells and studied the consequences of depletion on cell cycle progression and on cell death. Cell cycle progression was analyzed by fluorescence activated cell sorting analysis of synchronized cells, and the apoptosis rate by annexin V incorporation.

Results: Mechanistic investigations revealed that D2 inactivation accelerates cell cycle progression thereby enhancing the proportion of S-phase cells and cyclin D1 expression. Conversely, D3 mutagenesis drastically suppressed cell proliferation and enhanced apoptosis of BCC cells. Furthermore, the basal apoptotic rate was oppositely regulated in D2- and D3-depleted cells.

Conclusion: Our results indicate that BCC cells constitute an example in which the TH signal is finely tuned by the concerted expression of opposite-acting deiodinases. The dual regulation of D2 and D3 expression plays a critical role in cell cycle progression and cell death by influencing cyclin D1-mediated entry into the G1-S phase. These findings reinforce the concept that TH is a potential therapeutic target in human BCC.

Keywords: deiodinases, thyroid hormone metabolism, basal cell carcinoma

Introduction

THYROID HORMONE (TH) EXERTS pleiotropic effects during organ development and in adulthood by regulating such cellular processes as cell survival and differentiation and cellular homeostasis and metabolism (1,2). The active thyroid hormone, triiodothyronine (T3), in the target tissues can derive either from circulating T3 levels or from the in-

tracellular conversion of the prohormone thyroxine (T4) into T3. Three iodothyronine deiodinase enzymes catalyze the removal of the iodine moiety—a process that results in TH activation or inactivation. Type 2 deiodinase (D2) is the TH-activating enzyme in the skin, while type 3 deiodinase (D3) terminates TH action and attenuates the signal. The canonical action of T3 is to regulate gene expression by binding with nuclear receptors (TRs) that are encoded by two genes, *Thrx*

◀ AU4

AU3 ▶
AU3 ▶

¹Department of Clinical Medicine and Surgery, University of Naples “Federico II”, Napoli, Italy.

²IRCCS SDN, Naples, Italy.

³CEINGE–Biotechnologie Avanzate Scarl, Naples, Italy.

*D.S. and M.D. contributed equally to this work.

and *Thrb*, thereby giving rise to different isoforms, whose active receptors are TR α 1, TR β 1, and TR β 2 (3). Nuclear receptors bind to thyroid response elements (TREs) present in the promoter regions of the target genes, thus forming homo- or heterodimers with other nuclear receptors and finally resulting in activation or repression of transcription. The actions of T3 are also modulated by co-repressors and co-activators (3).

Thyroid hormone has been reported to be a critical regulator of cell differentiation during development and in adulthood (4). Accordingly, the TH inactivating enzyme, D3, is overexpressed in several mouse and human cancers. This concept is exemplified by basal cell carcinoma (BCC), which is characterized by sustained D3 expression, and in which the TH signal attenuates cell proliferation thereby reducing BCC tumorigenicity (5). The skin is very sensitive to the action of TH. Indeed, TH influences both epidermal homeostasis and the pathogenesis of skin cancer (6). Moreover, normal TH levels are required for efficient epidermal homeostasis, function and regeneration (7). By binding to TRs, T3 regulates the expression of several keratins and skin-specific genes (8,9–11). This regulation is critical for fetal epidermal differentiation, barrier formation, hair growth, sebum production, wound healing, epidermal oxygen consumption, and keratinocyte proliferation (8,12–14).

The molecular mechanisms by which TH regulates rates of cell cycle progression and the relative contributions of deiodinases in this process have not yet been completely elucidated. We previously showed that D3 depletion and TH treatment influence the proliferation and survival of BCC cells. An intriguing and unexpected finding of the present study was that D2 is also highly expressed in BCC, which suggests that the D3-activating enzyme might play a role in BCC tumorigenesis and that the regulation of BCC tumorigenesis by TH can be more complex than previously thought.

The aim of the present study was to identify the molecular changes associated with cell cycle progression and apoptosis induced by TH and mediated by the deiodinases D2 and D3. Our data provide evidence that the BCC cell population is a unique cell model that is exquisitely sensitive to TH modulation and expresses high levels of both activating (D2) and inactivating (D3) TH enzymes. Co-expression of D2 and D3 raises the possibility of studying in detail the opposite effects of intracellular TH modulation and is thus a cellular model with which to unravel the molecular mechanisms of cell cycle control by TH.

Materials and Methods

Cell cultures, transfections, and reagents

BCC cells (G2N2c) are derived from transgenic mice expressing a constitutively active form of *GLI2* under the control of the keratin 5 promoter (15), which generates BCC-like tumors called “trichoblastomas,” which are referred to as “BCC cells” throughout this article. Mouse primary keratinocytes were purified from wild-type (C57) mice and cultured under low-calcium conditions with 8% Ca²⁺-chelated fetal bovine serum and keratinocyte growth factor (Sigma-Aldrich, Saint Louis, MO) (16) Transient transfections were performed with Lipofectamine 2000 (Life Technologies Ltd., Paisley, Scotland) according to the manufacturer’s instructions. Monoclonal anti-cyclin D1

anti-Erk antibodies were from Santa Cruz Biotechnology (Santa Cruz, CA). BCC cells were treated with 2.5 μ M and 12.5 μ M doxorubicin for 16 hours and with 0.2 μ g/mL and 1 μ g/mL tunicamicin for 24 hours.

Dio2 and Dio3 targeted mutagenesis

Depletion of *Dio3* and *Dio2* in mouse BCC cells was obtained using the CRISPR/Cas9 system from Santa Cruz Biotechnology (*Dio3* CRISPR/Cas9 Knockout [KO] Plasmid, catalog sc-430733; *Dio2* CRISPR/Cas9 KO Plasmid, catalog sc-420003) and control plasmid (Control CRISPR/Cas9 Plasmid, catalog sc-418922) as previously described (17). BCC cells were transfected with 500 ng of the D3, D2, or control CRISPR/Cas9 KO plasmids with Lipofectamine 2000 (Life Technologies). Three days after transfection, the cells were sorted using fluorescence activated cell sorting (FACS) for green fluorescent protein expression, single clones were analyzed by PCR to evaluate coding region alterations, and *Dio2* exon 1 was sequenced to identify the inserted mutations. D3KO and control cells have already been checked for effective and specific D3 depletion as reported in Di Girolamo *et al.* (17).

Western blot analysis

Total protein extracts from BCC cells were run on a 10% SDS-PAGE gel and transferred onto an Immobilon-P transfer membrane (Millipore). The membrane was then blocked with 5% nonfat dry milk in phosphate-buffered saline (PBS), probed with anti-cyclin D1 and anti-PARP antibodies overnight at 4°C, washed, and incubated with horseradish peroxidase-conjugated anti-mouse immunoglobulin G secondary antibody (1:3,000), and detected by chemiluminescence (Millipore, cat. WBKLS0500). After extensive washing, the membrane was incubated with anti-Erk or anti-tubulin specific antibodies (Santa Cruz Biotechnology) as loading control. All Western blots were run in triplicate, and bands were quantified with ImageJ software.

Real-time PCR (RT-PCR)

Messenger RNAs were extracted with Trizol reagent (Life Technologies Ltd). Complementary DNAs were prepared with Vilo reverse transcriptase (Life Technologies Ltd.) as indicated by the manufacturer. The cDNAs were amplified by PCR in an iQ5 Multicolor Real Time Detector System (BioRad, Hercules, CA) with the fluorescent double-stranded DNA-binding dye SYBR Green (Applied Biosystems). Specific primers for each gene were designed to work under the same cycling conditions (95°C for 10 min followed by 40 cycles at 95°C for 15 s and 60°C for 1 min), thereby generating products of comparable sizes (about 200 bp for each amplification). Primer combinations were positioned whenever possible to span an exon–exon junction and the RNA digested with DNase to avoid genomic DNA interference. Primer sequences are indicated in the Supplementary Table S1 (Supplementary Data are available online at www.liebertpub.com/thy). For each reaction, standard curves for reference genes were constructed based on six four-fold serial dilutions of cDNA. All samples were run in triplicate. The template concentration was calculated from the cycle number when the amount of PCR product passed a threshold

◀ AU5

◀ ST1

DEIODINASES D2 AND D3 CONTROL PROLIFERATION OF BCC CELLS

established in the exponential phase of the PCR. The relative amounts of gene expression were calculated with cyclophilin A expression as an internal standard (calibrator). The results, expressed as *N*-fold differences in target gene expression, were determined as follows: $N * target = 2^{(Ct_{sample} - Ct_{calibrator})}$.

Colony formation assay

To evaluate colony formation, cells were seeded out in appropriate dilutions to form colonies. Three and six days after plating, cells were washed with PBS and stained with 1% crystal violet in 20% ethanol for 10 min at room temperature. Cells were washed with PBS twice and visible colonies were counted.

DNA transfection and Luciferase (Luc) expression assays

G2N2C cells were transiently transfected using Lipofectamine 2000 (Life Technologies Ltd.) according to the manufacturer’s instructions. The reporter plasmids (pCcnD1CTR-Luc or T3TK-Luc) and CMV-Renilla were co-transfected into G2N2C. Luc activities were measured 48 hours after transfection with the Dual Luciferase Reporter Assay System (Promega), and differences in transfection efficiency were corrected relative to the level of Renilla Luciferase. Each construct was studied in triplicate in at least three separate transfection experiments.

Cell cycle analysis

For DNA content analysis, G2N2C cells were first synchronized by a double thymidine block protocol (18). Briefly, cells were grown in 100 mm plates to 40–50% confluence and then incubated for 14 h with growth medium supplemented with 2 mM thymidine. After two washes with PBS, cell medium was replaced by growth medium without thymidine for 24 h. Cells were then subjected to an additional incubation with 2 mM thymidine for 14 h followed by a release in growing medium until harvesting at the indicated time points (Fig. 1). Cells were fixed in ice-cold 70% ethanol at –20°C. At least 10,000 cells were analyzed by FACS (FACS Canto2, Becton Dickinson) after staining with 5 µg/mL propidium iodide and exposure to 0.25 mg/mL RNase I (Sigma Aldrich). Data were analyzed with the MODFIT Lt3.0 Software.

For carboxy-fluorescein succinimidyl ester (CFSE) *in vivo* labeling, the CFSE labeling solution (1 µM) was added to 1 mL cell suspensions in PBS and incubated for 10 min at room temperature, after which cells were washed with regular medium to quench any free dye in solution. Cells were then plated in regular growing medium for different time points and harvested for cell sorting using a FACS Aria system (BD).

Cell synchronization measurements

Cells were synchronized through a double thymidine block (18). G2N2C cells were grown to 25–30% confluence, suspended in media containing 2 mM thymidine, and grown for 18 h (first block). Cells were then suspended with trypsin-EDTA (Life Technologies), divided into multiple containers, left to grow in normal growth media for 9 h, and then incubated for 17 h in media containing 2 mM thymidine (second block). Cells were released from the second block by incu-

bation in growth media without thymidine and were harvested at the indicated time-points.

Statistical analysis

Differences between samples were assessed by Student’s two-tailed *t*-test for independent samples; *p*-values <0.05 were considered significant. Relative mRNA levels (in which the first sample was arbitrarily set as one) are reported as the results of RT-PCR in which the expression of cyclophilin A served as housekeeping gene. All experiments were repeated and analyzed from three to five times.

Results

BCC cells express both the activating and inactivating thyroid hormone enzymes D2 and D3, respectively

We previously reported that BCC cells and tumors are characterized by elevated expression of the TH inactivating enzyme D3 (5). To probe in greater detail the mechanisms underlying TH metabolism in BCC cells, we analyzed the expression of other proteins related to TH metabolism, namely, D2, THRα, THRβ, MCT8, and MCT10, and compared their expression with that of normal mouse primary keratinocytes (Supplementary Fig. S1A; Supplementary Data are available online at www.liebertpub.com/thy). Surprisingly, BCC cells showed sustained expression of D2 mRNA; Furthermore, receptors and transporters were expressed at slightly lower levels in BCC cells than in mouse keratinocytes (Supplementary Fig. S1). Since sustained D2 expression was unexpected, we compared D2 expression in BCC cells with its expression in solid BCC and in known D2-expressing tissues, namely pituitary and brown adipose tissue, compared with a “low-expressing tissue,” namely, skeletal muscle. PCR analysis showed that BCC cells and tumors express consistent levels of D2, similar to unstimulated brown adipose tissue (Fig. S1B). These data demonstrate that BCC cells represent a complex TH-sensitive system with which to study the intracellular regulation of TH action.

◀SF1

D2 and D3 depletion inversely regulate intracellular TH availability

To address the functional relevance of D2 and D3 co-expression in BCC cells, we genetically depleted *DIO2* (D2) or *DIO3* (D3) gene expression using CRISPR/Cas9 technology. The generation of the CRISP-CTR and D3KO clones is reported elsewhere (17). D2 was depleted using the same CRISPR/Cas9 system used for D3-depletion (see methods section). Four different D2KO clones were selected, and effective D2 depletion was confirmed by DNA sequencing (Supplementary Fig. S2). To assess whether D2- and D3-depletion affect nuclear TH availability, we transfected the generated cells with a T3-dependent artificial promoter that drives the luciferase gene (TRE3-Tk-Luc promoter). As expected, TH activity was reduced in D2KO cells and enhanced in D3KO cells (Supplementary Fig. S3A). Interestingly, the T3 signal in D2KO cells was even lower than in normal BCC cells (which are already characterized by an “intracellular hypothyroid state”). This finding shows that D3 is not the only enzyme controlling the total thyroid signal within these cells. Similar results were obtained by measuring the

◀SF2

◀SF3

F1 ▶
AU6 ▶

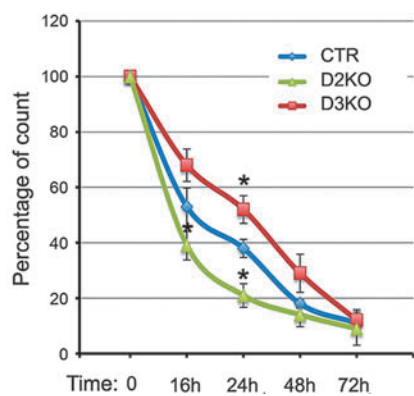
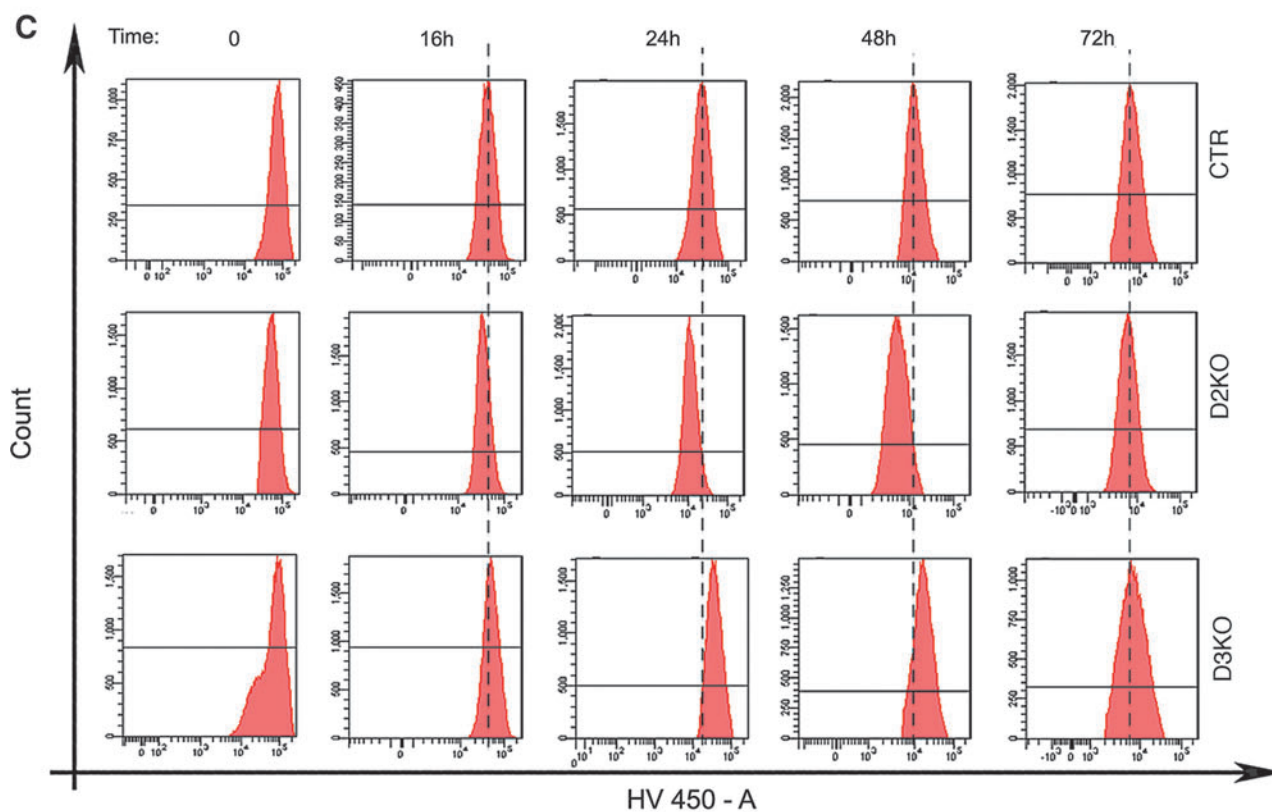
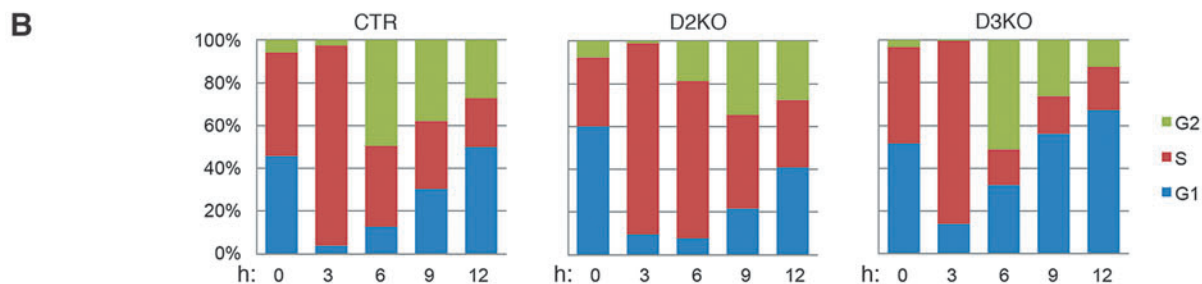
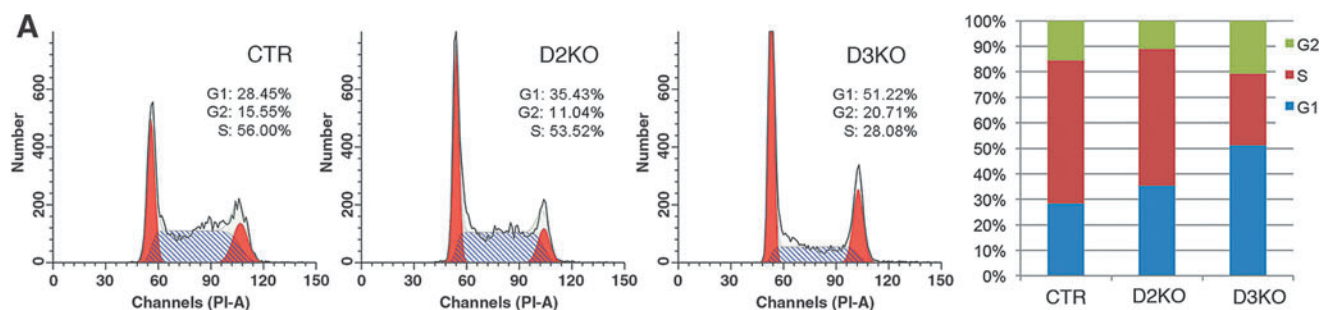
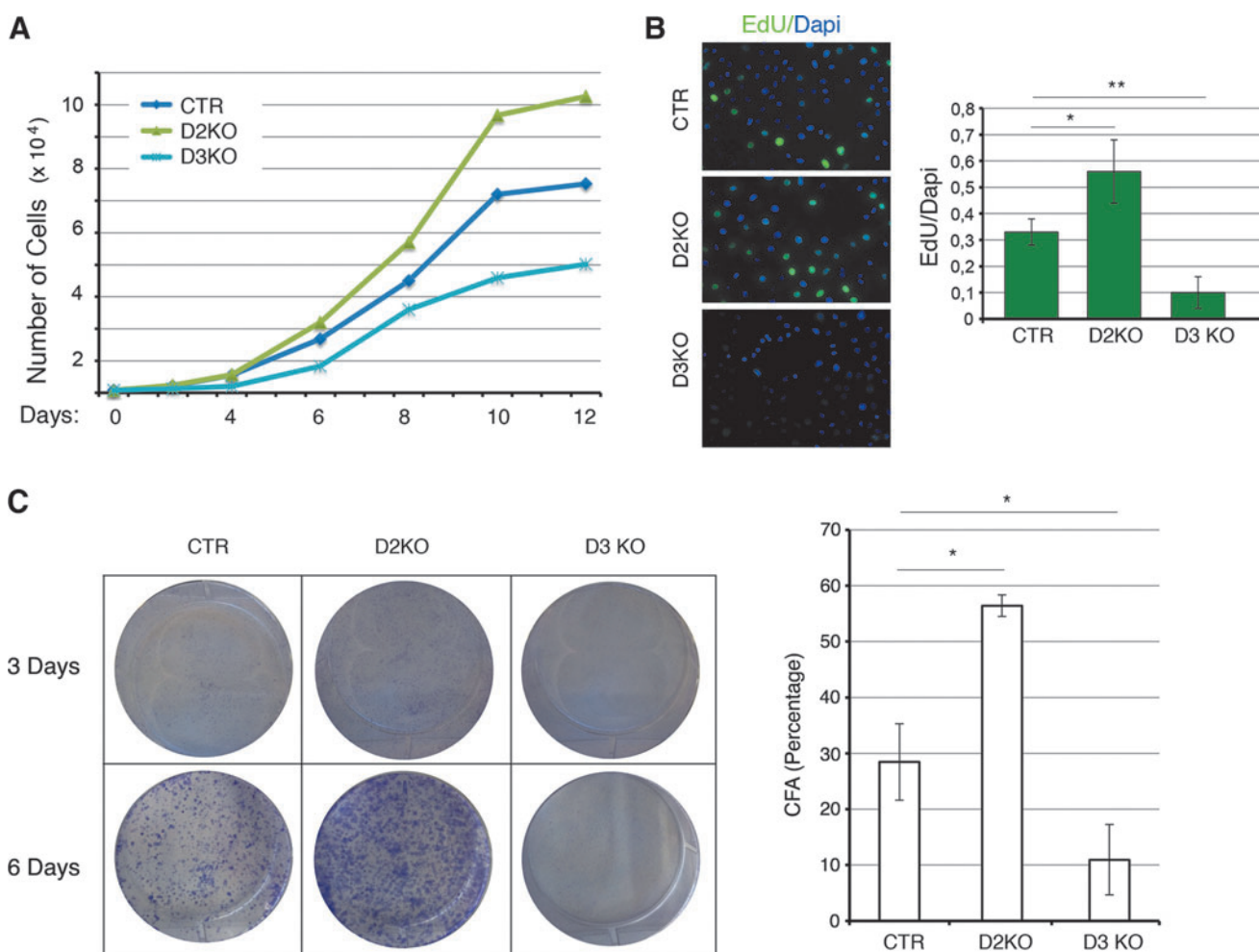


FIG. 1. Cell cycle progression is significantly altered in D2- and D3-depleted cells. (A) Cell cycle distribution was measured in asynchronized cells by flow cytometry using propidium iodide staining; the percent of cells in each cell cycle phase is shown in a bar graph. (B) Cell cycle profile of synchronized CTR, D2KO, and D3KO cells at 0, 3, 6, 9, and 12 h upon release from a double thymidine block. Cells were analyzed with flow cytometry upon propidium iodide staining. $n=3$. (C) CTR, D2KO, and D3KO cell proliferation was followed for 72 h using the carboxy-fluorescein succinimidyl ester (CFSE) CellTraceTM Violet reagent. The discrete peaks in this histogram represent successive generations of live, CFSE-positive cells. The percentage of count is represented for the three cell lines. Data are represented as mean of three experiments done in duplicates. Differences between CTR cells and D2KO or D3KO cells at each time point were assessed by Student's two-tailed t -test for independent samples. p -Values <0.05 were considered significant.

◀AU6

◀4C

DEIODINASES D2 AND D3 CONTROL PROLIFERATION OF BCC CELLS



4C ▶

FIG. 2. Selective type 2 and type 3 deiodinase (D2, D3) mutagenesis inversely regulates cell proliferation. (A) Cell growth curves of CRISPR/Cas9 control cells (CTR), and D3 knockout (D3KO) and D2KO cells. The means of three independent experiments, each conducted in triplicate, are shown. (B) Edu/Dapi staining performed to detect proliferating cells. (C) Clonogenic assay of CRISP-CTR, D3KO, and D2KO cells grown for 3 and 5 days as indicated; representative images of petri dishes are shown. Statistical significant differences were evaluated by two-way analysis of variance with the Bonferroni post-test to compare all data from D3KO and D2KO clones to those from CRISP-CTR at each time point.

expression of two TH-target genes in the skin, K10 and K14 (Supplementary Fig. S3B).

Targeted mutagenesis of D2 and D3 influences cell proliferation

To investigate and compare the functional consequences of genetic inactivation of D2 and D3 in BCC cells, we first evaluated cell proliferation in three clones for each condition (CTR, D2KO, and D3KO). Representative cell proliferation curves of one clone for each condition showed that D2KO cells grow faster than control cells, while D3-depletion in D3KO cells inhibits cell growth (Fig. 2A). EdU incorporation confirmed a growth advantage for the D2-depleted cells and a drastically decreased number of proliferative cells in a D3-null background (Fig. 1B). Similarly, colony assay demonstrated that D2-depletion accelerates cell proliferation, and that the opposite occurred in D3-depleted cells (Fig. 2C). These findings indicate that deiodinases D2 and D3 exert opposite effects on cell cycle control: D2-

F2 ▶

AU7 ▶

AU6 ▶

depletion accelerates cell proliferation, while D3-depletion inhibits cell replication.

We also treated D2KO clones with physiological T3 concentrations to assess if D2KO-dependent increases in cell proliferation were due to TH signal inactivation. T3 treatment decreased the proliferation rate of D2KO cells to almost that of CTR cells (Supplementary Fig. S4A). Analogously, we cultured D3KO cells in medium containing TH (normal serum) and in TH-deprived medium (charcoal stripped, CH). TH deprivation rapidly rescued the slow cycling profile of D3KO cells, which indicates that the reduced proliferation of D3KO cells depends on increased intracellular TH concentration (Supplementary Fig. S4B).

◀ SF4

TH modulation by D2 and D3 affects cell cycle progression

We examined the cell cycle phase distribution in asynchronized cells using flow cytometry. D3 depletion decreased S-phase cells and increased the population of G1-phase and

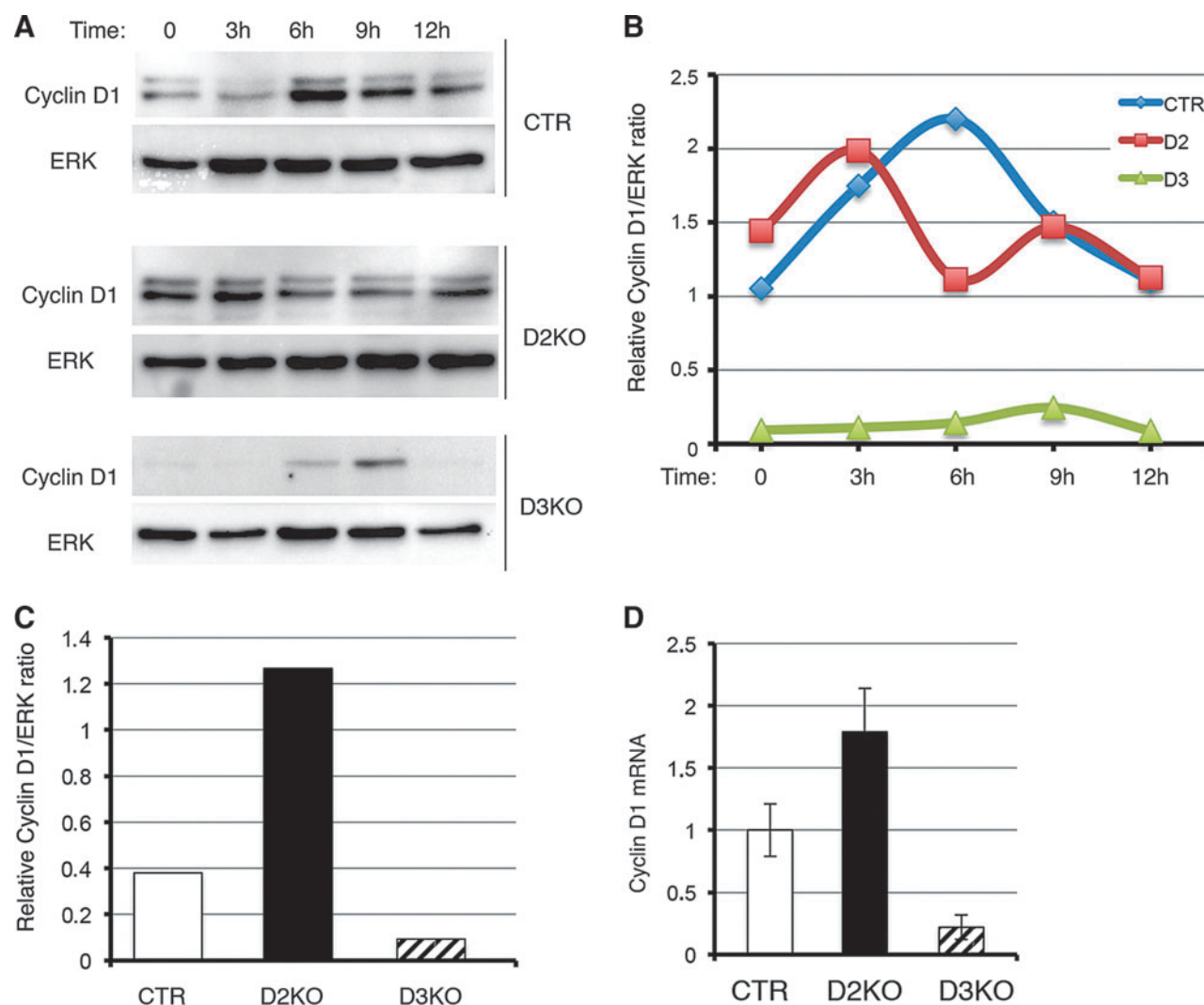
G2-phase cells (Fig. 2A); D2KO cells had a reduced number of G2-phase cells. To gain further insight into the effects of D2 and D3 depletion on cell cycle progression, we analyzed this process in S-phase synchronized cells by blocking the cell cycle with double-thymidine block and by forcing the cells to reenter the cell cycle by replacing thymidine in the medium. Cells were collected at different time points after thymidine removal. FACS analysis demonstrated that control cells recovered after thymidine block and that 37% of cells were in S-phase 6 hours after thymidine removal. Interestingly, D2-depleted cells divided more rapidly, and 73% of cells were in S-phase 6 hours after thymidine removal (Fig. 1B, Supplementary Fig. S5). On the contrary, the proportion of S-phase cells was much lower in the D3KO population (16%) than in control cells, with a consequent shift toward the G1 and G2 phases of the cell cycle. These data suggest that cell cycle progression of D3KO cells is drastically compromised. As a complementary approach, we used a

SF5 ▶

fluorescence-based method for tracing the dividing cells. Cells were labeled with a fluorescent dye (CFSE) able to mark live cells so that when they divide, the daughter progeny receives approximately half the fluorescence of the parent. After labeling, cells were harvested at different time points to measure the dye incorporation by FACS analysis. Figure 2C shows that D2KO cells retained the dye for a shorter time compared with CTR cells, while D3KO cells were the longest retaining cells, thus implicating slower replication timing for these cells.

To determine the biochemical changes underlying these altered cell cycle profiles, we examined the cyclin D1 expression profile. Thymidine-treated cultures were released from thymidine block at different time points, and total lysates were analyzed for cyclin D1 by Western blotting (Fig. 3A, B). After synchronization, cyclin D1 increased more rapidly in D2KO cells than in control cells. Conversely, cyclin D1 levels were consistently very low in

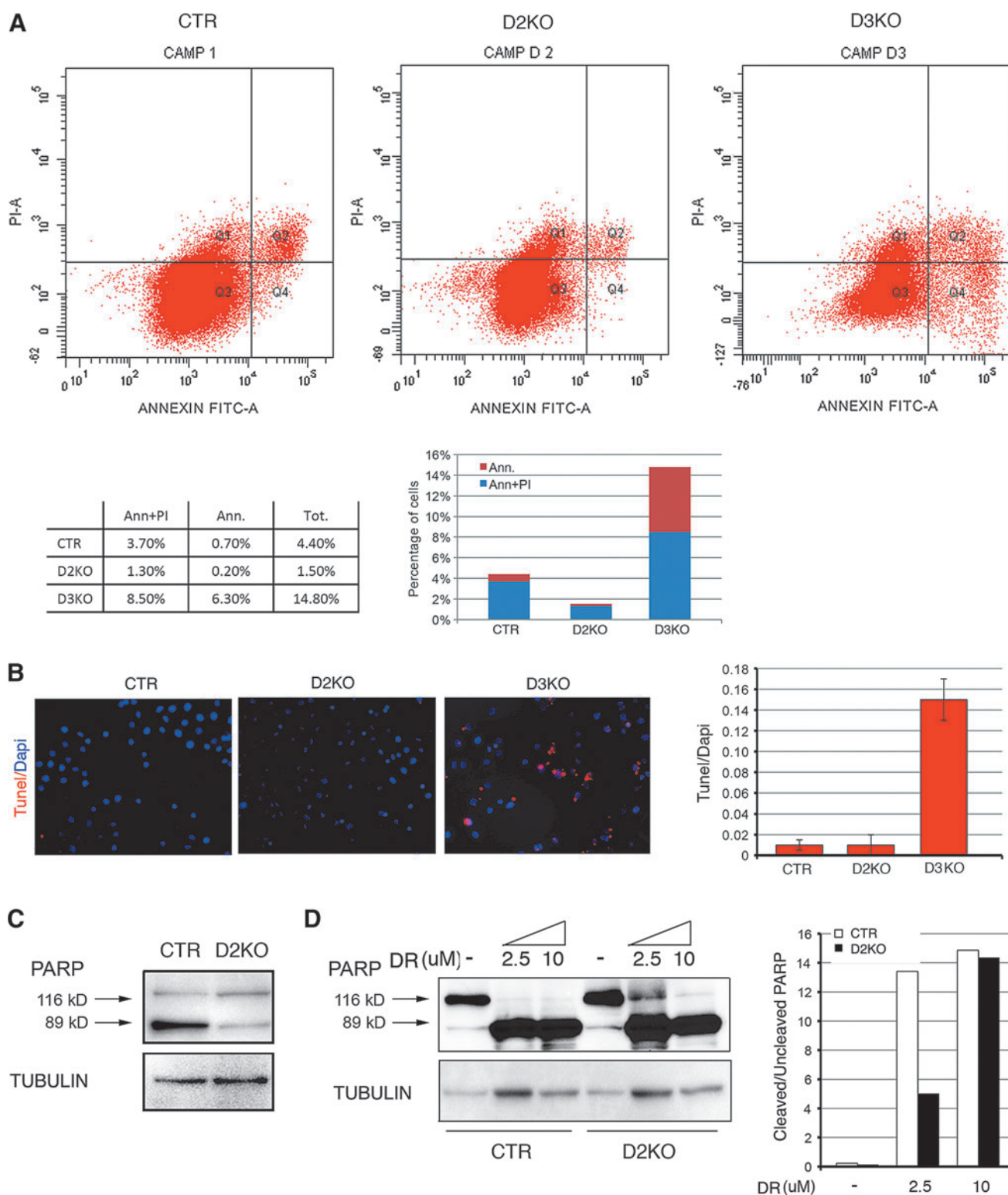
◀ F3



4C ▶

FIG. 3. Cyclin D1 expression reflects alterations in cell cycle in D2- and D3-depleted cells. (A) Cyclin D1 protein levels from synchronized CTR, D2KO, and D3KO cells at 0, 3, 6, 9, and 12 h upon release from a double thymidine block were measured by Western blotting. (B) Band intensities of Cyclin D1 and ERK levels were quantified by densitometric analysis with the ImageLab software and the levels of Cyclin D1/ERK are represented during the different time points. (C) Band intensity of the levels of cyclin D1/ERK from the Western blot reported in A and relative to time 0. (D) Basal levels of cyclin D1 mRNA from CTR, D2KO, and D3KO cells were measured by real-time PCR.

DEIODINASES D2 AND D3 CONTROL PROLIFERATION OF BCC CELLS



4C **FIG. 4.** Elevated TH levels in D3KO cells enhance basal apoptosis. **(A)** Flow cytometry detection of phosphatidylserine exposure analyzed with annexin V and propidium iodide (PI). Flow cytometry showed the increased population at early apoptosis (annexin V⁺/PI⁻) and at late apoptosis (annexin V⁺/PI⁺) in D3-depleted clones. **(B)** Apoptosis was measured with a TUNEL assay in CTR, D2KO, and D3KO clones. The blue signal represents DAPI-positive cells and the red signal represents TUNEL-positive cells. Percentages of TUNEL/DAPI-positive cells in each sample are represented in the graph bar. **(C)** PARP and Bcl-2 levels were measured by Western blotting in CRISP CTR, D3KO, and D2KO clones. Band intensity was quantified by densitometric analysis with the ImageLab software. **(D)** Western blot analysis of PARP cleavage in D2KO and CTR cells treated with 2.5 and 10 μ M doxorubicine. Ratio of cleaved versus un-cleaved PARP is represented by bars.

D3KO cells and increased slightly only nine hours after synchronization (Fig. 3A, B). Basal levels of cyclin D1 were lower in D3KO cells and higher in D2KO cells than in controls (Fig. 3C). A similar expression profile was observed at mRNA level (Fig. 3D). Taken together, these data indicate that concerted D2 and D3 action regulates S-phase entry and cyclin D1 expression.

D2-depletion protects BCC cells from cell death

Lastly, we analyzed the effects of D2 and D3 depletion on cell death. Annexin V incorporation and FACS analysis demonstrated that while apoptotic cells represent 4.4% of the control cell population, apoptosis was reduced to 1.5% in D2KO cells and increased to 14.8% in D3KO cells (Fig. 4A). TUNEL assay confirmed this result (Fig. 4B). PARP expression and cleavage confirmed that D2KO cells have a reduced basal apoptotic rate versus control cells (Fig. 4C). Interestingly, D2-depletion protected BCC cells also from doxorubicin- and tunicamycin- (data not shown) induced apoptosis, thus revealing a hitherto unrecognized role of hypothyroidism as an anti-apoptotic condition (Fig. 4D).

Discussion

The goal of this work was to dissect the role of deiodinases D2 and D3 in the regulation of intracellular TH signaling and their relative contribution to BCC cell tumorigenesis. Using a system of genetic depletion of the deiodinases D2 and D3, we generated D2KO and D3KO BCC cells, which have reduced and enhanced nuclear TH action respectively. The most prominent feature of these cells was a drastic alteration in cell proliferation rate, which reinforces the concept that TH plays a critical role in controlling cell proliferation. Given the pleiotropic roles played by TH in cell differentiation, growth, and metabolism, it is not surprising that the effects of TH on cell proliferation differ widely depending on the cellular context (19). Differential interaction with co-activator and co-factors, tissue-specific expression of different receptor isoforms, and the presence or absence of additional chromatin modifiers can explain the context-related effects of TH on cellular proliferation.

The BCC model is an example of high D3 expression within a tumor highly sensitive to TH (5,7,17). We have demonstrated that both treatments of BCC, with topical T3 or intracellular enhancement of the T3 signal by D3-depletion, affect BCC tumorigenesis by modulating multiple oncogenic signals, among them Shh/Gli2 (5) and miR21 (20). Consequently, we used the BCC cell line to unravel the molecular mechanisms by which TH interferes with the cell cycle machinery in a tumoral environment. Interestingly, while D3 was hitherto considered the deiodinase most frequently linked to tumoral transformation (19), we found robust levels of D2, the TH-activating enzyme, in BCC cells. Why is D2 expressed in BCC cells and what is its role in this tumoral context? We do not have a complete answer to this question, but the present study and our preliminary data indicate that BCC and colon cancer tumors (data not shown here) express D2 mRNA and protein besides D3, which implicates a possible role of D2 in tumorigenesis. Furthermore, other preliminary data on dual D2-D3 expression in BCC indicate that the two enzymes are partially co-expressed during tumor formation, with D3 being expressed in an early stage of tumorigenesis and D2 appearing

thereafter (data not shown). It is conceivable that in some cellular contexts the presence of both activating and inactivating TH mechanisms is a means with which to rapidly customize the TH signal as necessary. The regulator of D2 expression in BCC and in the tumorigenesis in general is not known. Preliminary data from *in vitro* transfections in BCC cells indicate that none of the well-known inducers of BCC tumorigenesis (i.e., Gli2, β -catenin, and miR21) drive D2 expression in BCC. Consequently, further studies are required to clarify the regulation of D2 *in vivo* in BCC.

The most obvious phenotype of the generated deiodinase knockout cells was a drastic variation in cell proliferation. D2KO cells have low TH nuclear activity, as demonstrated by transactivation studies and the levels of TH target gene expression, and consequently represent a model of a “hypothyroid” condition. These cells are characterized by a high proliferation rate and by a high proportion of S-phase cells. Conversely, D3KO cells are slowly cycling cells and are characterized by increased nuclear TH activity when compared with control cells. These results point to a model in which TH slows the proliferation rate in the BCC context.

Studies in both synchronous and asynchronous cells indicate that variations of the proliferative rate induced by deiodinase depletion are associated to the proportion of S-phase and to cyclin D1 expression. Cyclin D1 is a key player in cell cycle modulation (21) and is dynamically regulated at both transcriptional and post-transcriptional level during the cell cycle to ensure the G1 to S progression of cells (20). Cyclin D1 is also a TH target in several cell contexts (19). However, the transcriptional regulation of cyclin D1 by TH is dynamic and highly variable depending on the context. Breast cancer is an example of a tumor in which the TH-TR β complex reduces tumorigenesis by down-regulating cyclin D1 expression (22). Additionally, TR β suppresses estrogen-dependent tumor growth of human breast cancer cells (23). Recently, it was suggested that the mechanism by which TR β acts as tumor suppressor is via up-regulation of the nuclear receptor co-repressor 1 (NCOR1) and suppression of invasion, tumor growth, and metastasis in human hepatocarcinomas (24). Also in neuroblastoma cells, over-expression of TR β inhibits the transcriptional response of the RAS/mitogen-activated protein kinase/ribosomal-S6 pathway, thereby suppressing growth (25). Similarly, overexpressed TR β inhibited the AKT-mTOR-p70S6K pathway in human follicular thyroid cancer cells (26). Overexpression of cyclin D1 mRNA was detected in *Thr β ^{PV/PV}* mice in which the *Thr β* gene was mutated by an insertion leading to a frame-shift of TR β 1 and a total loss of triiodothyronine (T3) binding ability. The molecular mechanism by which this TR β mutation increases cyclin D1 expression in *Thr β ^{PV/PV}* mice was found to be due, at least in part, to the loss of the negative regulation of cyclin D1 promoter activity by wild-type receptor (27). On the other hand, there are many examples showing that TH and its receptors exert a positive effect on cell proliferation (28,29). Therefore, to better contextualize the transcriptional role of TH in cyclin D1 expression, we measured the levels of cyclin D1 mRNA and protein in synchronized BCC cells (5). Our data demonstrate that TH attenuation in D2KO cells potentiates the expression of this crucial cyclin, whereas the opposite occurs in D3KO cells.

Besides regulating cell cycle progression, modulation of T3 by D2 and D3 also affects BCC cell survival. Using our deiodinase loss-of-function BCC cell models, we evaluated the effects of T3 on apoptosis, and obtained evidence that T3 plays a pro-apoptotic role in BCC cells. Indeed, lower T3 levels in D2KO cells reduced basal apoptosis as measured by annexin V incorporation and FACS analysis, but they were also associated with stronger resistance to the apoptotic stimuli of doxorubicine and tunicamicine.

In conclusion, our results demonstrate that D2 and D3 are simultaneously expressed in BCC cells and that their action fine-tunes the TH signal. Manipulation of D2 or D3 dramatically affects the proliferative potential of BCC cells. Our results are compatible with the recent finding that precise regulation of the TH-dependent landscape of gene expression is essential in a vast range of biological processes, namely, embryonic development, tissue repair, and tumorigenesis (4). From a broad perspective, these novel concepts expand the use of deiodinases as a tool with which to interfere in diverse pathophysiological contexts in order to adapt the TH signal in a tissue-specific fashion.

Acknowledgments

AU9 ▶ This work was supported by grants from AIRC to M.D. (IG 13065) and D.S. (IG 11362). We thank Jean Ann Gilder (Scientific Communication srl., Naples, Italy) for writing assistance.

C.M., M.A.D.S., D.D.G., E.D.C. A.G.C. and T.P. performed *in vitro* experiments and prepared figures; R.A. generated plasmids and performed *in vitro* experiments; M.R. and L.D.V. performed fluorescence activated cell sorting analysis studies; D.S., provided observations, scientific interpretations, and contributed to experiment supervision and interpretation; M.D. designed the overall study, supervised the experiments, analyzed the results, and wrote the paper; and all authors discussed the results and provided input on the manuscript.

Author Disclosure Statement

The authors have declared that no conflict of interest exists.

References

1. Yen GG, Meesad P 2001 An effective neuro-fuzzy paradigm for machinery condition health monitoring. *IEEE Trans Syst Man Cybern B Cybern* **31**:523–536.
2. Sirakov M, Skah S, Nadjar J, Plateroti M 2013 Thyroid hormone's action on progenitor/stem cell biology: new challenge for a classic hormone? *Biochim Biophys Acta* **1830**:3917–3927.
3. Brent GA 2012 Mechanisms of thyroid hormone action. *J Clin Invest* **122**:3035–3043.
4. Gereben B, Zeold A, Dentice M, Salvatore D, Bianco AC 2008 Activation and inactivation of thyroid hormone by deiodinases: local action with general consequences. *Cell Mol Life Sci* **65**:570–590.
5. Dentice M, Luongo C, Huang S, Ambrosio R, Elefante A, Mirebeau-Prunier D, Zavacki AM, Fenzi G, Grachtchouk M, Hutchin M, et al. 2007 Sonic hedgehog-induced type 3 deiodinase blocks thyroid hormone action enhancing proliferation of normal and malignant keratinocytes. *Proc Natl Acad Sci U S A* **104**:14466–14471.
6. Antonini D, Sibilio A, Dentice M, Missero C 2013 An Intimate relationship between thyroid hormone and skin: regulation of gene expression. *Front Endocrinol (Lausanne)* **4**:104.
7. Dentice M, Salvatore D 2011 Deiodinases: the balance of thyroid hormone: local impact of thyroid hormone inactivation. *J Endocrinol* **209**:273–282.
8. Tomic-Canic M, Day D, Samuels HH, Freedberg IM, Blumenberg M 1996 Novel regulation of keratin gene expression by thyroid hormone and retinoid receptors. *J Biol Chem* **271**:1416–1423.
9. Engelhard A, Christiano AM 2004 The hairless promoter is differentially regulated by thyroid hormone in keratinocytes and neuroblastoma cells. *Exp Dermatol* **13**:257–264.
10. Puzianowska-Kuznicka M, Pietrzak M, Turowska O, Nauman A 2006 Thyroid hormones and their receptors in the regulation of cell proliferation. *Acta Biochim Pol* **53**: 641–650.
11. Qi JS, Yuan Y, Desai-Yajnik V, Samuels HH 1999 Regulation of the mdm2 oncogene by thyroid hormone receptor. *Mol Cell Biol* **19**:864–872.
12. Komuves LG, Hanley K, Jiang Y, Elias PM, Williams ML, Feingold KR 1998 Ligands and activators of nuclear hormone receptors regulate epidermal differentiation during fetal rat skin development. *J Invest Dermatol* **111**:429–433.
13. Slominski A, Wortsman J 2000 Neuroendocrinology of the skin. *Endocr Rev* **21**:457–487.
14. Hanley K, Rassner U, Elias PM, Williams ML, Feingold KR 1996 Epidermal barrier ontogenesis: maturation in serum-free media and acceleration by glucocorticoids and thyroid hormone but not selected growth factors. *J Invest Dermatol* **106**:404–411.
15. Sheng H, Goich S, Wang A, Grachtchouk M, Lowe L, Mo R, Lin K, de Sauvage FJ, Sasaki H, Hui CC, et al. 2002 Dissecting the oncogenic potential of Gli2: deletion of an NH(2)-terminal fragment alters skin tumor phenotype. *Cancer Res* **62**:5308–5316.
16. Antonini D, Rossi B, Han R, Minichiello A, Di Palma T, Corrado M, Banfi S, Zannini M, Brissette JL, Missero C 2006 An autoregulatory loop directs the tissue-specific expression of p63 through a long-range evolutionarily conserved enhancer. *Mol Cell Biol* **26**:3308–3318.
17. Di Girolamo D, Ambrosio R, De Stefano MA, Mancino G, Porcelli T, Luongo C, Di Cicco E, Scalia G, Vecchio LD, Colao A, et al. 2016 Reciprocal interplay between thyroid hormone and microRNA-21 regulates hedgehog pathway-driven skin tumorigenesis. *J Clin Invest* **126**: 2308–2320.
18. Bostock CJ, Prescott DM, Kirkpatrick JB 1971 An evaluation of the double thymidine block for synchronizing mammalian cells at the G1-S border. *Exp Cell Res* **68**:163–168.
19. Dentice M, Antonini D, Salvatore D 2013 Type 3 deiodinase and solid tumors: an intriguing pair. *Expert Opin Ther Targets* **17**:1369–1379.
20. Yang K, Hitomi M, Stacey DW 2006 Variations in cyclin D1 levels through the cell cycle determine the proliferative fate of a cell. *Cell Div* **1**:32.
21. Sherr CJ 1995 D-type cyclins. *Trends Biochem Sci* **20**:187–190.
22. Park JW, Zhao L, Willingham MC, Cheng SY 2016 Loss of tyrosine phosphorylation at Y406 abrogates the tumor

- suppressor functions of the thyroid hormone receptor beta. *Mol Carcinog*.
23. Park JW, Zhao L, Cheng SY 2013 Inhibition of estrogen-dependent tumorigenesis by the thyroid hormone receptor beta in xenograft models. *Am J Cancer Res* **3**:302–311.
 24. Martinez-Iglesias OA, Alonso-Merino E, Gomez-Rey S, Velasco-Martin JP, Martin Orozco R, Luengo E, Garcia Martin R, Ibanez de Caceres I, Fernandez AF, Fraga MF, et al. 2016 Autoregulatory loop of nuclear corepressor 1 expression controls invasion, tumor growth, and metastasis. *Proc Natl Acad Sci U S A* **113**:E328–337.
 25. Garcia-Silva S, Aranda A 2004 The thyroid hormone receptor is a suppressor of ras-mediated transcription, proliferation, and transformation. *Mol Cell Biol* **24**:7514–7523.
 26. Kim WG, Zhao L, Kim DW, Willingham MC, Cheng SY 2014 Inhibition of tumorigenesis by the thyroid hormone receptor beta in xenograft models. *Thyroid* **24**:260–269.
 27. Furumoto H, Ying H, Chandramouli GV, Zhao L, Walker RL, Meltzer PS, Willingham MC, Cheng SY 2005 An unliganded thyroid hormone beta receptor activates the cyclin D1/cyclin-dependent kinase/retinoblastoma/E2F pathway and induces pituitary tumorigenesis. *Mol Cell Biol* **25**:124–135.
 28. Lukas J, Bartkova J, Bartek J 1996 Convergence of mitogenic signalling cascades from diverse classes of receptors at the cyclin D-cyclin-dependent kinase-pRb-controlled G1 checkpoint. *Mol Cell Biol* **16**:6917–6925.
 29. Prall OW, Sarcevic B, Musgrove EA, Watts CK, Sutherland RL 1997 Estrogen-induced activation of Cdk4 and Cdk2 during G1-S phase progression is accompanied by increased cyclin D1 expression and decreased cyclin-dependent kinase inhibitor association with cyclin E-Cdk2. *J Biol Chem* **272**:10882–10894.

Address correspondence to:

Monica Dentice

◀AU10

Department of Clinical Medicine and Surgery

University of Naples “Federico II”

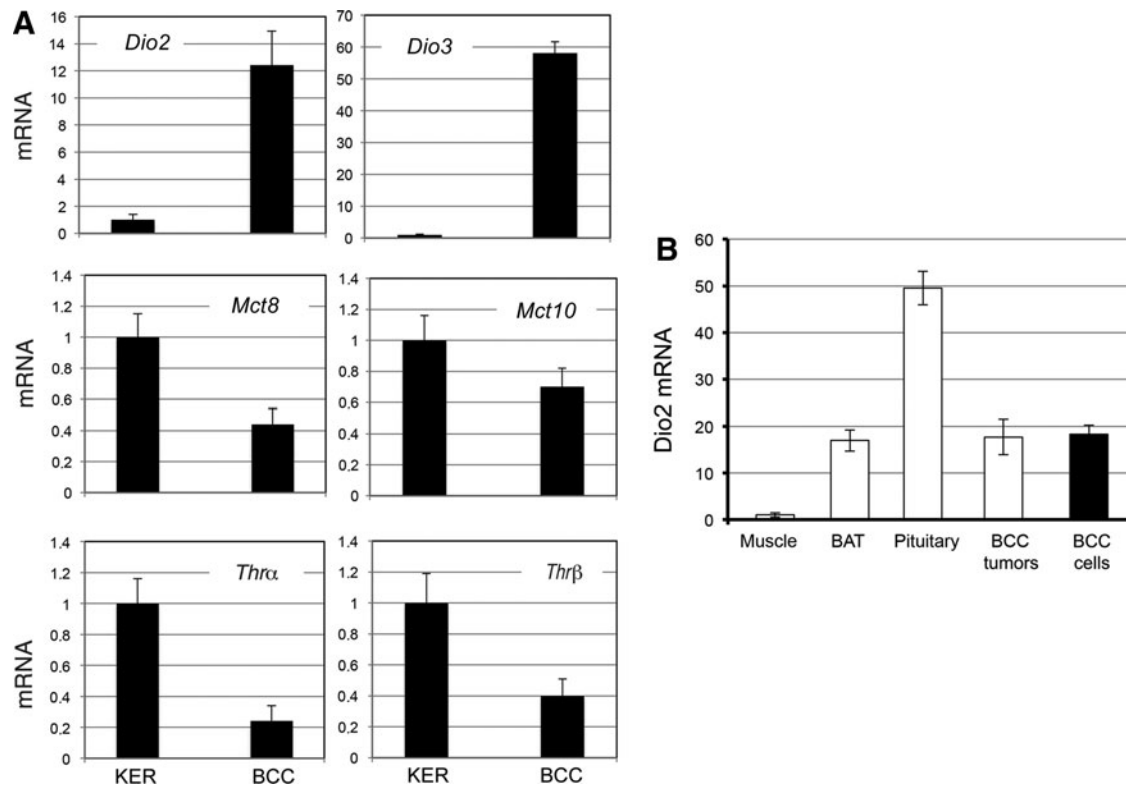
Via S. Pansini 5

Naples 80131

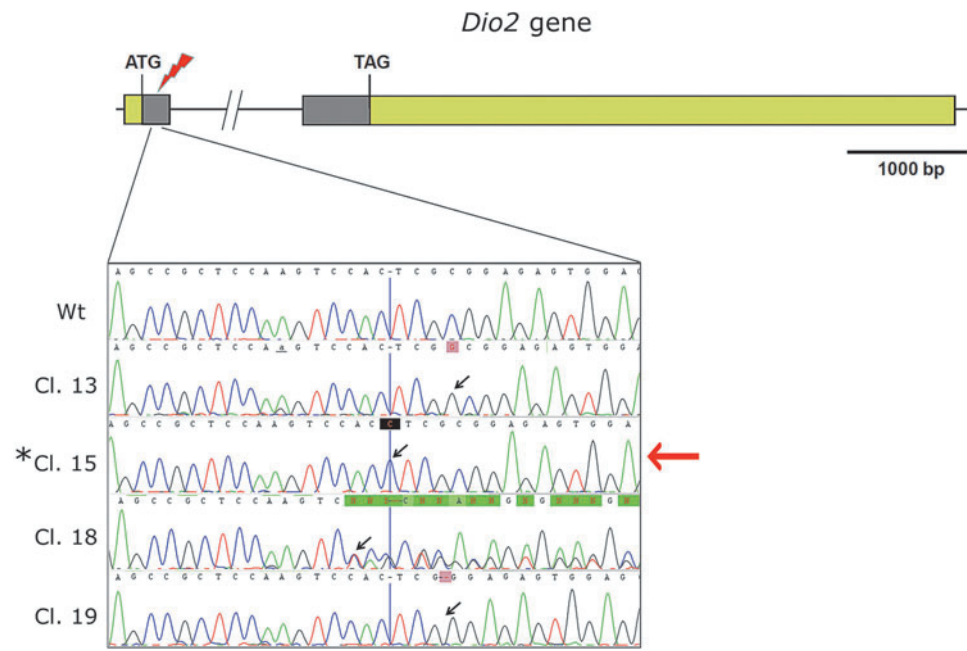
Italy

E-mail: monica.dentice@unina.it

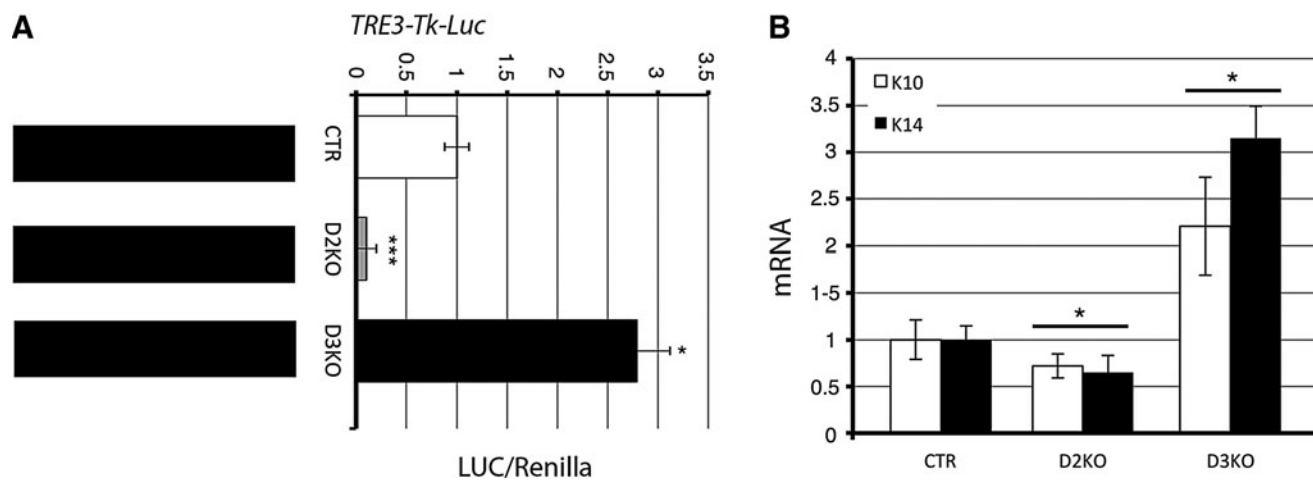
Supplementary Data



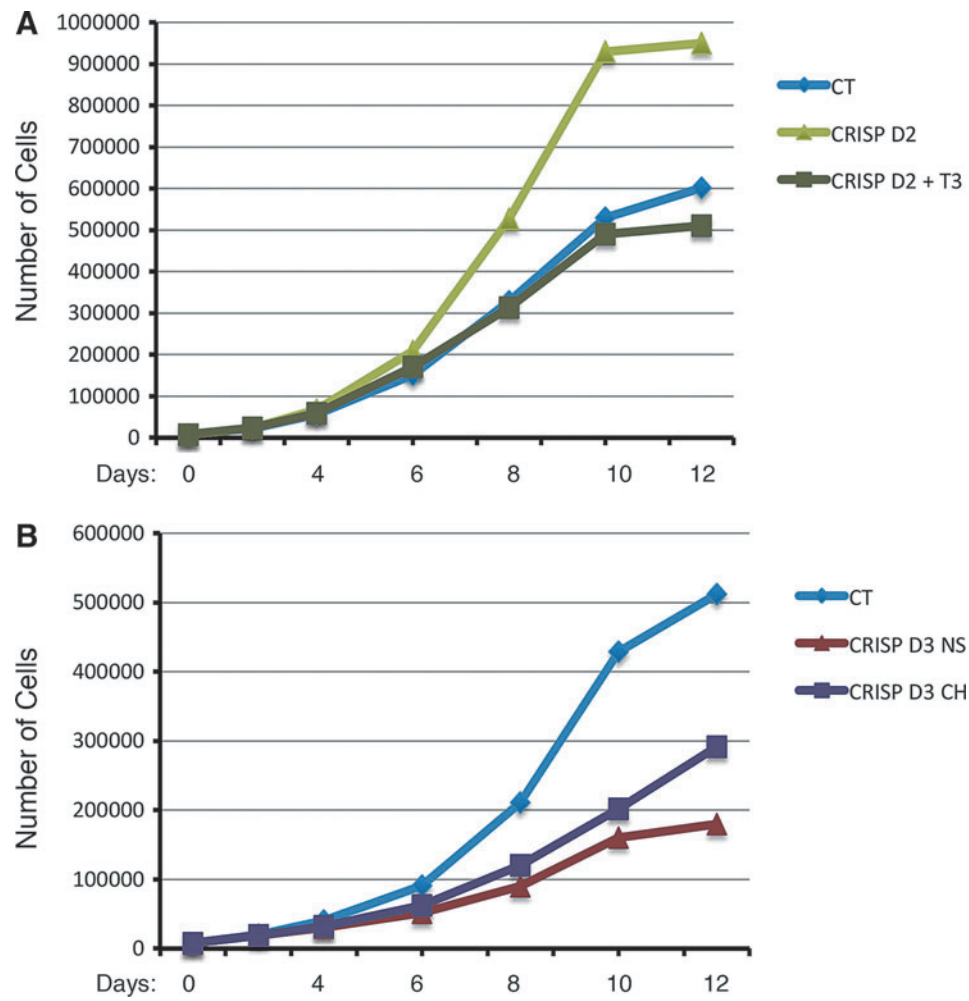
SUPPLEMENTARY FIG. S1. Expression of *Dio2*, *Dio3*, *THRα*, *THRβ*, *MCT8*, and *MCT10* in BCC cells and wild-type (WT) keratinocytes. mRNA expression levels were assessed by real-time quantitative reverse transcription-PCR in BCC cells and in WT keratinocytes. mRNA levels were normalized to those of the cyclophilin A gene. mRNA expression levels in BCC cells was calculated by the $2^{-\Delta\Delta Ct}$ method relative to WT keratinocytes, in which expression is reported as 1.



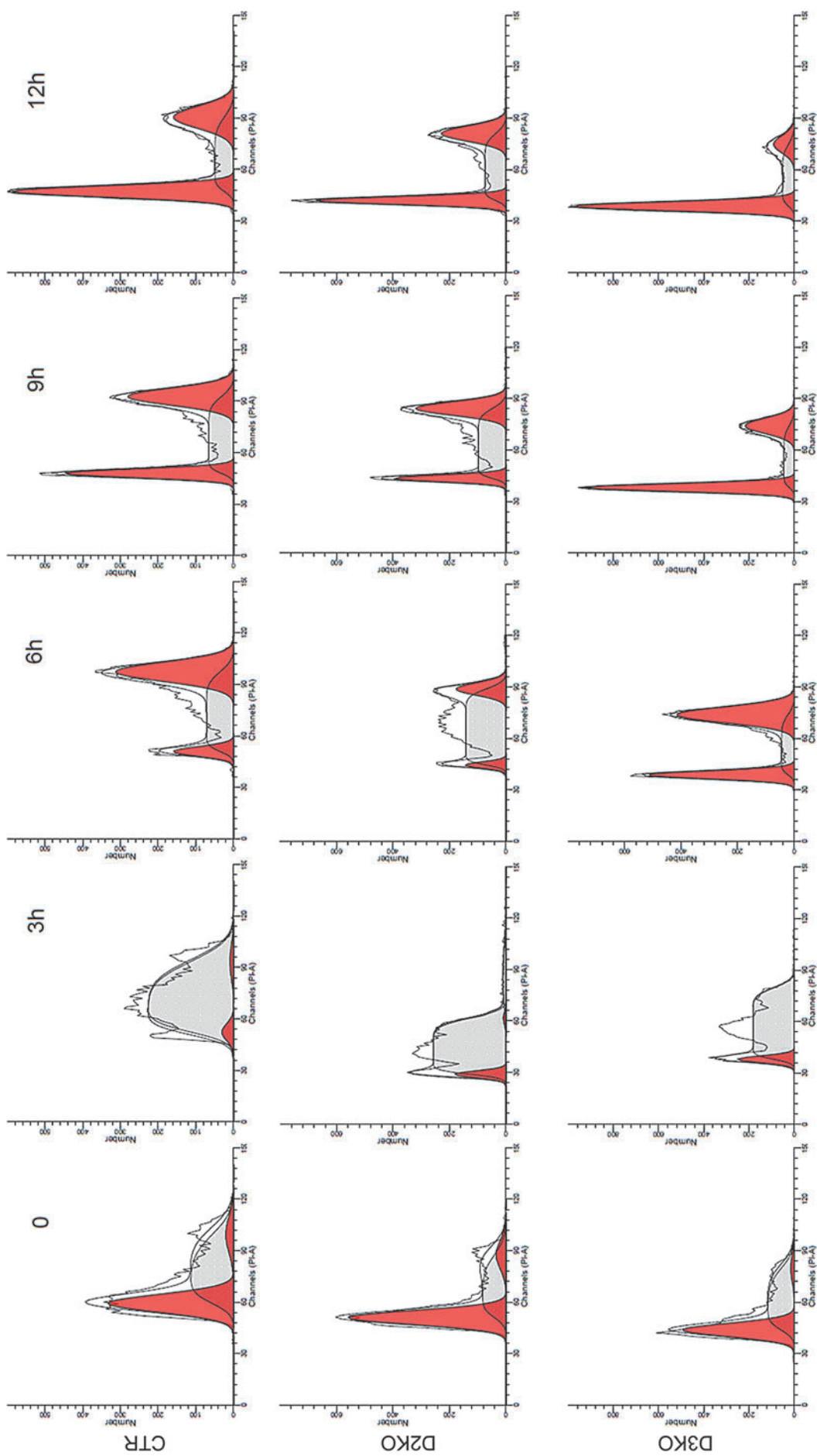
SUPPLEMENTARY FIG. S2. Mutagenesis of D2 in BCC cells. Schematic representation of the *DIO2* locus. Four clones are compared to WT BCC cells. The red arrow indicates the selected clone.



SUPPLEMENTARY FIG. S3. Mutagenesis of D2 and D3 expression drastically alters intracellular triiodothyronine (T3) signaling. **(A)** Control (CTR), type 2 deiodinase knockout (D2KO), and D3KO cells were transfected with the artificial T3-responsive promoter TRE3-TK-Luc and cells were analyzed for luciferase activity. The results are shown as means \pm standard deviation of the luciferase/renilla (LUC/Renilla) ratios from at least three separate experiments, performed in duplicate. * $p < 0.05$, ** $p < 0.01$, *** $p < 0.001$. **(B)** K10 and K14 mRNA expression levels were assessed by real-time quantitative reverse transcription-PCR in the CTR, D2KO, and D3KO clones. * $p < 0.05$.



SUPPLEMENTARY FIG. S4. Manipulation of T3 levels rescues the D2KO and D3KO phenotype. **(A)** Cell growth curves of D2KO cells cultured with normal serum with or without the addition of 3 nM T3. **(B)** CTR and D3-KO clones were plated in 60 mm dishes with 10% fetal bovine serum (FBS) (normal serum, NS) or with 10% Ch. St-FBS (charcoal stripped serum, CH). On alternative days, cells were harvested in PBS and counted. The graph shows the means of two independent experiments, each conducted in triplicate.



SUPPLEMENTARY FIG. S5. Deiodinase mutagenesis alters cell cycle progression. The figure shows the cell cycle profile of CTR, D2KO, and D3KO cells at 0, 2, 4, 6, 8, and 10 h after release from a double thymidine block. Cells were analyzed by flow cytometry upon propidium iodide staining. $n = 3$; * $p < 0.05$; ** $p < 0.01$.

SUPPLEMENTARY TABLE 1. LIST OF OLIGONUCLEOTIDES

Oligonucleotides used for real-time PCR

<i>Gene</i>	<i>Forward primer (5' → 3')</i>	<i>Reverse primer (5' → 3')</i>
<i>Cyclophilin A</i>	CGCCACTGTCGCTTTTCG	AACTTTGTCTGCAAACAGCTC
<i>Dio2</i>	CTTCCTCCTAGATGCCTACAAAC	GGCATAATTGTTACCTGATTCAGG
<i>Dio3</i>	CCGCTCTCTGCTGCTTCAC	CGGATGCACAAGAAATCTAAAAGC
<i>Thra1</i>	CCTGGATGACACGGAAGTGGCT	GGGCACTCGACTTTTCATGTG
<i>Thrb1/2</i>	CACAGGGTACCACTATCGCTGC	CAGCACCAAGTCTGTTGCCATGC
<i>Mct8</i>	TTCGGCTGGATAGTGGTGTGTTGCA	ATCATGCCCATAGCGAGGGCTC
<i>Mct10</i>	CCATCGTGAGTGTCTTCACGGACAT	GGAGCAGGATTGTGAAGACGCTGC
<i>Kyclin D1</i>	GCTCCTGTGCTGCGAAGTGGA	TCATGGCCAGCGGGAAGACCT
<i>Krt10</i>	CGAGCTGGAGGGTAAAATCA	CGTTGGCATTGTGTCAGTTGTC
<i>Krt14</i>	GATGTGACCTCCACCAACCG	CCATCGTGCACATCCATGAC
<i>Oligonucleotides used for genome analysis of CrispR/CAS clones</i>		
<i>gdi3U</i>	CGACCCAAGATTTCTGGGGCA	
<i>gdi3L</i>	AGCAGAGTCTCAAGTTAGCCAGAC	
<i>Dio2_ex1U</i>	AGAGCCTGAACCTGGTCTTT	
<i>Dio2_ex1L</i>	CACACCTTCCACACCCTAG	

AUTHOR QUERY FOR THY-2016-0532-VER9-MIRO 1P

AU1: Please note that the gene symbols in any article should be formatted as per the gene nomenclature. Thus, please make sure that the gene symbols, if present in this article, are italicized.

AU2: Please check all author names for accurate indexing.

AU3: Please expand abbreviated institution names.

AU4: Should this indicate thyroid hormone (e.g., nuclear thyroid hormone receptors)?

AU5: Reworded to add definition of FACS. Please check wording to ensure that it is acceptable.

AU6: Figures 1 and 2 reordered/renumbered to appear chronologically in the text.

AU7: Please expand EdU.

AU8: References 20 and 21 reordered/renumbered to appear chronologically.

AU9: Expand abbreviated term/institution name AIRC.

AU10: Please add degree abbreviations (ex., MD, PhD).